UNIVERSITY OF OKLAHOMA

GRADUATE COLLEGE

GLACIATION IN EQUATORIAL PANGAEA: TESTING THE HYPOTHESIS IN THE PENNYSLVANIAN-PERMIAN FOUNTAIN FORMATION (COLORADO)

A DISSERTATION

SUBMITTED TO THE GRADUATE FACULTY

in partial fulfillment of the requirements for the

Degree of

DOCTOR OF PHILOSOPHY

By

DUSTIN E. SWEET
Norman, Oklahoma
2009

GLACIATION IN EQUATORIAL PANGAEA: TESTING THE HYPOTHESIS IN THE PENNYSLVANIAN-PERMIAN FOUNTAIN FORMATION (COLORADO)

A DISSERTATION APPROVED FOR THE
CONOCOPHILLIPS SCHOOL OF GEOLOGY AND GEOPHYSICS

BY

Dr. Gerilyn S. Soreghan, Chair

Dr. Michael J. Soreghan

Dr. Richard D. Elmore

Dr. Susan E. Postawko

Dr. Charles F. Kluth

Acknowledgments

First and foremost, I would like to thank my advisor, Dr. Lynn Soreghan, for her unparalleled enthusiasm for geology and seemingly endless energy. Many of my papers and proposals reached seven or eight versions and she patiently forged through all the cryptic, unnecessary and nonsensical passages. Furthermore, she was always a sounding board for crazy ideas and life issues —for all these things I thank her again.

I thank my committee members Dr. Mike Soreghan, Dr. Doug Elmore, Dr. Susan Postawko and Dr. Chuck Kluth for timely and constructive comments throughout my dissertation process. A special thanks to Mike for his forbearance during unexpected office interruptions to ask Illustrator issues and, of course, for Friday beers!

I thank the many OU students who listened to me and offered advice, especially Vincent Heesakkers and Matthew Zeichmeister—even though they kept trying to postpone my defense date. To Dr. Ze'ev Reches, I appreciate all the conversations about fractures and for letting me play like a structural geologist. Also, I thank Sohini Sur and Kristen Marra who kept me from blowing myself up in the lab.

I thank my Mother for accepting that I needed to go get my doctorate even though it meant we saw each other once a year. I thank my father for listening when I needed to talk even though those times were probably far too few. I thank my grandparents for their unparalleled support and weekly Sunday phone calls asking me how "the paper" was coming along. I thank my brothers for pretending to care. Lastly, I thank Alisan for helping me see it through the end—thank you!

Table of Contents

List of Tables

List of Figures

Abstract

Recently, Soreghan et al. (2007, 2008) suggested that Unaweep Canyon of western Colorado was initially carved by Late Paleozoic equatorial glaciers that reached modest elevations (<1000 m). Furthermore, Soreghan et al. (in press) suggest that the Permian Cutler Formation cropping out at the mouth of Unaweep Canyon represents proglacial and ice-contact deposition. These new hypotheses are important because they challenge previously proposed models and they provide new ideas for Late Paleozoic climate states, chiefly low-latitude, low-elevation glaciation. However, if these hypotheses are valid, then the Cutler-Unaweep glacial system should not have been a singular event and other glacial systems should have been present within the ancestral Rocky Mountains. This study tests the hypotheses that glacial and proglacial conditions influenced sedimentation in the Late Paleozoic Fountain Formation where it crops out along the east flank of the Front Range of Colorado. In addition, data providing constraints on basin evolution in the Manitou Springs, Colorado, region and estimates of global sea level change are presented. The work is organized such that each chapter represents a stand-alone entity.

Chapter 2

Sedimentologic, stratigraphic and structural data indicate that the Fountain Formation at Manitou Springs consists of three tectonostratigraphic units, herein termed the lower, middle and upper Fountain units. The lower and middle Fountain units were deposited in a fan-delta setting adjacent to the active ancestral Ute Pass fault. The lower is thin and predominantly characterized by depositional stability as rcorded by abundant well-developed, deeply-rooted paleosols. The middle Fountain unit reflects fan

progradation and highland rejuvenation as a result of increased activity of the ancestral Ute Pass fault. This activity was likely the result of a basinward splay of the ancestral Ute Pass fault with reverse dip-slip motion as indicated by (1) exhumation of the lower Paleozoic Sawatch Formation and (2) fault-parallel folding. The upper Fountain unit reflects deposition in a NW-SE-trending, braided-river system and appears to post-date movement on the ancestral Ute Pass fault. Lithostratigraphic correlation allows for a Latest Pennsylvanian-early Permian age for the upper Fountain unit, thus constraining cessation of the ancestral Ute Pass fault to middle- to late Pennsylvanian time.

The Fountain Formation was deposited within a NW-SE oriented structural trough (i.e. Woodland Park trough) that separated the ancestral Front Range into a northern block (i.e. ancestral Front Range block) and a southern block (i.e. Ute Pass uplift). The Woodland Park trough was bounded on its southern margin by the ancestral Ute Pass fault which was active throughout deposition of the lower two Fountain tectonostratigraphic units, during which time sediments were shed northward across the ancestral Ute Pass fault into a marine environment. By the time of deposition of the upper Fountain unit, movement on the ancestral Ute Pass fault had ceased or dramatically decreased. During this time, the Fountain Formation records predominantly axially oriented braided-stream deposition.

Comparison of the timing and kinematic history of the ancestral Ute Pass fault with other documented reverse and strike-slip faults of the ancestral Rocky Mountains suggests that: 1) cessation of faulting within the ancestral Rocky Mountains displays a slight east-to-west younging, but the crude age resolution of adjacent basin fill also allows for the possibility of relatively synchronous cessation of faulting, and 2)

kinematics of all faults examined are consistent with a NE-SW oriented maximum horizontal compressional stress field. These inferences contrast with the proposed Laurentian-Gondwanan diachronous closure models for the ancestral Rocky Mountains, which require rotation of the maximum horizontal stress orientation through time and pronounced east-to-west younging of faulting. Rotation of the horizontal stress field may be recorded in multi-stage, kinematic histories of faults but multiple faults require study to assess this model. Age constraints on post-tectonic units of the ancestral Rocky Mountains, such as the upper Fountain Formation tectonostratigraphic unit defined herein, are poor and further refinement would greatly aid understanding of the enigmatic tectonics of these ancient mountains.

Chapter 3

Sand- and granule-filled polygonal fractures are present on bedding surfaces within the equatorial Fountain Formation (Pennsylvanian-Permian, Colorado). The surfaces are areally extensive (> 120,000 m^2) and occur within inferred braided-river deposits. The fractures penetrate downward into coarse sandstone to granule conglomerate and range from 3-55 cm and 13- >220 cm in width and depth, respectively. At one locality (Manitou Springs), both fracture fill and polygon interiors display a grain-supported texture and contain <14% clay; additionally, the fracture fill is microbrecciated. At the other locality (Loveland), both the fracture fill and polygon interiors display a grain-supported texture and contain <3.5% clay.

The polygonal fractures are inferred to have formed as frozen ground experienced thermal contraction induced by repeated cooling events. Owing to the equatorial location of the Fountain Formation, we suggest that diurnal, rather than seasonal, temperature

variations provided the repeated cooling mechanism. Alternative causes of polygonal fracturing, such as desiccation of clay-rich sediments or thermal contraction of evaporite minerals, are untenable because the hosting strata contain minimal clay (<14%) and are framework-supported, indicating that there was insufficient space for either clay or evaporite minerals. A thermal contraction origin for these features implies that the equatorial Fountain Formation experienced at least two episodes of remarkably cold conditions. Furthermore, using maximum reasonable stream gradients (~0.02) between the polygonally fractured surfaces and the shoreline (gauged from shallow-marine deposits of the Denver basin), the fractures formed at relatively low elevation (≤ 1800 m).

Chapter 4

Scanning Electron Microscopy (SEM) of first-cycle quartz grains from the equatorial, Pennsylvanian-early Permian Fountain Formation reveals microtextures that resulted from fracturing during depositional transport, even after diagenetic overprinting occurred under moderate burial conditions (up to 3.5 km depth and 100°C). Depositional transport microtextures can be grouped based on fracture process into: 1) high-stress fractures, consisting of fractures created through sustained high-shear stress, such as grooves, deep troughs, and gouges, and are inferred to occur predominantly during glacial transport; 2) percussion fractures, consisting of fractures created by grain-to-grain contact during saltation or traction flow, such as randomly oriented v-shaped cracks and edge rounding, and are inferred to occur predominantly during saltation and/or traction flow; and 3) polygenetic fractures, such as conchoidal fractures, arc-shaped steps, linear steps and linear fractures, occur under a wide range of transport processes and thus indicate no environmental significance. Using a ternary diagram that distinguishes high-

stress, percussion, and polygenetic fracture types, data from this study demonstrate that quartz grains from the Fountain Formation exhibit microtextures similar to both Quaternary till and glaciofluvial deposits, suggesting that periods of upland glaciation occurred in the Fountain Formation provenance region (Ute Pass uplift).

The frequency of high-stress fractures versus stratigraphic level shows three peak intervals (I, II, & III). These intervals are inferred to record the presence of ice within the Ute Pass uplift and are correlative with polygonally fractured bedding paleosurfaces within the Fountain Formation inferred to reflect cold-temperature weathering. Moreover, the peak intervals are roughly coeval to inferred episodes of ice maxima from high-latitude localities. Employing geologically reasonable stream gradients and estimated transport distance, elevation of the ice terminus is constrained to <1500 m. These data suggest that upland glaciers episodically existed within this equatorial setting and further use of this technique may reveal more evidence of ice in other proximal deposits of the ancestral Rocky Mountains, as well as other systems of various geologic ages.

Chapter 5

At Manitou Springs, Colorado, the lower ~ 240 meters of the Fountain Formation is composed of successive continental-marine cycles. Each cycle is characterized by alluvial-fan deposits overlain by a marine progradational package. A thin cobble conglomerate marks the base of marine strata and is inferred to represent a transgressive lag. Furthermore, each of these lags can be traced down depositional dip throughout the study area. The above field relationships allow for a minimum calculation of the magnitude of sea-level change because: 1) a minimum horizontal distance of transgression can be measured from the mapped transgressive lag deposits; and 2) the

slope of the surface over which transgression progressed can be estimated through paleohydraulic analysis of the fluvial deposits.

Magnitudes of sea level change over six successive cycles were calculated using an estimated depositional slope of 0.005; results suggest a minimum of 10-18 m of change. A large eustatic component is inferred for these six cycles because each marine package is separated throughout the study area by alluvial packages; conversely, inferred autogenic cycles of the Fountain Formation have alluvial components that grade laterally into marine strata. Tectonic pulses occur over too long a time frame to have produced these higher-frequency cycles.

Marine strata of the lower Fountain Formation have yielded Morrowan-Atokan conodonts (*Idiognathoides sinuatus*). Few estimates of the magnitude of sea-level change exist for this time period, but incised valley depths suggest 20-45 m of eustatic sea-level change and modeling of ice-volume and facies models suggest 40-60 m of sea-level change. Our estimates are absolute minimums and the method does reflect some sensitivity to variations in slope, such that an order-of-magnitude change in slope results in ~100 m of sea-level change. Nevertheless, the range given by our method approaches other estimates and provides a new method for estimating magnitudes of sea-level change.

Glacio-eustasy is the result of ice growth and ice melt due to cyclical climate change. The data presented here indicate low levels of interglacial ice melt when compared to other times in the late Paleozoic. However, high- and low-latitude records indicate that cold conditions may have prevailed during the Morrowan-Atokan possibly

suggesting that the estimates may reflect cooler interglacials with high-volume ice that experienced reduced melt.

1. INTRODUCTION TO THE DISSERTATION

Recently, Soreghan et al. (2007, 2008) suggested that Unaweep Canyon of western Colorado was initially carved by Late Paleozoic equatorial glaciers that reached modest elevations (<1000 m). Furthermore, Soreghan et al. (in press) suggest that the Permian Cutler Formation cropping out at the mouth of Unaweep Canyon represents proglacial and ice-contact deposition. These new hypotheses are important because they challenge previously proposed models and they provide new ideas for Late Paleozoic climate states, chiefly low-latitude, low-elevation glaciation. However, if these hypotheses are valid, then the Cutler-Unaweep glacial system should not have been a singular event and other glacial systems should have been present within the ancestral Rocky Mountains. This study tests the hypotheses that glacial and proglacial conditions influenced sedimentation in the Late Paleozoic Fountain Formation where it crops out along the east flank of the Front Range of Colorado. In addition, data providing constraints on basin evolution in the Manitou Springs, Colorado, region and estimates of global sea level change are presented. The work is organized such that each chapter represents a stand-alone entity and brief synopses of each are presented below.

Chapter 2

Sedimentological, stratigraphic and structural data indicate that the Fountain Formation at Manitou Springs, Colorado, consists of three tectonostratigraphic units—lower, middle and upper. Each unit is separated by a tectonic unconformity of varying duration and significance. This chapter presents: 1) a more detailed account of the variety of depositional styles recorded in the Fountain Formation; 2) constraints on the timing

and kinematics of the basin bounding fault, the ancestral Ute Pass fault; 3) a significant departure from other studies for the paleogeography of the region; and 4) a tectonostratigraphic framework that allows relative dating of events and better correlation to other regional climatic studies. Although this chapter does not present specific data on the low-latitude glacial hypothesis, the tectonostratigraphic framework is used extensively in subsequent chapters.

Chapter 3

Sand- and granule-filled polygonal fractures occur on two separate bedding surfaces within the Fountain Formation. The polygonal fractures are inferred to be the result of thermal contraction in frozen ground and thus hypothesized to record proglacial conditions. Because the polygons occur in granular sandstone with extremely low clay content and no evaporites, alternative explanations for the formation of the polygons fail. These polygonal surfaces occurred at <1800 m, but likely much closer to sea level as they occur intercalated with marine strata. This chapter is published in Sweet and Soreghan (2008).

Chapter 4

Scanning Electron Microscopy of quartz grains reveals a suite of microtextures indicative of grain-to-grain contact in a glacial environment. A ternary diagram was developed to present the microtextural data in terms of fracturing process. The diagram is a significant departure from classical methods of microtextural data presentation (although the classic method is used too) and allows for a better quantitative inter-sample comparison. The data show three stratigraphically distinct pulses of glacial-induced microtextures which are inferred to represent upland glaciation. Furthermore, placing the

pulses in the tectonostratigraphic framework developed in chapter 2 allows for crude correlation to Gondwanan glacial episodes. SEM microtextural studies applied to ancient (pre-Quaternary) strata are relatively rare, presumably owing to the diagenetic influence; however this technique has utility and should be considered when assessing the influence of glaciation in ancient strata.

Chapter 5

A novel approach to estimating the magnitude of sea level change is presented. The method utilizes simple trigonometric calculations taken from: 1) the horizontal map distance of the well-developed transgressive lag deposits recorded in the Fountain Formation, and 2) the slope of deposition estimated by paleohydraulic analysis. To my knowledge, this is the first application of this method. Magnitude of sea level change of 10-18 m is calculated depending on which transgressive surface is used. These results are minimums, but comparable with other estimates for this time period (Atokan) suggesting that either minimal global ice or extremely cool interglacials existed.

References

Soreghan, G.S., Sweet, D.E., Marra, K.R., Eble, C.F., Soreghan, M.J., Elmore, R.D., Kaplan, S.A., and Blum, M.D., 2007, An exhumed Late Paleozoic canyon in the Rocky Mountains. *Journal of Geology*, v. 115, p. 473-481.

Soreghan, G.S., Soreghan, M.J., Poulsen, C.J., Young, R.A, Sweet, D.E. and Davogustto, O.C., 2008, Anomalous cold in Pangaean tropics: Geology, v. 36, no. 8, p. 659-662.

Soreghan, G.S., Soreghan, M.J., Sweet, D.E., and Moore, K.D., 2009, Alluvial fan or proglacial outwash? An alternative interpretation for the proximal Cutler Formation (upper Paleozoic, Paradox Basin): *Journal of Sedimentary Research* [in press].

Sweet, D.E. and Soreghan, G.S., 2008, Polygonal cracking in coarse clastics records cold temperatures in the equatorial Fountain Formation (Pennsylvanian-Permian, Colorado): Palaeogeography, Palaeoclimatology, Palaeoecology, v. 268, no. 3-4, p. 193-204.

2. LATE PALEOZOIC TECTONICS AND PALEOGEOGRAPHY OF THE ANCESTRAL FRONT RANGE: STRUCTURAL, STRATIGRAPHIC AND SEDIMENTOLOGIC EVIDENCE FROM THE FOUNTAIN FORMATION (MANITOU SPRINGS, COLORADO)

Abstract

Sedimentologic, stratigraphic and structural data indicate that the Fountain Formation at Manitou Springs consists of three tectonostratigraphic units, herein termed the lower, middle and upper Fountain units. The lower and middle Fountain units were deposited in a fan-delta setting adjacent to the active ancestral Ute Pass fault. The lower is thin and predominantly characterized by depositional stability as rcorded by abundant well-developed, deeply-rooted paleosols. The middle Fountain unit reflects fan progradation and highland rejuvenation as a result of increased activity of the ancestral Ute Pass fault. This activity was likely the result of a basinward splay of the ancestral Ute Pass fault with reverse dip-slip motion as indicated by (1) exhumation of the lower Paleozoic Sawatch Formation and (2) fault-parallel folding. The upper Fountain unit reflects deposition in a NW-SE-trending, braided-river system and appears to post-date movement on the ancestral Ute Pass fault. Lithostratigraphic correlation allows for a Latest Pennsylvanian-early Permian age for the upper Fountain unit, thus constraining cessation of the ancestral Ute Pass fault to middle- to late Pennsylvanian time.

The Fountain Formation was deposited within a NW-SE oriented structural trough (i.e. Woodland Park trough) that separated the ancestral Front Range into a northern block (i.e. ancestral Front Range block) and a southern block (i.e. Ute Pass uplift). The

Woodland Park trough was bounded on its southern margin by the ancestral Ute Pass fault which was active throughout deposition of the lower two Fountain tectonostratigraphic units, during which time sediments were shed northward across the ancestral Ute Pass fault into a marine environment. By the time of deposition of the upper Fountain unit, movement on the ancestral Ute Pass fault had ceased or dramatically decreased. During this time, the Fountain Formation records predominantly axially oriented braided-stream deposition.

Comparison of the timing and kinematic history of the ancestral Ute Pass fault with other documented reverse and strike-slip faults of the ancestral Rocky Mountains suggests that: 1) cessation of faulting within the ancestral Rocky Mountains displays a slight east-to-west younging, but the crude age resolution of adjacent basin fill also allows for the possibility of relatively synchronous cessation of faulting, and 2) kinematics of all faults examined are consistent with a NE-SW oriented maximum horizontal compressional stress field. These inferences contrast with the proposed Laurentian-Gondwanan diachronous closure models for the ancestral Rocky Mountains, which require rotation of the maximum horizontal stress orientation through time and pronounced east-to-west younging of faulting. Rotation of the horizontal stress field may be recorded in multi-stage, kinematic histories of faults but multiple faults require study to assess this model. Age constraints on post-tectonic units of the ancestral Rocky Mountains, such as the upper Fountain Formation tectonostratigraphic unit defined herein, are poor and further refinement would greatly aid understanding of the enigmatic tectonics of these ancient mountains.

Introduction

The Late Paleozoic ancestral Rocky Mountains are an intraplate series of predominantly northwest-trending Precambrian basement highs with intervening coeval sedimentary basins. Plate tectonic models for the ancestral Rocky Mountains invoke either continent-to-continent collision along the southern margin of Laurentia (Kluth and Coney, 1981; Kluth, 1986; Dickinson and Lawton, 2003) or Andean-type subduction along the southwestern margin of Laurentia (Ye et al., 1996). Within the ancestral Rocky Mountains province, large-scale, basin-bounding fault zones have been identified for decades (e.g. Mallory, 1958, Baars, 1966; McKee, 1975); however timing of fault motion is only broadly constrained by the adjacent Pennsylvanian-Permian basin fill. Furthermore, fault geometry and slip are commonly poorly constrained due predominantly to crude dating of basin fill and overprinting by younger deformational events. Thus, determining a tectonic causation has been hobbled by the lack of timing, and lack of geometric and kinematic constraints from individual faults that ultimately provide the data to assess the regional stress field.

Key data to help unravel the regional tectonic history of the ancestral Rocky Mountains are recorded in basin fill. Relatively recently, synorogenic strata, intraformational unconformities, structural relationships, and modeling have been used to decipher the timing and style of individual faults of the ancestral Rocky Mountains from younger deformational events within the Central Colorado trough (Hoy and Ridgway, 2002) and the Paradox basin (Barbeau, 2003; Thomas, 2007; Moore et al., 2008). Offsets of magnetic anomalies and paleomagnetic analyses of fault gouge have been used to infer Late Paleozoic dextral motion of the Picuris-Pecos fault (Cather et al., 2006; Wawrzyniec

et al., 2007). These studies are focused on the Uncompahgre and adjacent basins (Paradox and central Colorado Trough) and the resultant data have been insufficient to better resolve a regional ancestral Rocky Mountains tectonic model. For example, Thomas (2007) has suggested a top-to-the-left model for the western margin fault of the Uncompahgre uplift, Hoy and Ridgway (2002), however, demonstrate top-to-the-right structural relationships for the eastern margin fault of the same uplift. While both senses of motion are possible in the same structural system, it is unclear how they interact at depth.

Here we provide sedimentological, stratigraphic and structural evidence for synorogenic and post-orogenic sedimentation within the Upper Paleozoic Fountain Formation. The Fountain Formation was deposited on the east flank of the ancestral Front Range, a major uplift within the central ancestral Rocky Mountains (Mallory, 1972). Accordingly, our study provides new data on kinematics and timing on a prominent ancestral Rocky Mountains structure and suggests that a northwest-southeast-oriented depositional trough divided the ancestral Front Range into northern and southern blocks. Put in a broader context with other studies these data help place additional constraints on the tectonic development of the ancestral Rocky Mountains.

Geologic Background and Setting

The ancestral Rocky Mountains are an intraplate collage of Precambrian basement-cored uplifts with intervening, structurally deep sedimentary basins possibly extending from southern Idaho to Oklahoma (Fig. 2.1; e.g. Mallory, 1972; Kluth and Coney, 1981; Kluth, 1986). However, the plate tectonic setting of the ancestral Rocky

Figure 2.1: Late Paleozoic tectonic elements of the greater Ancestral Rocky Mountains, specifically highlighting faults with inferred Pennsylvanian movement. Modified from Lindsey et al. (1986), Hoy and Ridgway (2002) and Kluth and McCreary (2006). Locations of paleo-equators are from Scotese (1997). CCT = Central Colorado trough; WPT = Woodland Park trough; UPU = Ute Pass uplift; ut = Uncompahgre thrust (slip-sense from Frahme and Vaughn, 1983); rf = Ridgeway fault (slip-sense from Stevenson and Baars, 1986; Thomas, 2007); pp = Picuris-Pecos fault (slip-sense from Cather et al., 2006; Wawrzyniec et al., 2007); ct = Crestone thrust (slip-sense from Hoy and Ridgway, 2002); aupf = ancestral Ute Pass fault (slip-sense data herein); fc = Freezeout Creek fault (slip-sense from Maher, 1953; McKee, 1975); at = Anadarko thrust (slip-sense from Brewer et al., 1983); wv = Washita Valley fault (slip-sense from Tanner, 1967).

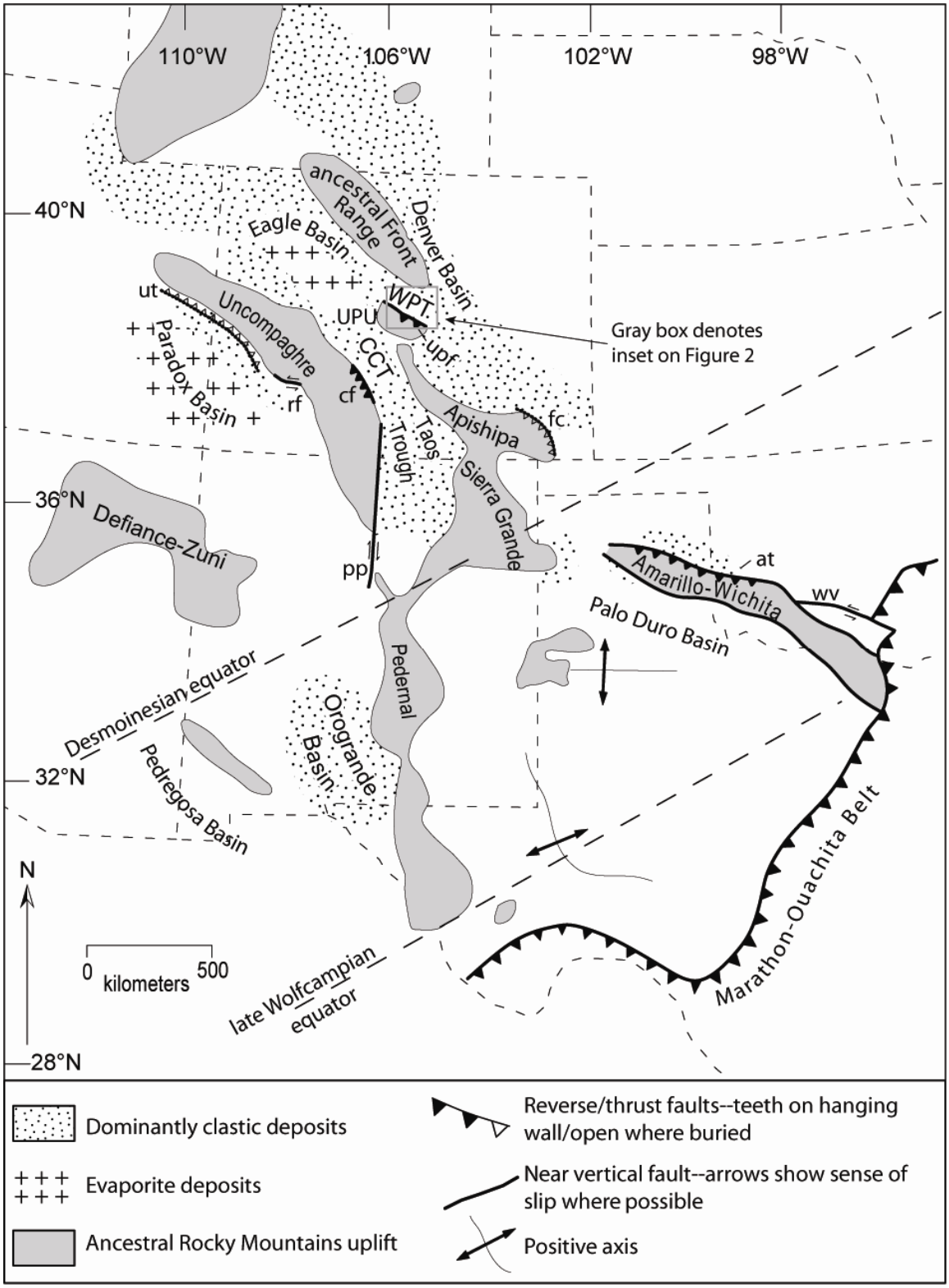
110°W
106°W
102°W
98°W
40°N
36°N
32°N
28°N
ancestral Front Range
Denver Basin
Eagle Basin
ut
Uncompaghre
Paradox Basin
rf
WPT
UPU
CCT
cf
upf
Gray box denotes inset on Figure 2
Apishipa
fc
Taos Trough
Sierra Grande
Defiance-Zuni
pp
Amarillo-Wichita
at
wv
Palo Duro Basin
Pedernal
Desmoinesian equator
Orogrande Basin
Pedregosa Basin
late Wolfcampian equator
Marathon-Ouachita Belt
N
0
kilometers
500
Dominantly clastic deposits
Evaporite deposits
Ancestral Rocky Mountains uplift
Reverse/thrust faults--teeth on hanging wall/open where buried
Near vertical fault--arrows show sense of slip where possible
Positive axis

Mountains has remained unclear owing to its intraplate location, with deformation extending up to 1500 km from any coeval plate margin; furthermore, subsequent Mesozoic and Cenozoic structural overprinting has complicated identification and interpretation of features of the ancestral Rocky Mountains. Timing of peak subsidence within basins of the ancestral Rocky Mountains broadly follows an arcuate path from early Pennsylvanian in the east-northeast to early Permian in the southwest that mimics the east-to-west suturing along the Ouachita-Marathon belt (Kluth and Coney, 1981; Kluth, 1986; Dickinson and Lawton, 2003). On the basis of this correlation, Kluth and Coney (1981) and Kluth (1986) suggested that the ancestral Rocky Mountains were related to Himalaya-style indenture of the South American plate along the Ouachita-Marathon suture. Because the polarity of subduction along the Ouachita-Marathon belt was opposite that of the Himalayan system, Dickinson and Lawton (2003) suggested that ancestral Rocky Mountains deformation was the result of far-field torsional stresses created through the oblique closure of the Ouachita-Marathon suture. Conversely, Ye et al. (1996) argued that the northwest-southeast trending structural elements of the ancestral Rocky Mountains are better explained by Andean-type subduction along the southwestern margin of Laurentia. However, the plausibility of a subduction zone along the southwestern margin remains debated (Kluth, 1998; Ye at al., 1998; Dickinson, 2000; Dickinson and Lawton, 2001).

The Fountain Formation consists of first-cycle, arkosic sediments shed eastward off the ancestral Front range and Ute Pass uplifts—centrally located uplifts of the ancestral Rocky Mountains—and now exposed along the east flank of the modern Front Range from southern Colorado to southern Wyoming (e.g. Hubert, 1960; Fig. 2.1, 2.2 &

2.3). The Fountain Formation lies unconformably upon Precambrian crystalline rocks to the north of Perry Park (Fig. 2.2), but upon lower Paleozoic strata between Cañon City and Perry Park (Trimble and Machette, 1979). Regionally, depositional models for the Fountain Formation portray fluvial braid-plain (Hubert, 1960; McPherson et al., 1987) and coalesced alluvial-fan environments (Howard, 1966; Mallory, 1972; Wilson, 1975).

In the Manitou Springs study area, the Fountain Formation crops out as a diamond-shaped body centered on the town of Manitou Springs (Fig. 2.2). Here the unit lies unconformably upon lower Paleozoic strata to the northwest, is structurally juxtaposed against younger strata to the northeast, and is conformably overlain by the Permian Lyons Formation to the southeast (Trimble and Machette, 1979). To the south, the Ute Pass fault juxtaposes Mesozoic and Paleozoic strata against Precambrian crystalline basement. The Ute Pass fault was also inferred to have a Late Paleozoic history as indicated by Fountain Formation sediment dispersal patterns and fining away from the fault (Suttner et al., 1984; Kluth, 1997). However, the exact location of this late Paleozoic fault plane is unknown; thus, it is herein termed the ancestral Ute Pass fault to distinguish it from the mappable Laramide feature.

Accumulation of sediments to the north of the ancestral Ute Pass fault has informally been assigned to two phases: 1) ~ 200 m of intertonguing continental-marine facies proximal to the AUPF ("lower" Fountain Formation) and lagoonal to shallow marine facies distally (Glen Eyrie Member); and 2) ~ 600 m of entirely continental sedimentation ("upper" Fountain Formation, Suttner et al., 1984; Maples and Suttner, 1990). The first phase has been interpreted as fan-delta deposits owing to the intercalation of marine and continental strata, close proximity to the ancestral Ute Pass fault, common

Figure 2.2: Geologic Map of the Manitou Springs study area. Location of mapped area and geographic coordinates shown by dashed black box displayed in inset. Sxn I = measured section I; sxn II = measured section II; sxn III = measured section III; sxn IV = measured section IV. Inset: Geographic locations of the places mentioned in text. Location of inset shown by gray box on Figure 2.1.

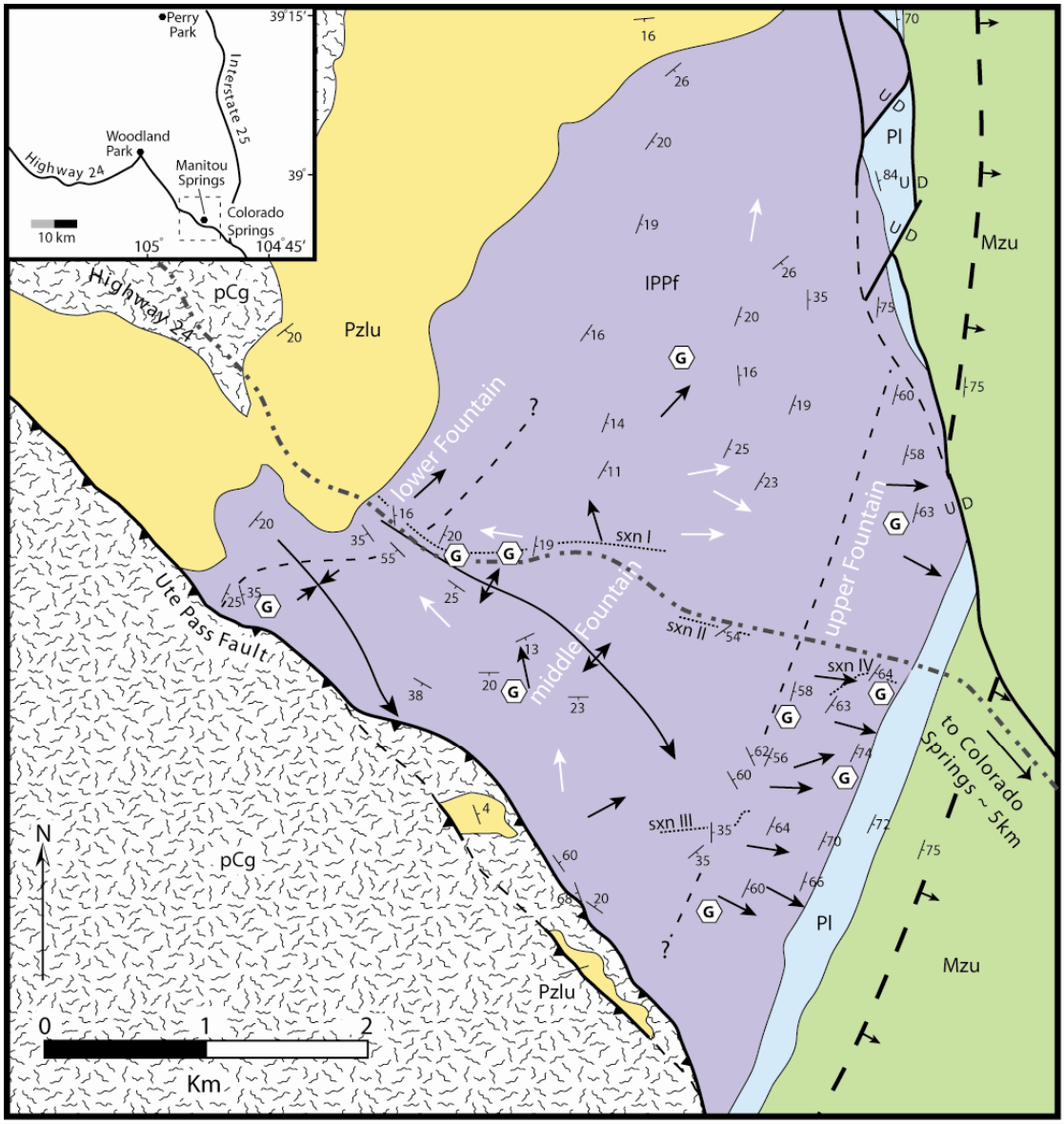

Mzu Undifferentiated Mesozoic strata

Pl Permian Lyons Formation

IPPf Pennsylvanian-Permian Fountain Formation

Pzlu Undifferentiated Lower Paleozoic

pCg Precambrian granitoid

G Grain size distribution site

23 Strike and dip of bedding

Anticline

Syncline

U D High angle fault

Thrust Fault (teeth on hanging wall)

Monocline axis

Measured stratigraphic section

Paleocurrent mean vector. White arrows are from Suttner et al. 1984

Fountain Tectonostratigraphic boundary

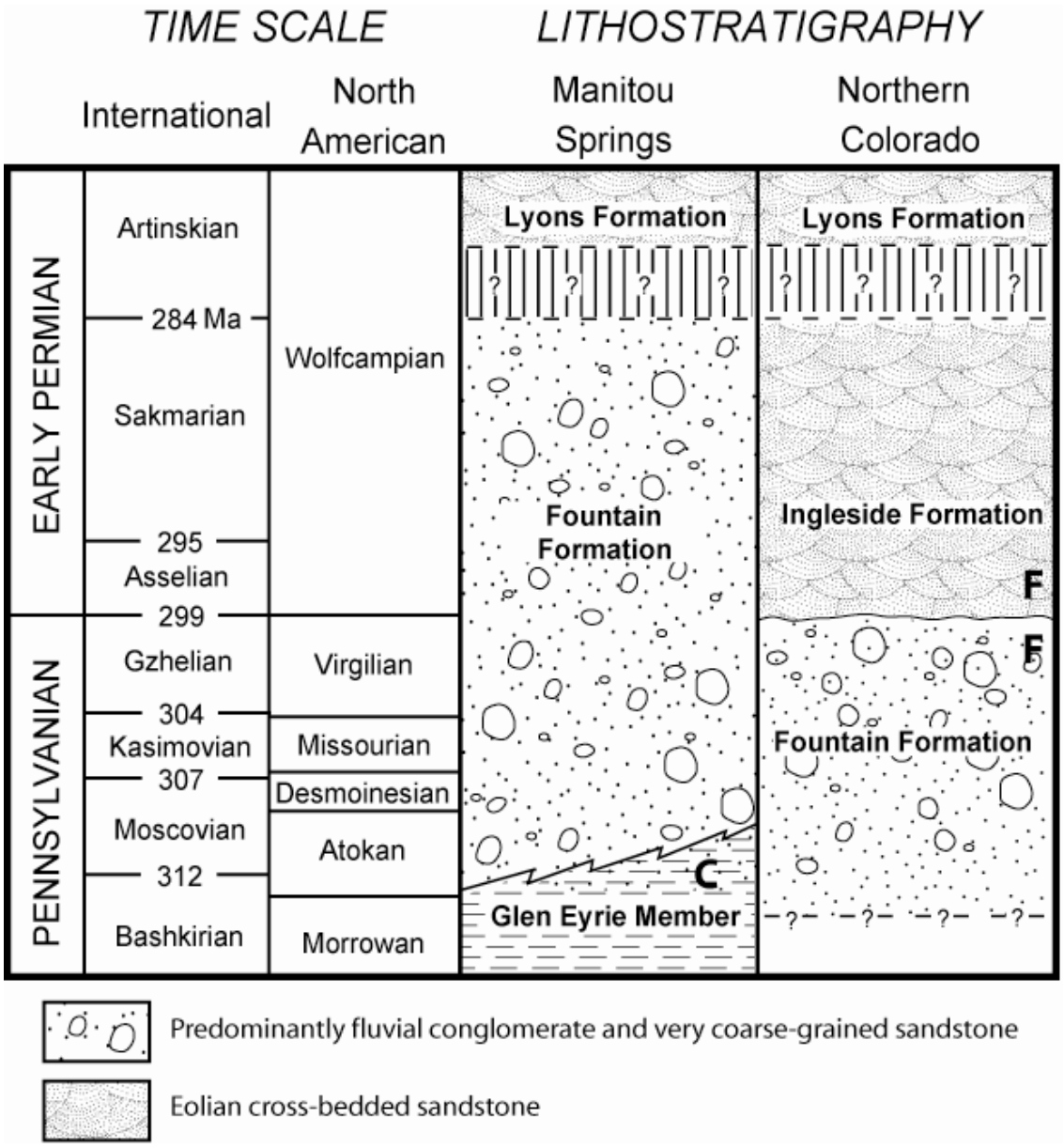

Figure 2.3: Late Pennsylvanian-Early Permian stratigraphy along the east flank of the ancestral Front Range. Vertical black lines denote hiatuses. Bold F = recovered fusulinid. Bold C = recovered conodont. Age of lithostratigraphic units at Manitou Springs is from Chronic and Williams (1978), Trimble and Machette (1979) and Suttner et al. (1984). Age of lithostratigraphic units in northern Colorado is from Maughan and Ahlbrandt (1985). Timescale is from Gradstein et al. (2004).

boulders and cobbles of mass-flow origin proximally, semi-radial paleocurrents and wedge-like geometry (Fishbaugh, 1980; O'Connell, 1981; Langford, 1982; Suttner et al., 1984; Maples and Suttner, 1990). The second phase has received much less study, but has been generally considered a braid-plain deposit (Suttner et al., 1984).

The age of the Fountain Formation is inferred from paleontological data recovered from a few marine interbeds, and from its overall stratigraphic position. At Manitou Springs, Morrowan-Atokan (Bashkirian) marine invertebrate and plant fossils were recovered from the basal Glen Eyrie Member (Fig. 2.3; Chronic and Williams, 1978; Suttner et al., 1984). Northward, near Loveland, Colorado, limestone beds containing Virgilian (Gzhelian) fusulinids interfinger with the uppermost Fountain Formation (Maughan and Albrandt, 1985) suggesting that the Fountain Formation may span the entire Pennsylvanian. Moreover, the Fountain Formation gradationally underlies the lower Permian Ingleside and Lyons Formations locally (Schatz, 1986; Sweet and Soreghan, 2008) suggesting that the Fountain Formation could range to early Permian in age.

Methods

Facies of the alluvial-fluvial continental strata were analyzed using a modified version of Miall's (1977) field classification for fluvial lithofacies (Table 1). Marine facies within the Fountain Formation have been extensively studied (Fishbaugh, 1980; O'Connell, 1981; Langford, 1982; Suttner et al., 1984; Maples and Suttner, 1990) and findings herein do not differ from those interpretations; rather, we focus here on the

continental facies. Paleosols identified within the section were named according to the classification scheme of Mack et al. (1993).

Paleocurrent data were collected by measuring the orientation of trough and channel axes as well as the attitudes of planar and trough cross-stratification. Rose diagrams, structural restorations and stereoplots were done with GEOrient© v.9.2 developed by R. Holcombe.

Grain-size anaylses were conducted on the coarsest beds (inferred from visual inspection) to quantitatively assess the spatial and temporal degree of fining away from the AUPF. Data on the > 2 cm fraction was obtained by placing a 0.5 m^2 net with ~5 cm grid size on the outcrop and recording sizes of clasts > 2 cm (A-axis) at grid intersections. For clasts larger than the grid size, all intersections were counted. Data for the > 2 cm fraction was tallied into 5 cm bins. The matrix (< 2 cm fraction) of each site was then sampled for further grain size analysis through disaggregation and standard sieve analysis.

Hematite and/or hematite-stained clays commonly form the primary cement within the Fountain Formation (e.g. Hubert, 1960). Disaggregation was achieved by dissolution of the iron using the citrate-bicarbonate-dithionite (CBD) method (Mehra and Jackson, 1960; Janitzky, 1986). Disaggregated sand was then wet sieved through -1.5, -.5, .5 1.5 and 3 φ meshes. Grain-size-distribution histograms, used to calculate the 90^{th} percentile (D90) and 50^{th} percentile (D50) of clast diameters, were compiled from the percentages of the >2 cm fraction (area data from net method) and sieve analysis data normalized to the matrix percentage recovered by the net method. The relative

proportions of clay and silt-sized grains were analyzed with a Beckman-Coulter LS-230 laser particle size analyzer.

Facies analysis

The study area represents the thickest accumulation (~913 m) of Fountain Formation exposed along the Front Range (Fig. 2.4,2. 5, 2.6, & 2.7; Appendix E). The lower ~200 m of the Fountain Formation is characterized by the intercalation of marine and alluvial facies (Fig. 2.4; Suttner et al., 1984; Maples and Suttner, 1990). Owing to our focus on the continental portion of the Fountain Formation, we describe the marine facies only briefly and employ the interpretive terms introduced by the more complete work of Suttner et al. (1984), Maples and Suttner (1990) and Kairo et al. (1993).

Marine Facies

Marine facies are distinguished from continental facies by their lateral continuity, presence of transgressive lag deposits and overall predictable progradational vertical facies associations (Suttner et al., 1984; Maples and Suttner, 1990). Complete or partial incision by overlying alluvial facies is common. A typical marine progradational cycle consists of a thin basal conglomerate, off-shore mudstone, hummocky cross-stratified sandstone, shoreface sandstone and a foreshore sandstone cap (Fig. 2.8; Suttner et al., 1984; Maples and Suttner, 1990). However, proximal to the ancestral Ute Pass fault (along our measured section) marine cycles are commonly abbreviated, consisting of shoreface and foreshore sandstone and missing offshore deposits.

Table 2.1: Fountain Formation Descriptions and Interpretations of Continental Facies

Name	Code	Description	Interpretation
Massive coarse sandstone/conglomerate	S-GRm	Poorly to moderately sorted, predominantly clast supported, very coarse-grained, poor lateral persistence, local rip-up clasts	Stream deposit, channel fill
Muddy granular sandstone	Sm-g	Very poorly sorted mixture of granule, sand and mud, distinct deep maroon color	Debris flow often pedogenically altered
Horizontal stratified sandstone	Sh	Moderately sorted, very coarse- to coarse-grained, poor lateral persistence	Upper-flow-regime stream deposit
Crudely stratified sandstone/conglomerate	S-GRch	Very coarse- to coarse-grained, low-angle scour and scour-fill, floating cobbles (up to 25 cm) and graded bedding in some deposits	Hyperconcentrated flood flow (when floating cobbles & grading bedding is present). High discharge stream deposit (when floating cobbles & graded bedding are absent)
Cobble conglomerate	Gm-ch	Massive to crudely stratifed, predominantly matrix supported, pockets of clast support, clasts up to 30 cm	Stream flood deposit
Trough cross-bedded sandstone	Sx	Medium- to very coarse-grained, locally granular rich, high-angle foresets 7-25° ranging 5-25 cm thick	Lower-flow-regime stream deposit, dune migration
Planar cross-stratified	Sp	Very coarse- to coarse-grained, high-angle cross-stratification, granules and pebbles common	Lower-flow-regime stream deposit, bar formation
Massive to laminated siltstone/sandstone	F-Sm	Massive very fine sandstone and siltstone, distinct orange color, local laminations and/or small scours, periodic dolomitic nodules and tubules	Eolian-transported silt and sand, locally reworked and pedogenically altered

Figure 2.4: Measured stratigraphic section I. The boundary between the lower and middle Fountain tectonostratigraphic units, as defined in text, is not well represented on the measured section, but is inferred to occur within the vertical gray rectangle displayed in upper left-hand corner of figure. Note the abrupt occurrence of fine-grained igneous clasts at approximately 70 meters above base. Location shown on Figure 2.2. See Figure 2.6 for key to symbols.

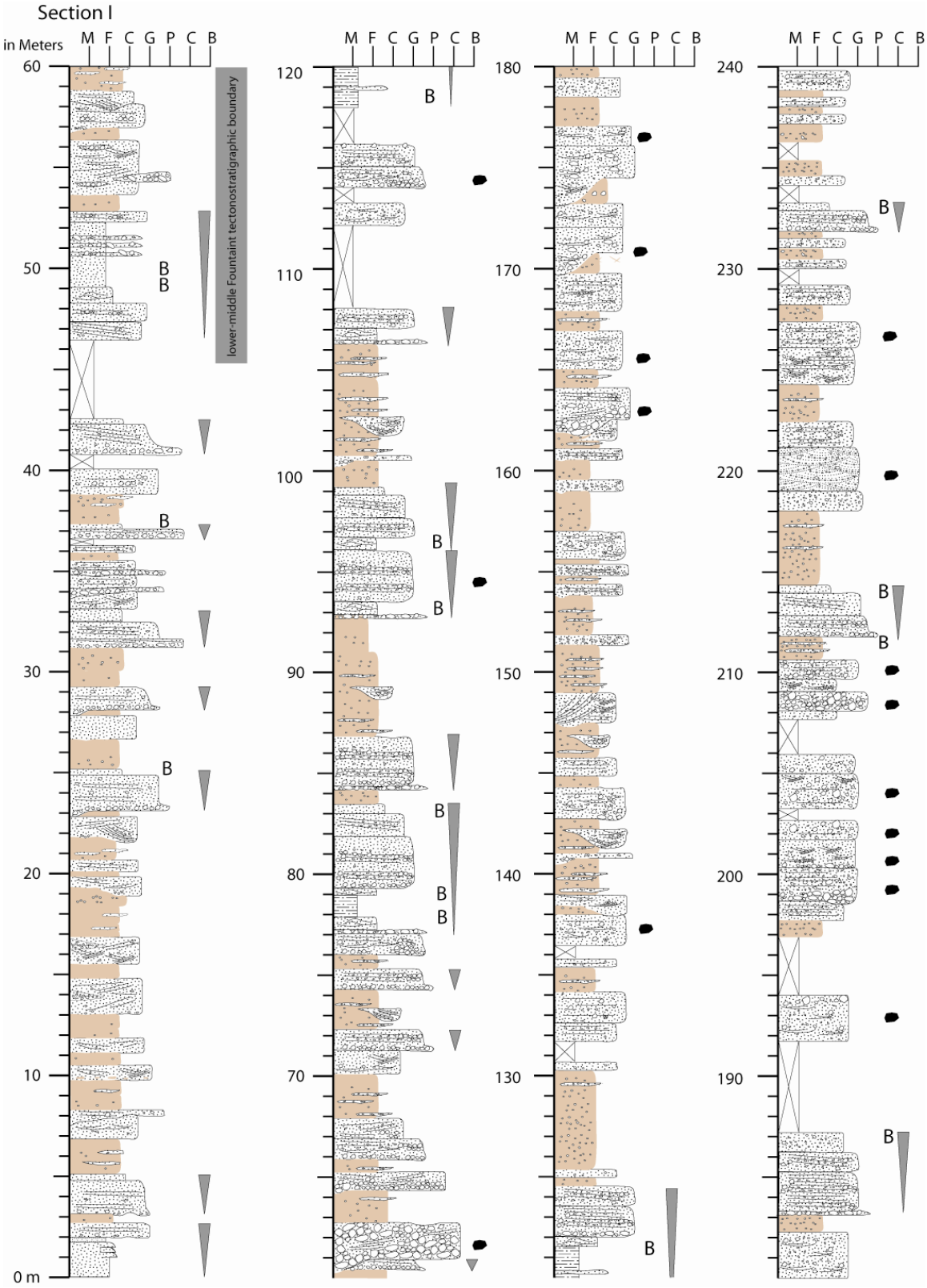
Section I
in Meters
M F C G P C B
lower-middle Fountaint tectonostratigraphic boundary
0 m
10
20
30
40
50
60
70
80
90
100
110
120
130
140
150
160
170
180
190
200
210
220
230
240
B

Figure 2.5: Measured stratigraphic section II. Gray numbers indicate estimated cumulative meters above base. Location shown on Figure 2.2 and Appendix A. See Figure 2.6 for key.

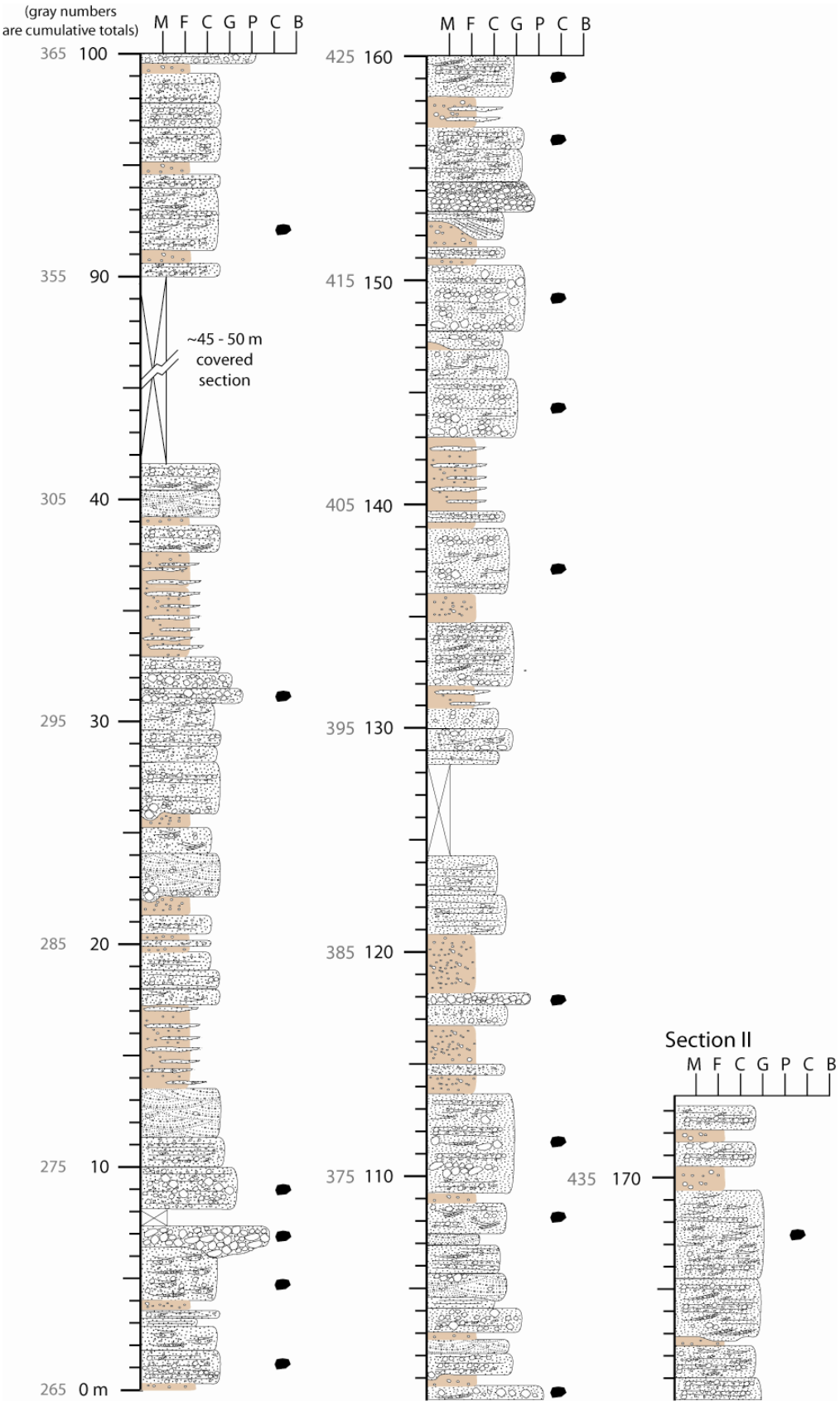
(gray numbers are cumulative totals)
M F C G P C B
365 100
355 90
~45 - 50 m covered section
305 40
295 30
285 20
275 10
265 0 m
425 160
415 150
405 140
395 130
385 120
375 110
Section II
435 170

Figure 2.6. Measured stratigraphic section III. Note the unconformity (upper left-hand corner) separating the middle and upper Fountain tectonostratigraphic units. The unconformity is represented by the abrupt occurrence of boulders and cobbles of Fountain Formation origin. Gray numbers indicate estimated cumulative meters above base. Location shown on Figure 2.2 and Appendix A.

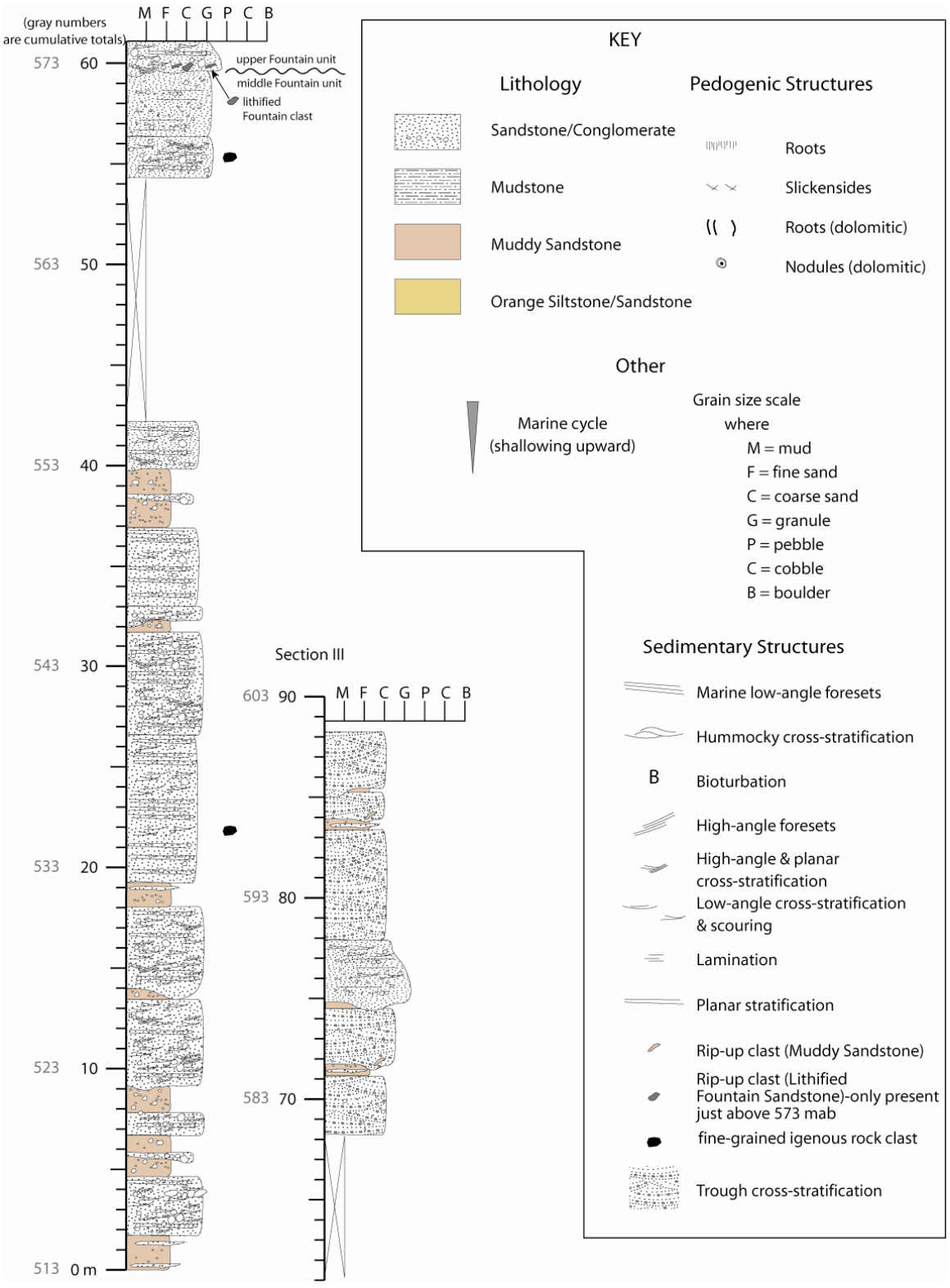
(gray numbers are cumulative totals)
M F C G P C B
573 60
563 50
553 40
543 30
533 20
523 10
513 0 m
upper Fountain unit
middle Fountain unit
lithified Fountain clast
Section III
603 90
593 80
583 70
KEY
Lithology
Sandstone/Conglomerate
Mudstone
Muddy Sandstone
Orange Siltstone/Sandstone
Pedogenic Structures
Roots
Slickensides
Roots (dolomitic)
Nodules (dolomitic)
Other
Marine cycle (shallowing upward)
Grain size scale where
M = mud
F = fine sand
C = coarse sand
G = granule
P = pebble
C = cobble
B = boulder
Sedimentary Structures
Marine low-angle foresets
Hummocky cross-stratification
B
Bioturbation
High-angle foresets
High-angle & planar cross-stratification
Low-angle cross-stratification & scouring
Lamination
Planar stratification
Rip-up clast (Muddy Sandstone)
Rip-up clast (Lithified Fountain Sandstone)-only present just above 573 mab
fine-grained igenous rock clast
Trough cross-stratification

Figure 2.7: Measured stratigraphic section IV. Note the common occurrence of the orange siltstone facies within this column. Gray numbers indicate estimated cumulative meters above base. Location shown on Figure 2.2 and Appendix A. See Figure 2.6 for key to symbols.

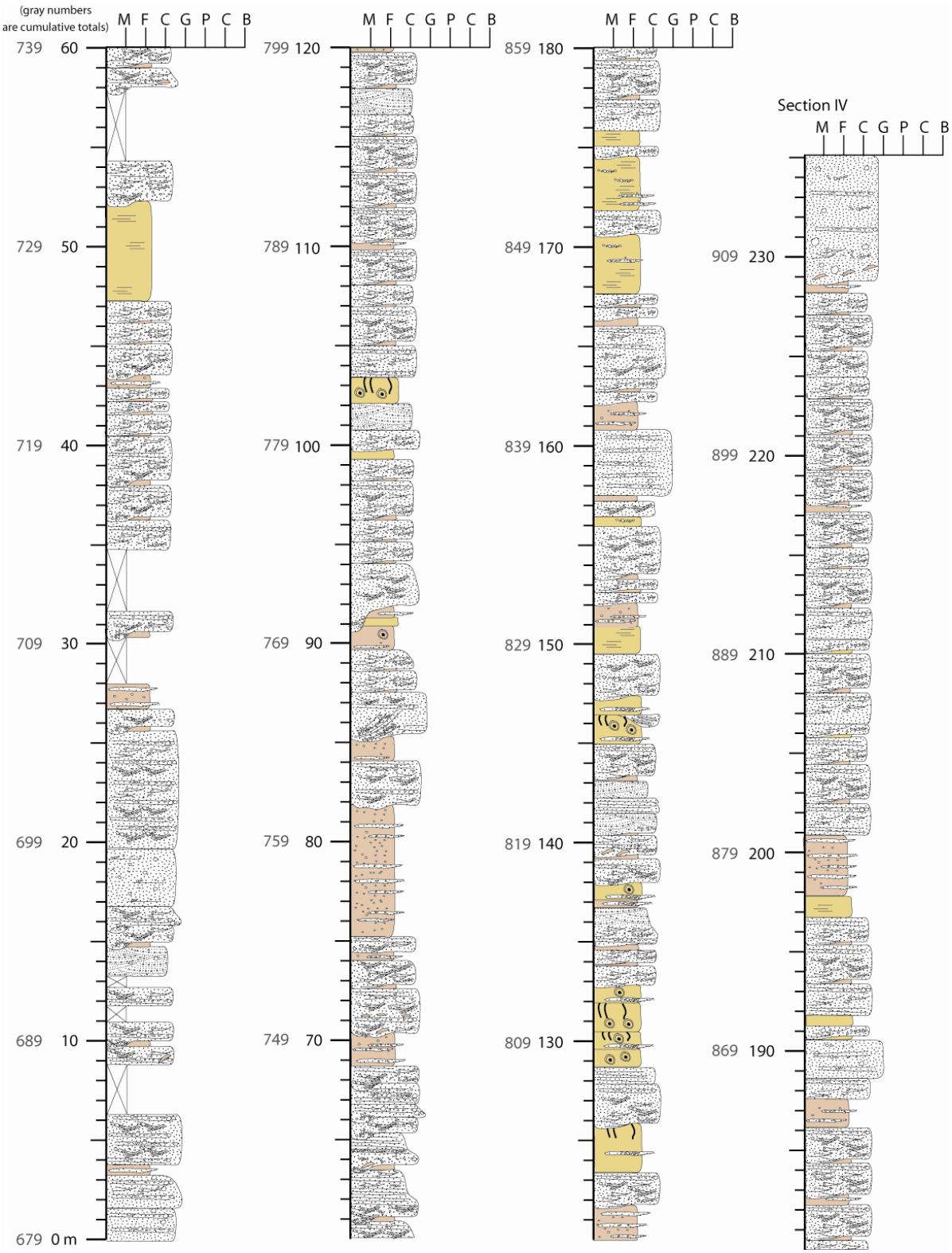
(gray numbers are cumulative totals)
M F C G P C B
739 60
729 50
719 40
709 30
699 20
689 10
679 0 m
799 120
789 110
779 100
769 90
759 80
749 70
859 180
849 170
839 160
829 150
819 140
809 130
Section IV
909 230
899 220
889 210
879 200
869 190

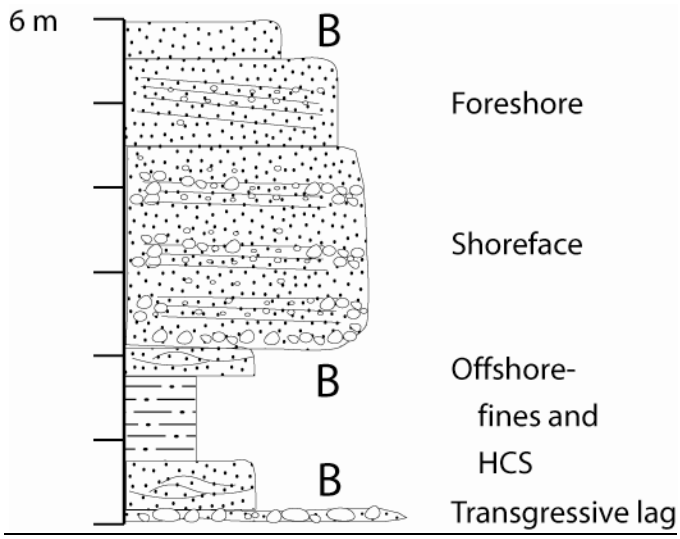

Figure 2.8: Typical marine progradational cycle originally defined by Suttner et al. (1984). See Figure 2.6 for key to symbols. HCS = hummocky cross-stratification

Continental Facies

Table 2.1 summarizes individual facies that are described in detail below. Vertical facies relationships are shown in Figures 2.4, 2.5, 2.6 and 2.7.

Crudely stratified sandstone/conglomerate (S-GRch)

This facies consists of pale pink to variegated maroon-pink, very coarse- to coarse-grained sandstone to granule conglomerate. Crude horizontal stratification is denoted by internal low-angle cross stratification, scour-and-fill structures and horizontal stratification. Bedding ranges from 0.5 -1.5 m with typically sharp, or rarely scoured bases. Beds either pinch out or are truncated laterally within <75 m. In a few deposits,

normal or inverse grading (Fig. 2.9a, b & c) and/or floating and outsized cobbles (up to 30 cm) occur, particularly below 573 meters above base.

Interpretation—The characteristic scour-and-fill structures, low-angle cross-strata and poor sorting are indicative of high-discharge, high-sediment-concentration stream conditions (Smith and Lowe, 1991). In many deposits of this facies, local high-angle cross-stratification also occurs, suggesting reworking by waning flow and/or continuous lower-discharge conditions. Deposits that contain floating or outsized cobbles or boulders and/or graded bedding suggest non-Newtonian conditions, indicating possible hyperconcentrated flood flows (Smith, 1986; Smith and Lowe, 1991).

Horizontal-stratified sandstone/conglomerate (S-GRh)

This facies consists of pale pink, moderately sorted, very coarse- to coarse-grained planar-stratified sandstone and granular conglomerate with beds 0.1-1.5 m thick (Fig. 2.9d & e). Outsized cobbles occur locally. Internal laminae are defined by heavy minerals. The basal contact is gradational or sharp where juxtaposed atop the muddy granule sandstone facies. Laterally, beds range from 10-75 m long, and either pinch out or are truncated. This facies is uncommon, but occurs throughout the section.

Interpretation—This facies represents traction flow in upper-flow-regime conditions. Where this facies occurs in association with planar cross-stratified sandstone, it most likely represents bar deposition as shown in Miall (1978). This relationship is most prevalent above 573 meters above base. Below this horizon, isolated occurrences of this facies tend to be more common. Here, this facies consists of thinner deposits (10-30

Figure 2.9: Photographs of various facies and paleosols within the Fountain Formation. A) Normal grading within crudely stratified granule conglomerate (e.g. hyperconcentrated flood flow). B) Reverse grading within crudely stratified sandstone (e.g. hyperconcentrated flood flow). C) Floating cobble in crudely stratified granule conglomerate (e.g. hyperconcentrated flood flow). D) Horizontal-stratified sandstone (e.g. upper flow-regime channel fill). E) Horizontal stratified granule conglomerate (e.g. sheet flood deposit). F) Cobble conglomerate bed (e.g. high-discharge flood event). Note the underlying remnants of marine shoreface facies shown by the white arrow. G) Trough cross-bedded sandstone (e.g. 3D dune migration). Ten cm divisions on base of staff for scale. H) Massive sandstone to granule conglomerate (e.g. channel fill). Note rip-up clast of massive siltstone in center of photograph. I) Muddy granule sandstone with rooting and scattered cobbles (e.g. fine-grained debris flow). J) Calcic-Protosol atop laminated siltstone. Note the root in center of photograph. Red division on staff is 50 cm. K) Heavily rooted horizon within muddy granule sandstone. L) Slickenside planes housed within a Vertisol.

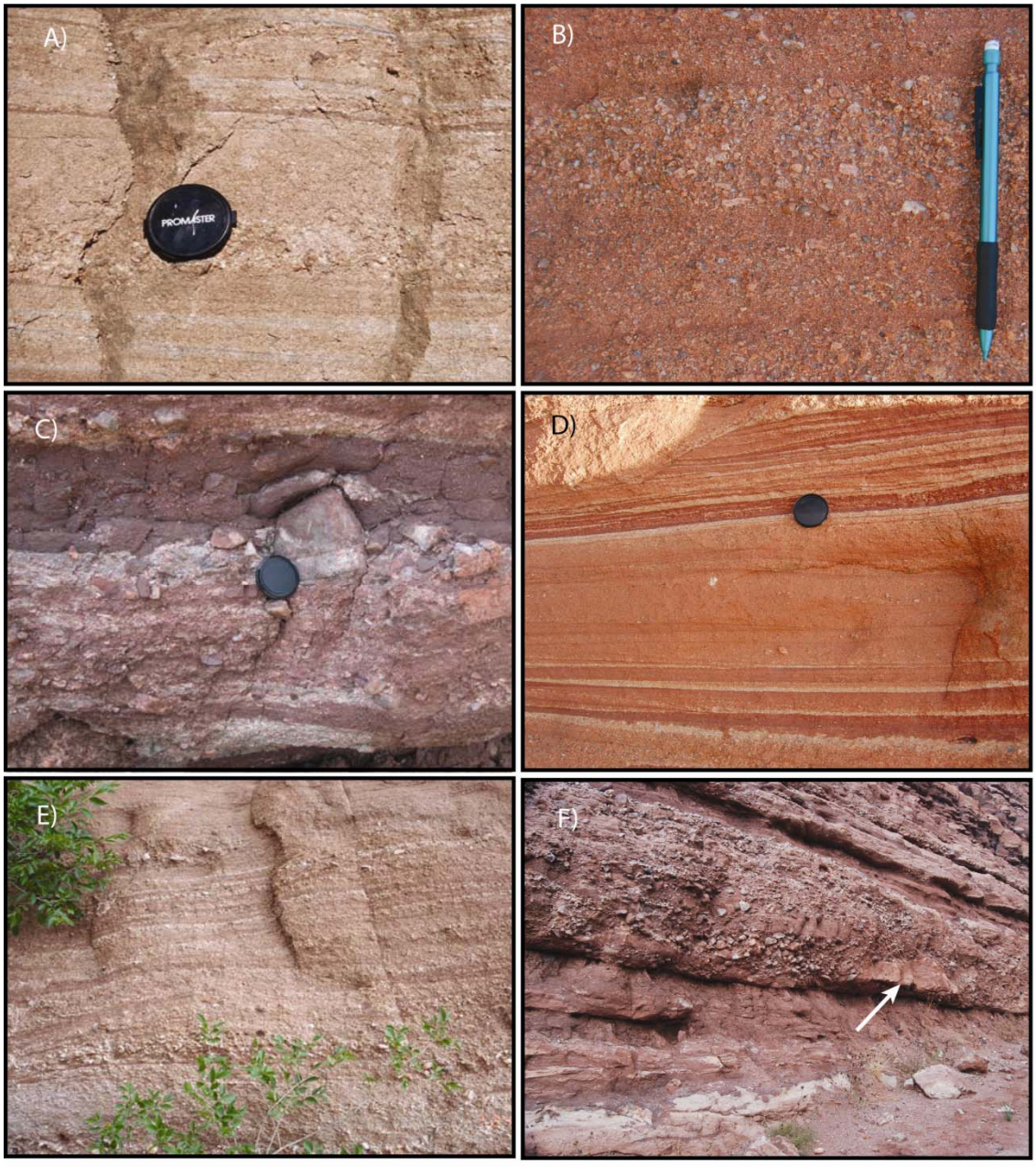
A)
PROMASTER
B)
C)
D)
E)
F)

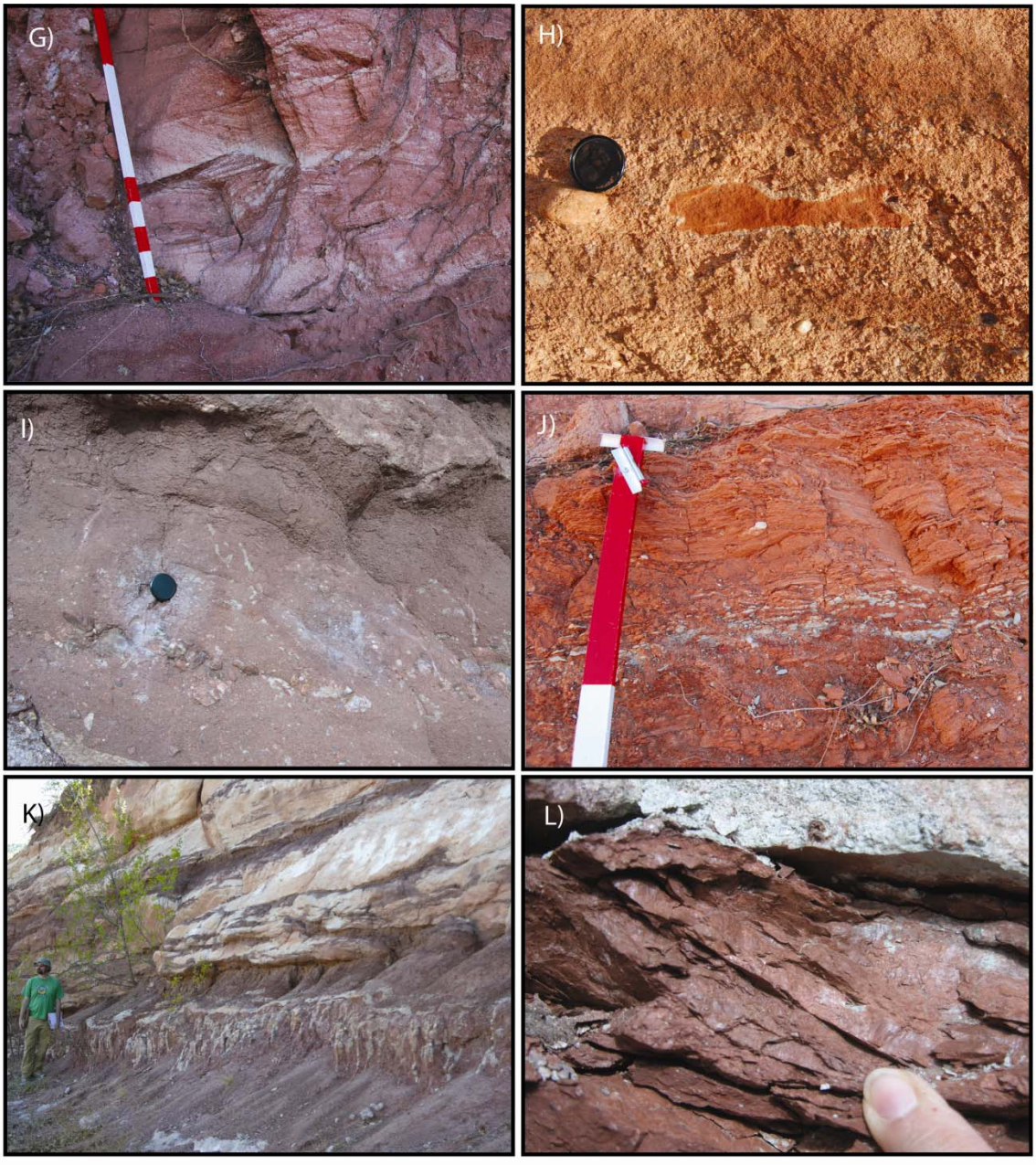
G)
H)
I)
J)
K)
L)

cm) associated with the muddy granule sandstone facies described above, and are interpreted as intermittent, shallow-stream-flow events, such as sheet-flood deposits.

Cobble conglomerate (Gm-ch)

This facies consists of massive, matrix-supported, cobble to boulder conglomerate with crude horizontal stratification and clast-supported pockets locally. Clasts are 8-20 cm (locally up to 30 cm) in diameter and imbricated only in clast-supported pockets. Beds range from 0.75-2 m and basal contacts exhibit deep scouring (Fig. 2.9f). This facies is relatively rare and only occurs between 60-425 meters above base.

Interpretation—Local pockets of crude stratification and imbricated clasts suggests stream flow and subsequent channel fill deposition. The extremely coarse grain size and deep basal scouring indicate that these deposits record high-discharge flood events.

Trough cross-bedded sandstone (Sx)

This facies consists of pale pink to variegated maroon-pink, medium- to very coarse-grained, cross-bedded sandstone with abundant granules, common heavy mineral laminations and trough cross bedding with foresets 5-25 cm thick (Fig. 2.9g). The basal contact is gradational and this facies typically overlies the massive coarse sandstone and/or crudely stratified sandstone facies, forming lens-shaped bodies up to tens of meters wide. This facies is more abundant in the upper 340 m of the section.

Interpretation—This facies records traction deposits in lower-flow-regime conditions. Trough cross-bedding is commonly interpreted as down-channel migration of 3D dunes (e.g. Miall, 1996) and these are interpreted similarly. Beds of this facies are commonly underlain by massive, planar, or crudely stratified sandstone facies.

Planar cross-stratified sandstone (Sp)

This facies consists of pale pink medium- to very coarse-grained, planar cross-bedded sandstone commonly containing abundant granules. Foresets dip at 10-20° in sets ranging from 10-25 cm thick. Basal contacts are sharp and planar. This facies occurs throughout the section, but is most abundant above 340 m.

Interpretation—This facies records traction deposits in lower-flow-regime conditions. Deposits with similar characteristics are typically interpreted to reflect migration of 2D dunes in the latter stages of channel fill, or atop bars (e.g. Miall, 1996), and likely represent a similar environment here. Beds of this facies are commonly underlain by either trough-, planar- or crudely cross-stratified sandstone.

Massive coarse-grained sandstone/conglomerate (S-GRm)

This facies consists of poorly to moderately sorted, massive very coarse-grained arkosic sandstone to granule conglomerate (Fig. 2.9h). Outsized cobbles (8- 20 cm) are present locally. Beds range from 0.5-2 m thick, exhibit sharp, locally scoured bases and local mudstone intraclasts near bases, and extend laterally for 10s of meters, terminating in a pinch out or truncation. This facies is not abundant, but occurs throughout the study section commonly atop muddy granular sandstone facies.

Interpretation—The sharp bases, local scouring, and mudstone intraclasts (e.g. rip-ups) resembling both massive siltstone and muddy granular conglomerate facies indicate a high-energy, turbulent deposit. Scouring and incorporation of underlying finer-grained deposits suggest channel-fill deposition.

Muddy granule sandstone (Sm-g)

This facies consists of massive, very poorly sorted granule-, sand- and mud-sized debris with common small (1-3 cm) pebbles (Fig. 2.9i). Grain-size analyses show that clay-size particles compose 5-20% if the total. Cobbles are rare and occur near bases of beds. This facies is a distinct deep-maroon color and crops out recessively. The basal contacts appear to fill in or drape existing surfaces and are not erosive. Beds of muddy granular sandstone are more laterally continuous in the lower 573 m. This facies is ubiquitous throughout the section, but more prevalent in the lower 573 m.

Interpretation—The lack of sorting and organization combined with presence of clay matrix suggests a mass-flow origin. The paucity of coarse pebble and larger material suggests an origin as a fine-grained debris flow (Hampton, 1975). Furthermore, the occurrence of the coarse material near the bases (i.e. crude grading) of flows indicates that these flows were non-cohesive (Hampton, 1975; Scott et al., 1992). However, the 5-20 wt% of clay-sized material suggests a high clay-mineral content typical of cohesive flows, which should have had the competence to entrain the cobbles and boulders present in this system. Hence, the behavior of these flows is not fully understood.

Massive to laminated siltstone/sandstone (F-Sm)

This facies consists of typically massive, well-sorted, very fine-grained sandstone and siltstone with a distinct orange color. Lenses of coarser sand or granules that define well-laminated intervals occur locally (Fig. 2.9j). Bedding ranges from 0.5 to 5 m and basal contacts are commonly gradational, but locally sharp. Massive coarse sandstone and/or crudely stratified sandstone facies are typically in erosional contact with this (siltstone) facies. This facies only occurs in the upper 300 m of the Fountain Formation.

Interpretation—The massive, well-sorted character with silt and subrounded, very fine sand grains suggests an eolian origin. Locally, the presence of scour, and coarse-grained fill indicates water reworking. Laminated portions are also inferred to reflect the influence of local water reworking.

Pedogenesis

Throughout the section, horizons exhibiting downwardly-penetrating, tubular features (up to 20 cm diameter), randomly oriented slickensides, clay enrichments, blocky to wedge-like peds and localized gray-green, Fe-reduction zones (i.e. gleying) occur within the muddy granule sandstone facies (Fig. 2.9i, j, k & l). The tubular features are interpreted as root traces and are most common in the lower ~ 60 m of the study section. Clayey horizons, gleyed zones and slickensides associated with wedge-shaped peds are all commonly associated with rooted horizons and are interpreted as Argillisols, Gleysols and Vertisols, respectively. From ~ 200~573 meters above base, Argillisols and Vertisols predominate.

Within the upper 340 m of section, calcified root traces (up to 2 cm diameter) and nodule and laminar (1-6 cm thick) carbonate occur within the massive to laminated siltstone facies (Fig. 2.9j). The carbonate laminae and nodules form horizons 5-15 cm below bed tops and are interpreted as Calcisols or calcic-Protosols.

Paleocurrent and Grain-Size Distribution Data

Paleocurrent data collected from throughout the study section indicate two distinct modal directions, confined to discrete stratigraphic intervals. In the lower ~ 573 m,

paleocurrents exhibit a semi-radial pattern with a mean flow to the northeast (x = 024°, 95% confidence = ±17°; Fig. 2.2 & 2.10a), which agrees with data presented by Suttner et al. (1984) from this part of the Fountain Formation. In the upper ~ 340 m, however, paleocurrents show flow to the southeast (x = 101°, 95% confidence = ±7°; Fig. 2.2 & 2.10b), nearly orthogonal to the data from the lower section and similar to the findings of Howard (1966).

Grain-size data also show a systematic shift upward in the section, as exhibited by trends in D90 relative to distance from the Ute Pass fault (Fig. 2.11). The lower ~ 573 m of section displays a distal fining from the fault (also documented by Suttner et al. (1984)), whereas the upper ~ 340 m shows no relationship or perhaps a slight increase in D90.

Depositional Systems

Within the lower ~ 573 m of section, continental strata of the Fountain Formation are best characterized by stacked muddy granular sandstone beds (i.e. fine-grained debris flows) episodically punctuated by 1-2 m beds of cobble conglomerate, planar-stratified sandstone, crudely-stratified sandstone and conglomerate, or massive sandstone facies (i.e. fluvial deposits; Fig. 12). Tops of individual fine-grained debris flows are commonly heavily rooted Vertisols or Gleysols. The bases of fluvial facies are predominantly sharp and planar, but are commonly deeply erosional (up to 5 m) into underlying strata. Fluvial facies are also characterized by poor lateral continuity, large width-to-thickness ratios of beds, chaotic ordering of facies and predominantly upper flow-regime sedimentary structures. Taken together this association records surface stability (i.e. pedogenesis)

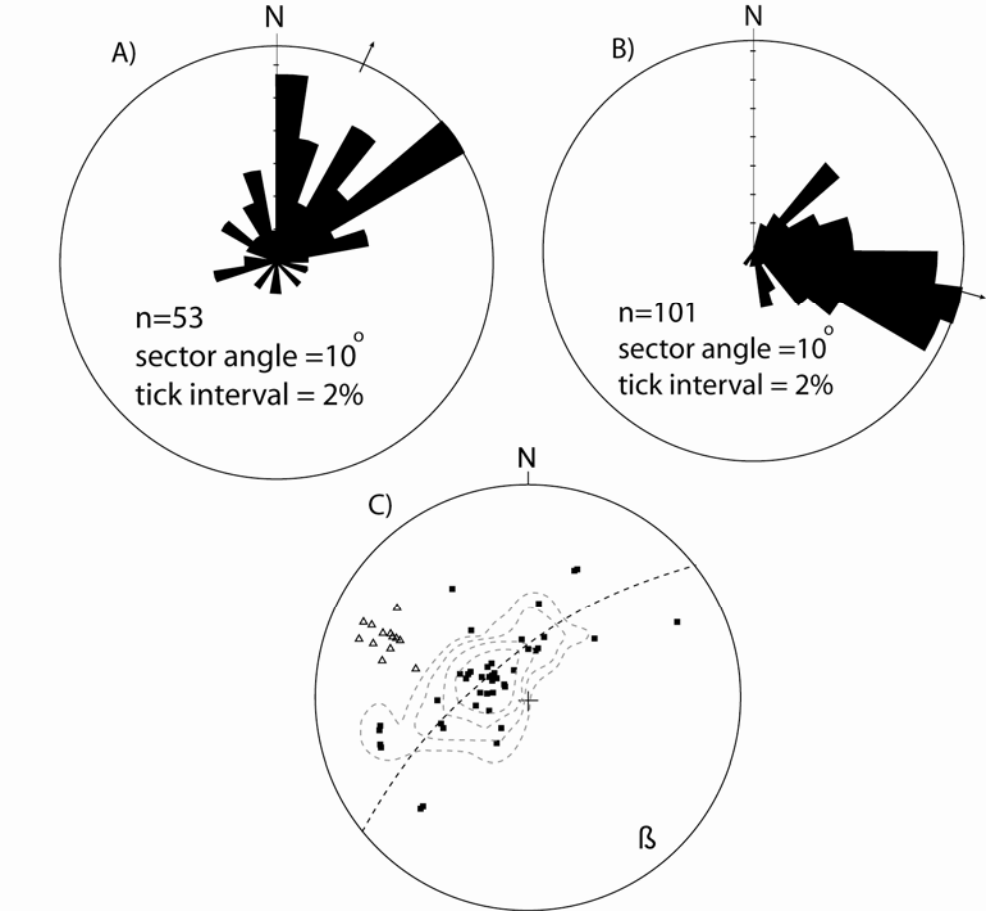

Figure 2.10: A) Rose diagram of paleocurrents collected from the lower and middle Fountain Formation. Arrow on outer circle indicates mean direction for data set. See Figure 2.2 for areal coverage. B) Rose diagram of paleocurrents collected from the upper Fountain Formation. Arrow on outer circle indicates mean direction for data set. C) Equal-area stereoplot of bedding attitudes from the Fountain Formation. Black squares (n = 38) are data collected from the lower and middle Fountain Formation within 1 km of fold axis depicted on Figure 2.2. Open triangles (n = 17) are data collected from the upper Fountain Formation. Contour intervals (from outside to inside) are 3%, 6%, 12% and 24%. Beta orientation is 141/17.

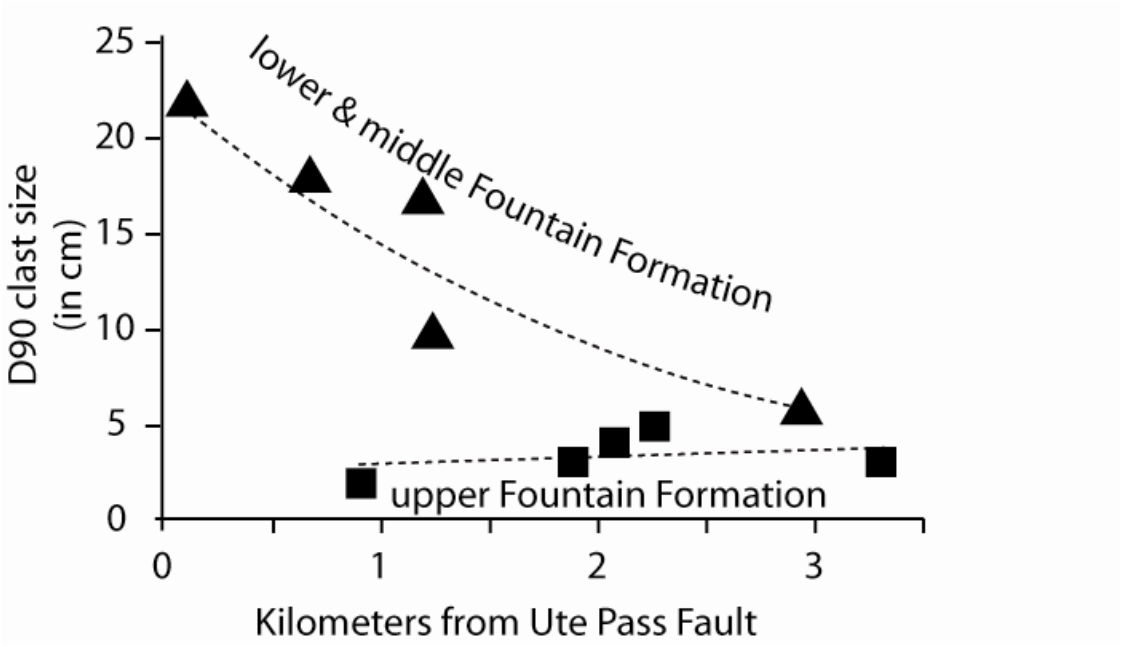

Figure 2.11: Plot of D90 grain size versus distance from Ute Pass fault. Black triangles are data collected from the lower and middle Fountain Formation. Black squares are data collected from the upper Fountain Formation.

episodically punctuated by depositional events of either stream-flow or mass-flow deposition. Crudely stratified sandstone and conglomerate facies interpreted as hyperconcentrated flood flows occur predominantly within this part of the section, further highlighting the intermittent nature of deposition. From 0-573 m, records of stream deposits and intercalated marine deposits suggest a fan-delta environment of deposition, an interpretation consistent with the findings of Suttner et al. (1984) and Maples and Suttner (1990).

In contrast, facies associations within the upper 340 m are characterized by a relatively consistent, stacked succession of planar cross-stratified sandstone, trough cross-bedded sandstone, crudely stratified sandstone, horizontally stratified sandstone and massive sandstone (i.e. fluvial deposits) overlain and/or episodically punctuated by a 0.5-4 meter thick unit of muddy granular sandstone (e.g. fine-grained debris flow) or massive siltstone/sandstone (e.g. eolian deposits; Fig. 12). In this part of the section, fluvial deposits predominate and form a series of stacked multi-story channels. Multi-story bodies range from ~ 30-200+ m wide and are separated laterally and vertically from each other by muddy granular sandstone and/or massive sandstone and siltstone. Mapping demonstrates that this system is at least 4 km wide, yet lacks true fine-grained, laminated overbank deposits, suggesting that the system is best characterized as a broad braided river system (e.g. Miall, 1978; 1996).

The most abundant facies in the entire section is muddy granular sandstone, interpreted as deposits of fine-grained debris flows. Owing to the presence of large pebbles and cobbles in other facies, the paucity of material larger than pebble size within

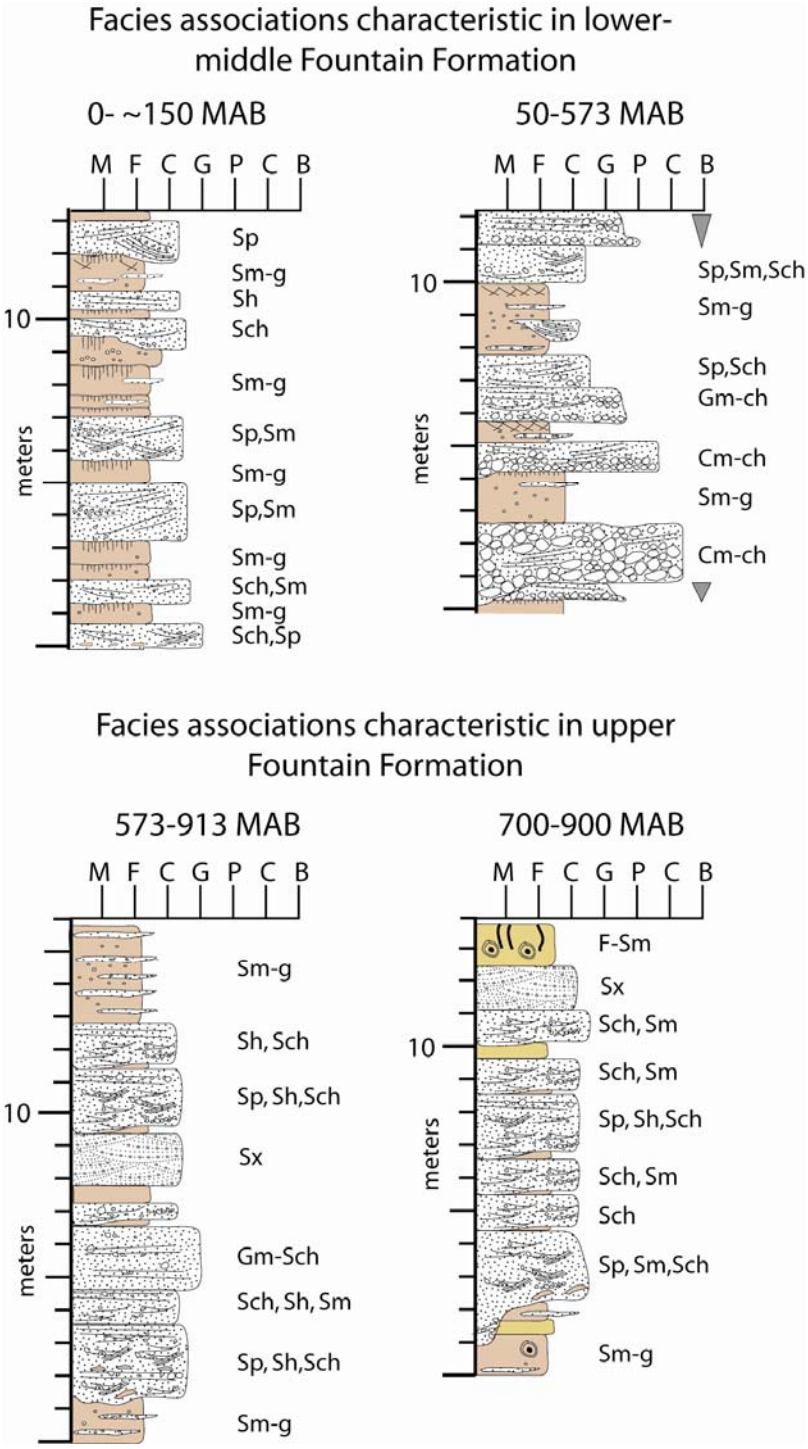

Figure 2.12: Idealized facies associations sketches within continental strata. See Figure 2.6 for sedimentary structures key and text for facies nomenclature and discussion.

these fine-grained debris flows is troubling. One explanation is that the fine-grained debris flows were derived exclusively from pre-sorted material. However, this possibility is unlikely because such presorted "source" material does not occur in the section. Another possibility is that the flow processes on the fan varied down flow (i.e. flow transformation). Scott et al. (1992) demonstrated that debris flows on Mount Rainier span a spectrum of flow processes; for example, flood events initiate as stream flow and steadily incorporate material to first form hyperconcentrated flows, then debris flows. The debris flows ultimately freeze downslope by dewatering, which can provide the fluid to initiate a fine-grained debris flow. In the Manitou Springs area, debris flows containing cobbles and boulders are rare but preserved predominantly in a more proximal location than our measured section. Thus, it is plausible that dewatering of proximal boulder debris flows could have provided the trigger to the fine-grained debris flows so ubiquitous throughout the section. However, the relatively high percentage of clay-sized material within these deposits suggests a high clay-mineral content, whereas Scott et al. (1992) observed that debris-flow deposits with >5% clay-mineral content (e.g. cohesive debris flows) generally do not transform into other flows. Furthermore, the rare occurrence of proximal coarse-grained debris flows is inconsistent with the amount of muddy granular sandstone observed in the section.

Paleoslope Calculations

Slope of deposition strongly affects flow velocity and hence bedform development; thus angle of depositional slope could be responsible for the dearth of cross-stratification in the lower 573 m of the study section and the abundance of cross-

stratification in the upper 314 m. Paola and Mohrig (1996) have shown that slope relates to mean grain size and flow depth by:

$$S = 0.094D^{*}H^{-1} \quad (1)$$

where S = depositional slope, D = mean grain size (D50), and H = mean water depth.

Four key assumptions in using this method are quasi-steady-state flows, noncohesive channel banks, bedform-free beds and dominantly bedload transport. Thus, application is best applied to deposits that: 1) lack signs of rapid deposition, plant roots and muddy overbank deposits, and 2) contain massive to crudely bedded channel deposits. Fountain Formation strata above 573 meters above base are best suited to this method because of the presence of massive, basal channel fill, scarce roots and little mudstone. We did not apply this method to strata within the lower 100 m because of the abundance of rooted horizons. The middle 100-573 m is not well suited for such analyses either, but intervals of cobble conglomerate and crudely stratified fluvial sandstone facies meet all criteria with the exception of quasi-steady flow due to the inferred intermittent nature of flows and possible "backwater effects" from close proximity to shoreline. Hence, we calculated slopes for the middle strata for cautious comparison.

Water depth for the upper and middle sections are estimated (Table 2.2) using thicknesses of upwardly fining inferred channel-fill units. These estimates were corroborated with data from nearby trough cross-stratified and planar cross-stratified beds by estimating water depth from the relationship of ripple height to water depth shown by Allen (1968). D50 was obtained by methods previously discussed. Depositional slope estimate calculated from Eq. (1) is ~0.0008 for the upper 314 m, whereas beds from 100-573 meters above base have an estimated slope of ~0.005. Modern sand- and gravel-

bedded rivers have slopes that typically range from 0.0004 – 0.001, whereas many modern fan-deltas and alluvial fans have slopes that range from 0.002 - 0.005 (references in Blair and McPherson, 1994). We infer that the steeper slope of the lower strata analyzed inhibited development of cross-stratification.

Table 2.2: Parameters and slope estimations of the middle and upper Fountain Formation

Middle Fountain	D50 (cm)	Water Depth (cm)
	8	160
	5	203
	8	229
	20	177
		195
Average	10.25	192.8
Upper Fountain		
	1.7	109
	0.5	126
	1.6	116
	0.2	137
		131
Average	1.00	122

Structural Data

In general, bedding in the study area dips and steepens to the east, forming a large monocline dipping into the Denver basin (Fig. 2.1 & 2.2). Inasmuch as overlying Mesozoic strata also form the monocline, this structure has long been attributed to Laramide-age shortening (Trimble and Machette, 1979). Similarly, tight folds parallel to and within 0.5 km of the Ute Pass fault trace have been attributed to Laramide shortening (Suttner et al., 1984; Kluth, 1997), as well as a broad, open syncline-anticline pair

occuring about 2 km north of the Ute Pass fault (Fig. 2.2; Trimble and Machette, 1979; Suttner et al., 1984), despite the contrasting styles of deformation. This syncline-anticline pair is at a high angle to the N-S trending Laramide monocline and is also folded within that monocline, such that the plunge of the anticline steepens eastward. Bedding attitudes collected from the lower 573 m within 1 km of the anticline fold axis shown on Figure 2.2 indicate an average fold axis (β = 141/17°), however, the upper 340 m shows no indication of folding (Fig. 2.10c). Hence, these data suggest that folding in the lower 573 m occurred before deposition of the upper 340 m of the Fountain Formation.

Fountain Tectonostratigraphy

The above sedimentologic, stratigraphic and structural data (summarized in Table 2.3) are collectively interpreted to indicate the presence of two intraformational unconformities within the Fountain Formation, which divide the unit into three tectonostratigraphic intervals, hereafter termed the lower Fountain, middle Fountain and upper Fountain units.

The lower Fountain Formation (0 - ~ 60 m) is defined by abundant laterally continuous beds of muddy granular sandstone commonly containing deeply rooted paleosols (commonly Vertisols, Argillisols and Gleysols), minor marine progradational cycles, and a relatively minor component of fluvial and marine facies. The middle Fountain Formation (~60 – 573 m) is characterized by prominent marine progradational cycles, presence of cobble conglomerate stream deposits, and Vertisols and Argillisols. Moreover, the middle Fountain Formation contains minor amounts (2% of the overall >2 cm fraction; data repository) of pebble-to-boulder sized, quartz-arenite clasts that most

resemble strata of the Cambrian Sawatch Formation that crops out within the area (Fig. 2.13), as well as distinctive clasts of fine-grained igneous rocks (10% of the overall > 2 cm fraction; data repository). Despite these differences, the lower and middle Fountain units both display similar paleocurrent dispersal patterns and grain-size distributions, suggesting that they are linked to the same depositional system.

Table 2.3: Characteristics of tectonostratigraphic units in the Fountain Formation

MAB*	Unit	Depositional environment	Slope of deposition	Paleosols	Marine strata	paleocurrent orientation	D90 distribution	Pebble-cobble composition
0- ~60	Lower Fountain	fan-delta	not calculated	Vertisols, Gleysols, Argillisols, roots common	minor	northeast	fines northward	granite, gneiss
~60-573	Middle Fountain	fan-delta	$\sim 10^{-3}$	Vertisols, Argillisols, roots uncommon	prominent in lower part, absent in upper part	northeast	fines abruptly northward	granite, gneiss, quartz-arenite, fine-grained igneous
573-913	Upper Fountain	braided river	$\sim 10^{-4}$	Calcisols, calcic-Protosols	absent	southeast	invariant	granite, gneiss

* meters above base of study section

The lower-middle Fountain contact is subtle in most regions, owing to limited exposure, but is well defined within 1 km of the Ute Pass fault by an angular unconformity (Fig. 2.14). Here the middle Fountain unit exhibits a larger D90, contains clasts of the Sawatch Formation (Fig. 2.13) of up to boulder size, and truncates lower Fountain beds to the northeast, all suggesting facies progradation and highland rejuvenation. More distally (northward), the contact is either diffuse, less angular or not

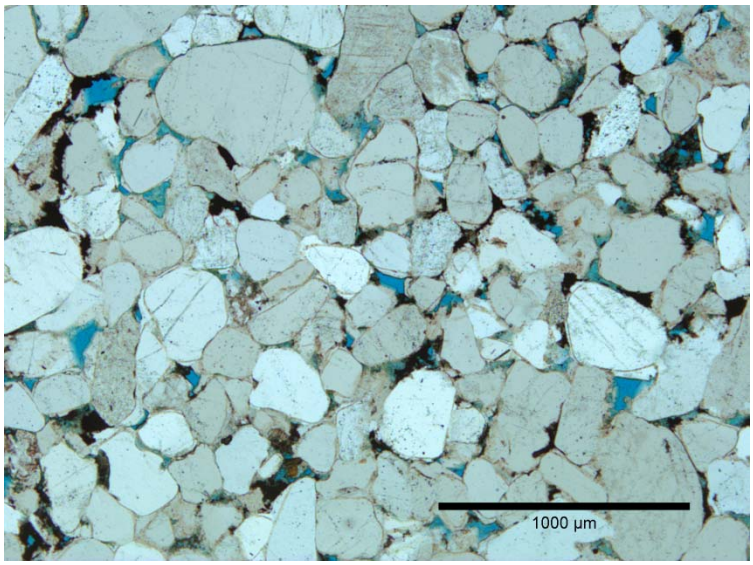

Figure 2.13: Photomicrograph of Quartz arenite clast recovered from the overlying strata shown in Figure 2.14, and inferred to be recycled from the Cambrian lower Sawatch Formation. Photomicrograph is in plain light.

well exposed, but can be estimated by the occurrence of clasts of fine-grained igneous rocks and cobble conglomerate facies (Fig. 2.4, 2.5 & 2.6).

Suttner et al. (1984) have demonstrated that the lower 200 m of the Fountain Formation interfingers to the north with the Glen Eyrie member which contains Morrowan-Atokan conodonts and plant fragments (Chronic and Williams, 1978; Jennings, 1980; Suttner et al., 1984), thus indicating an early Pennsylvanian age for the lower Fountain tectonostratigrahic unit. Because the middle and lower Fountain tectonostratigraphic units are linked to the same depositional system, the angular unconformity likely represents only a modest amount of time, and thus the middle

Fountain unit should be slightly younger (early- to mid-Pennsylvanian) than the lower unit (Fig. 2.15).

The upper Fountain tectonostratigraphic unit (~ 573-913 meters above base) is distinguished from the lower and middle units by abundant and relatively ordered fluvial facies, the presence of Calcisols and of massive (eolian) siltstone, a nearly 90° shift in paleocurrent orientations, and an invariant proximal-to-distal D90 distribution. Taken together the data reflect a different style of deposition from the lower tectonostratigraphic units. The contact between the upper and middle Fountain units is denoted by the first occurrence (at 573 meters above base) of cobbles and boulders recycled from the older Fountain Formation and by a slight angularity of bedding (Figs. 2.2, 2.10c).

Constraining the age of the upper Fountain tectonostratigraphic unit is difficult. Within the study area, predominantly fluvial deposition of the upper Fountain Formation intercalates into the overlying eolian unit, thus dating the overlying unit provides a minimum constraint on the upper Fountain unit. In northern Colorado, the upper Fountain Formation consists of interfingered eolian and fluvial sandstone overlain by predominantly eolian units of the Ingleside and Lyons Formations (Schatz, 1986; Sweet and Soreghan, 2008). However, whereas the Ingleside Formation is earliest Permian in age the Lyons Formation is younger and thought to be of early to middle Permian age. Within the study area, the eolian unit overlying the Fountain Formation is mapped as the Lyons Formation (Trimble and Machette, 1979). However, this assignment is based primarily on long-distance lithostratigraphic correlation such that the eolian unit in the study area could correlate in time to either the Ingleside or Lyons Formations. In northern Colorado, the Fountain-Ingleside contact is tightly constrained by Virgilian fusulinids

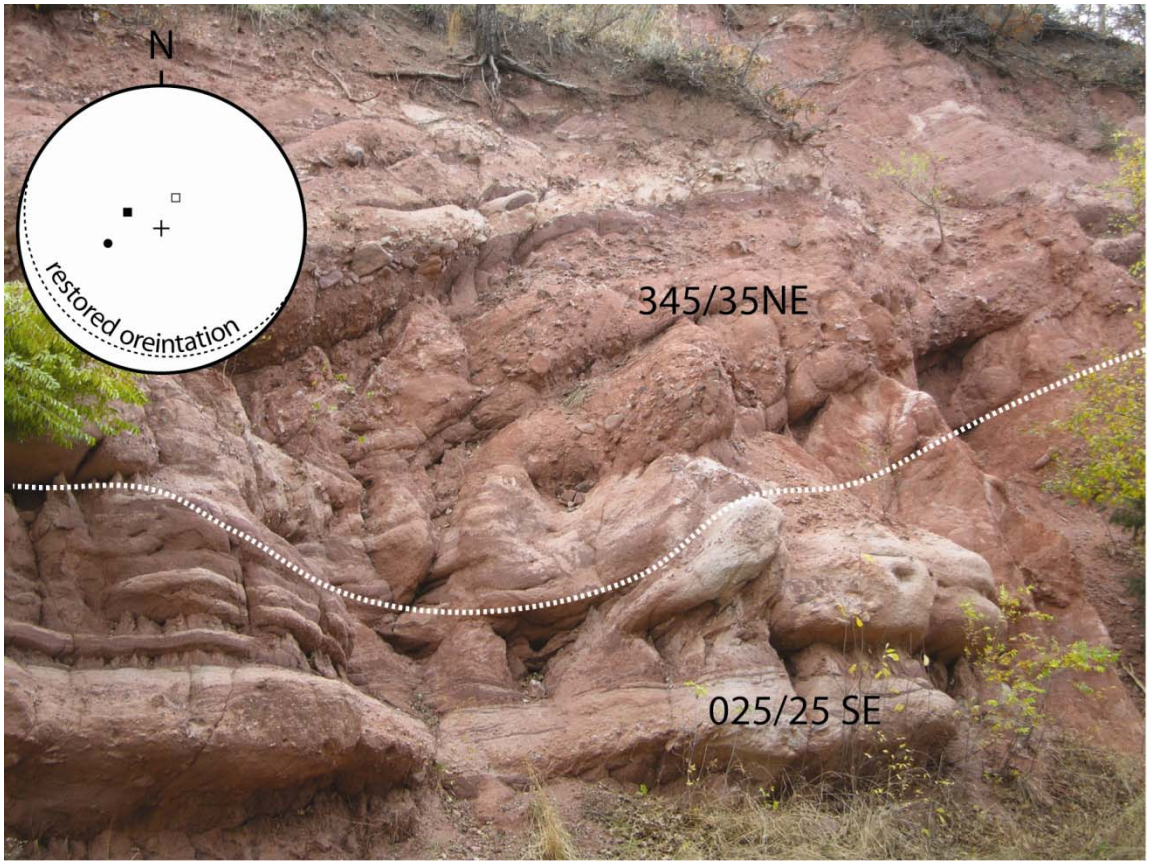

Figure 2.14: Lower-Middle Fountain contact located within 1 km of Ute Pass fault trace. Overlying beds contain cobbles and boulders of the Cambrian Sawatch Formation. Outcrop is ~ 10-12 m tall. Inset: Equal-area stereonet showing the orientation (dashed great circle trace) of underlying beds when upper beds are flattened. Solid circle = present orientation of overlying beds. Solid square = present orientation of underlying beds. Open square = pole to dashed great circle trace.

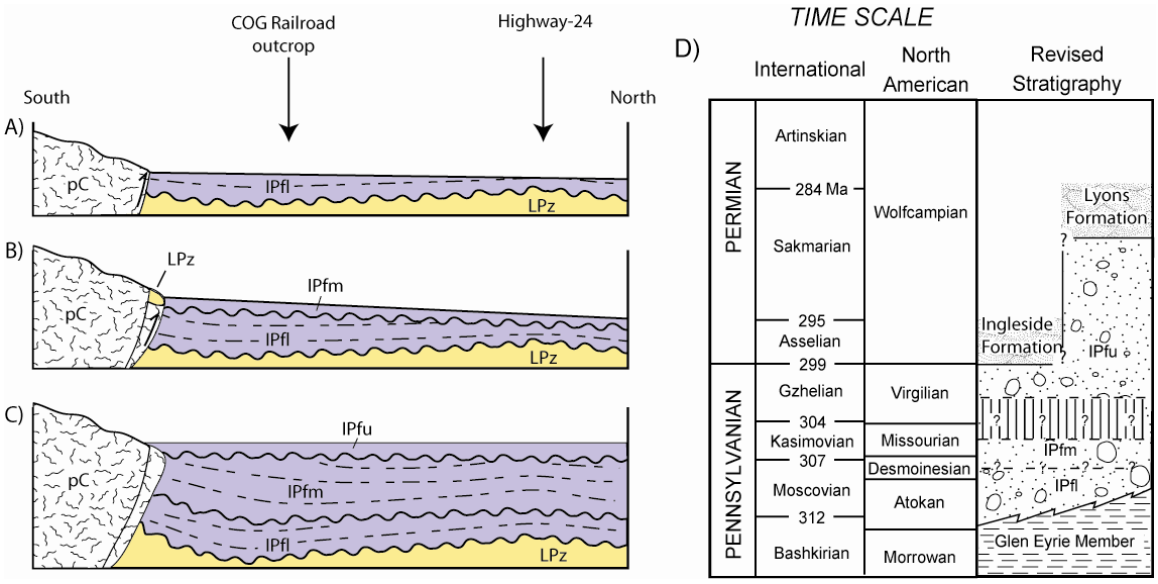

Figure 2.15: Evolution of the Fountain Formation stratigraphy. Wavy lines indicate unconformities discussed in text. Dashed lines represent bedding. A) Lower Fountain deposition. B) Middle Fountain deposition. Note basinward splay of the ancestral Ute Pass fault as described in text. C) Upper Fountain deposition is post tectonic, constraining the timing of movement on the ancestral Ute Pass fault. D) Revised Fountain stratigraphy of the Manitou Springs region. Note the Fountain Formation is gradational with either the Lyons Formation or Ingleside Formation; however, which one is unknown at this time. Time scale is from Gradstein, et al. (2004). pC = Precambrian granite, LPz = lower Paleozoic strata undifferentiated, IPfl = Lower Fountain tectonostratigraphic unit, IPfm = Middle Fountain Tectonostratigraphic unit, IPfu = Upper Fountain tectonostratigraphic unit.

recovered 4 m below the contact and Wolfcampian fusulinids recovered from the overlying Ingleside Formation (Maughan and Ahlbrandt, 1985). Northward, the Lyons Formation is atop both the Ingleside and Fountain Formations and hence considered as entirely Permian (Maughan and Wilson, 1963). Thus, the Upper Fountain Formation could be as young as late Virgilian to early Wolfcampian in age (Fig. 2.15).

The unconformity between the middle and upper Fountain tectonostratigraphic units is a significant boundary marking a change in depositional systems. As evinced by structural deformation (Fig. 2.10) and stratigraphic and sedimentological data, the lower two tectonic units record syntectonic sedimentation in a fan-delta system. The upper Fountain Formation tectonostratigraphic unit thus appears to record post-tectonic deposition in a braided-stream system. Moreover, the paleosols in the lower two units are predominantly Vertisols, Argillisols Gleysols, and Protosols, whereas paleosols in the upper Fountain unit are Protosols and Calcisols, signaling a switch from humid and seasonal to semi-arid conditions, respectively.

Implications for Timing and Kinematics of the Ancestral Ute Pass Fault

The ancestral Ute Pass fault is inferred to have been active during deposition of the Fountain Formation on the basis of the semi-radial paleocurrent dispersal pattern and the abrupt distal fining (from boulders to pebbles/sand over <3 km) relative to the inferred fault location (Suttner et al., 1984; Kluth, 1997). Our data corroborate this inference for the lower and middle Fountain tectonostratigraphic units; however, the upper Fountain unit shows no grain-size trends (Figure 11) and exhibits a shift to fault-parallel paleocurrents (Figure 2.2 & 2.10b). We interpret these data to indicate that the

ancestral Ute Pass fault was active during deposition of the lower to middle Fountain Formation, but had ceased or drastically reduced motion by the time of deposition of the upper Fountain Formation (latest Pennsylvanian, Virgilian (?)) (Fig. 2.15).

The ancestral Ute Pass fault zone experienced at least one major episode of activity as indicated by the presence of an intraformational unconformity separating the lower and middle Fountain units. Within <1 km of the inferred locality of the ancestral Ute Pass fault, this unconformity is exposed. By flattening the beds above the unconformity (middle Fountain), the lower Fountain beds restore (295/21sw) to gently dipping towards the fault (Fig. 2.14). However, it is unclear whether those beds continue to dip towards the fault proximally, thus implying a normal fault, or roll over to form a syncline, thus implying a thrust or reverse geometry.

Sedimentologic data, however, provide additional constraints on fault geometry. Increased activity of the ancestral Ute Pass fault produced a pulse of coarser, predominantly fluvial deposits that record the abrupt introduction of Cambrian Sawatch Formation and fine-grained igneous rock clasts. The lack of Sawatch clasts in the lower Fountain unit suggests that lower Paleozoic strata were absent from the upthrown block during lower Fountain deposition, thus the lower Paleozoic strata must have been exhumed to source these clasts. This exhumation of lower Paleozoic strata indicates that a basinward splay to the ancestral Ute Pass fault must have developed with some component of reverse dip-slip motion (Fig. 2.15b). The trace of the inferred ancestral Ute Pass fault location (i.e. either coincident with or near/subparallel to the Laramide feature) parallels the strike of the fold axis housed within the lower and middle Fountain Formation (Fig. 2.2), indicating that reverse faulting rather than transpression was the

predominant regime for the fault motion. However, some component of strike-slip motion cannot be ruled out.

The Laramide Ute pass fault trace continues to the northwest and veers northerly in the Woodlands Park region where a swath of Fountain Formation and lower Paleozoic strata are preserved in the easterly, downthrown block (Trimble and Machette, 1979). Inasmuch as the uplifts of the ancestral Rocky Mountains were delineated by the absence of lower Paleozoic strata atop the uplift (Kluth and Coney, 1981), the presence of lower Paleozoic strata beneath the Fountain Formation in the Manitou Springs and Woodland Park regions indicates that the area was a structural low that separated a northern block from a southern block. This relationship has been poorly depicted on most paleogeographic maps of the ancestral Rocky Mountains (e.g Kluth and Coney, 1981; Lindsey et al., 1986), but has recently been proposed by Kluth and McCreary (2006) in their portrayal of a northwest-southeast trending structural trough (i.e. Woodland Park trough) that separated a northern uplifted block (i.e. Front range) from a southern uplifted block (i.e. Ute Pass uplift; Fig. 2.1 & 2.16). The ancestral Ute Pass fault likely continued the more westerly trend observed in the study area and formed the southern basin-bounding fault of the Woodland Park trough during deposition of the lower and middle Fountain tectonostratigraphic units (Fig. 2.16). However, during deposition of the upper Fountain unit, the fault had ceased or dramatically decreased activity and sediments likely onlapped the Ute Pass uplift (Fig. 2.16). Hence, accommodation for the upper Fountain Formation must have been created through regional rather than local subsidence.

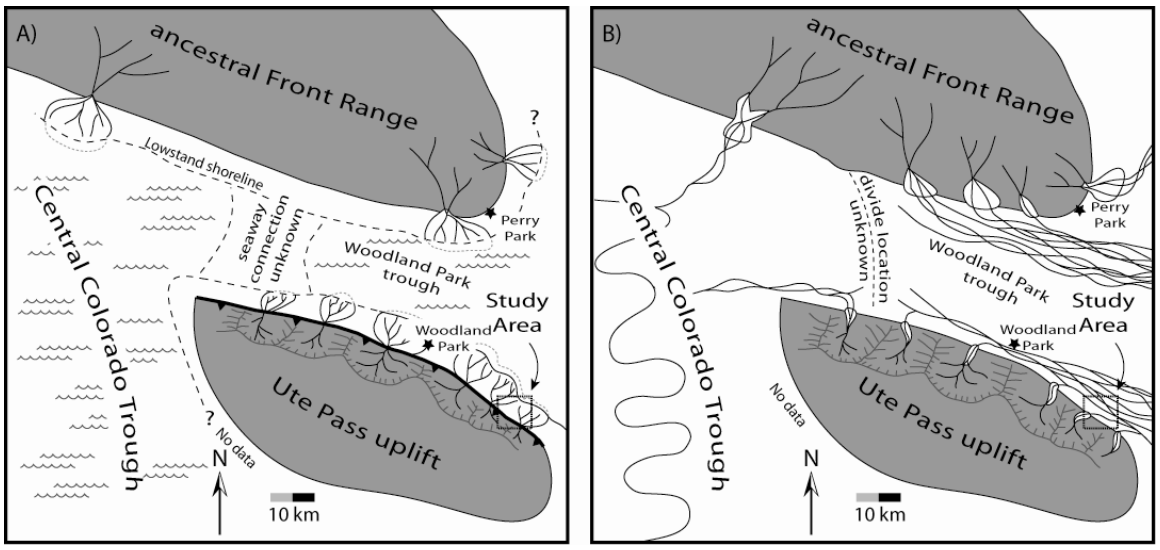

Figure 2.16: Paleogeography of the southern ancestral Front Range A) Early Pennsylvanian configuration during deposition of the lower and middle Fountain tectonostratigraphic units. Data for the Central Colorado trough is from Hoy and Ridgway (2002). Data from Perry Park region is from Hendrickson (1986) and Trimble and Machette (1979). B) Late Pennsylvanian-Early Permian configuration during deposition of the upper Fountain tectonostratigraphic unit. Data for the Central Colorado trough is from Hoy and Ridgway (2002). Data for the Perry Park region is from Hendrickson (1986), Howard (1966) and Trimble and Machette (1979).

Implications for the Greater Ancestral Rocky Mountains

Most syntheses of the ancestral Rocky Mountains address structural timing and kinematics by analyzing basin fill. For example, estimating peak deposition in adjacent basins has been used to propose east-to-west diachronous basin development within the ancestral Rocky Mountains (Kluth and Coney, 1981; Dickinson and Lawton, 2003), and sedimentary facies patterns have been used, in part or wholly, to propose individual basin-formation mechanisms (e.g. transpressional or thrust-loading regimes; Stevenson and Baars, 1986; Lawton and Giles, 2002; Barbeau, 2003). However, as demonstrated in this paper, the Fountain Formation records syntectonic *and* post-tectonic strata. Indeed, data from many studies have also shown that significant portions of basin fill within the ancestral Rocky Mountains post date associated local faulting (Maher, 1953; Devoto et al., 1971; Hoy and Ridgway, 2002; Thomas, 2007; Moore et al., 2008); hence, regional synthesis models based on basin fill alone are unsatisfactory because structural uplift may have ceased prior to deposition of the youngest Pennsylvanian-Permian strata within the basin.

Examination of faults with a documented late Paleozoic history shows a slight east-to-west younging (Fig. 2.17). However, as a result of crude dating of the post-faulting strata, the east-to-west age pattern may be less pronounced than the trend determined from basin fill alone (i.e. Dickinson and Lawton, 2003). For example, the age of the upper Fountain tectonostratigraphic unit postdates movement on the ancestral Ute Pass fault, yet the upper Fountain age constraints allow for a range from late Pennsylvanian-early Permian (e.g. 5-8 Ma difference). Thus, when the poorly constrained ages of basin fill and subsequent fault movement are considered, the possibility of a

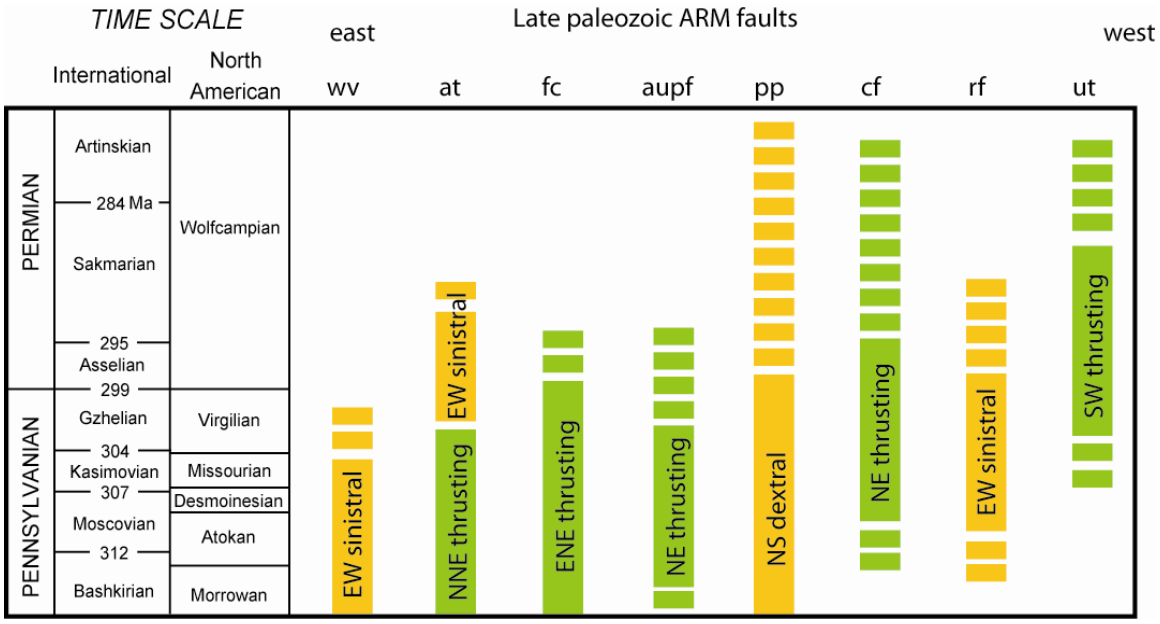

Figure 2.17: Inferred timing and kinematics of faults with a documented ancestral Rocky Mountains history. Light gray represents predominantly strike-slip motion whereas dark gray indicates predominantly reverse motion. Dashed bars indicate range of time faulting is thought to have initiated (bottom of figure) or ceased (top of figure). ut = Uncompahgre thrust (slip-sense from Frahme and Vaughn, 1983); rf = Ridgeway fault (slip-sense from Stevenson and Baars, 1986; Thomas, 2007); pp = Picuris-Pecos fault (slip-sense from Cather et al., 2006; Wawrzyniec et al., 2007); ct = Crestone thrust (slip-sense from Hoy and Ridgway, 2002); aupf = ancestral Ute Pass fault (slip-sense data herein); fc = Freezeout Creek fault (slip-sense from Maher, 1953; McKee, 1975); at = Anadarko thrust (slip-sense from Brewer et al., 1983); wv = Washita Valley fault (slip-sense from Tanner, 1967). Time scale is from Gradstein, et al. (2004).

relatively synchronous termination of faulting is permissible within the ancestral Rocky Mountains (Fig. 2.17). If the latter possibility holds, then current plate tectonic models invoking the diachronous closure of Laurentia and Gondwana may be compromised and better dates of basin fill and post-tectonic strata are needed to resolve the issue.

Faults of the ancestral Rocky Mountains striking NW-SE have predominantly reverse slip, whereas faults oriented east-west and north-south have sinistral and dextral strike-slip, respectively (Fig. 2.1 & 2.17). These geometries and slip directions are all consistent with a maximum horizontal compressional stress oriented NE-SW, possibly indicating a relatively stable stress orientation throughout the evolution of the greater ancestral Rocky Mountains. This stress stability does not appear to mesh well with the torsional stresses invoked by a diachronous closure (Dickinson and Lawton, 2003). However, the Anadarko fault has a well-documented early reverse and late sinistral-slip components (Fig. 2.17) which could indicate either (1) that the strike of the Anadarko fault more closely approximates east-west than the other thrusts, or (2) orientation of the maximum horizontal stress component rotated during the history of the greater ancestral Rocky Mountains, or (3) a combination of both. Other workers have proposed strike-slip motion on predominantly reverse-slip faults (Stevenson and Baars, 1986), thus it is possible that other faults of the ancestral Rocky Mountains may display the multi-slip histories.

Conclusions

1. Sedimentologic, stratigraphic and structural data indicate that the Fountain Formation in the Manitou Springs study area is divisible into three separate tectonostratigraphic

2. Rejuvenation of the ancestral Ute Pass fault zone created the intraformational unconformity separating the lower and middle units of the Fountain Formation. This event produced a basinward-propagating splay with reverse dip slip, as indicated by exhumation marked by the abrupt introduction of lower Paleozoic clasts into the Fountain depositional system, and by fault-parallel folding of the strata below the upper Fountain Formation.

3. Intermittent fluvial sedimentation and an estimated steep depositional slope (~0.005), coupled with the intercalation of prograding marine cycles is inferred to reflect deposition in a fan-delta setting for the lower and middle Fountain strata. Conversely, the upper Fountain Formation records a braided-river depositional setting as indicated by >4 km wide system of multi-story fluvial bodies, yet lacking true fine-grained, laminated overbank deposits and an estimated lower depositional slope (~0.0008).

4. Deposition of the lower Fountain unit began in the Morrowan-Atokan, as indicated by conodonts present in distal marine facies, and reasonably could have continued through Desmonesian (?) time for the middle Fountain Formation. The upper Fountain Formation is undated, but its gradational relationship between the overlying eolian unit (Lyons or Ingleside) in the study area, which elsewhere are fossil-bearing suggesting earliest Permian to middle-early Permian age. These relationships indicate that the ancestral Ute Pass fault had ceased movement by latest

Pennsylvanian-early Permian time, whereupon the upper Fountain Formation onlapped the Ute Pass uplift.

5. All three tectonostratigraphic units were deposited within a northwest-southeast-oriented structural trough, previously proposed as the Woodland Park trough (Kluth and McCreary, 2006). The lower and middle Fountain Formation record deposition influenced by structural subsidence of that trough during peak ancestral Rocky Mountains tectonism. The upper Fountain depositional system appears to have aligned axially with the Woodland Park trough, yet it was not influenced by structural subsidence of that trough; thus, accommodation for the upper Fountain Formation must have been created through regional rather than local subsidence.

6. Comparison of the kinematics of the ancestral Ute Pass fault to other regional ancestral Rocky Mountain faults suggests that these faults formed under similar stress regimes (NE-SW compression). Comparison of the timing of the same faults suggests an east-to-west younging of activity, but much more subdued than the east-to-west younging trend inferred (by others) on the basis of basin fill alone. The relatively poor age dating of ancestral Rocky Mountains strata also allows for t synchronous termination of faulting—a relationship that challenges the current diachronous closure model for ancestral Rocky Mountains.

Acknowledgements

This work was funded in part by GSA graduate student research grants, Sigma Xi Grants-in-Aid of Research, Colorado Scientific Society Research Grant, J.D. Love Field Geology Fellowship, SEPM Presidential Fund—student grant and NSF grant #EAR-0230332. I thank Z. Reches, L. Suttner, C. Kluth, and M. Soreghan for field visits and/or data sharing. Special thanks to K. Schroeder of the City of Colorado Springs Parks, Recreation & Cultural Services division for access to Red Rock Canyon and Garden of the Gods parks and sampling permission in Red Rock Canyon.

References

Allen, J.R.L., 1968, Current Ripples, their relation to Patterns of Water and Sediment Motion. North Holland Publishing Co., Amsterdam. 433 p.

Baars, D.L., 1966, Pre-Pennsylvanian paleotectonics—Key to basin evolution and petroleum occurrences in Paradox basin, Utah and Colorado: American Association of Petroleum Geologists Bulletin, v. 50, p. 2082-2111.

Barbeau, D.L., 2003, A flexural model for the Paradox Basin: Implications for the tectonics of the ancestral Rocky Mountains: Basin Research, v. 15, p. 97-115.

Blair, T.C. and McPherson, J.G., 1994, Alluvial fans and their natural distinction from rivers based on morphology, hydraulic processes, sedimentary processes, and facies assemblages: Journal of Sedimentary Research, v. A64, p. 450-489.

Brewer, J.A., Good, R., Oliver, J.E., Brown, D. and Kaufman, S., 1983, COCORP profiling across the southern Oklahoma aulocogen: overthrusting of the Wichita Mountains and compression within the Anadarko basin: Geology, v. 11, p. 109-114.

Cather, S.M., Karlstrom, K.E., Timmons, J.M. and Heizler, M.T., 2006, Palinspastic reconstruction of Proterozoic basement-related aeromagnetic features in north-central New Mexico: Implications for Mesoproterozoic to late Cenozoic tectonism: Geosphere, v. 2, p. 299-323.

Chronic, B.J. and Williams, C.A., 1978, The Glen Eyrie Formation (Carboniferous) near Colorado Springs, *in* Pruitt, J.D. and Coffin, P.E. (eds.), Energy Resources of the Denver Basin: Rocky Mountain Association of Geologists field conference guidebook, p. 199-206.

DeVoto, R.H., Peel, F.A., and Pierce, W.H., 1971, Pennsylvanian and Permian stratigraphy, tectonism, and history, Northern Sangre de Cristo Range, Colorado, *in* James, H.L. (ed.) New Mexico Geologic Society guidebook, 22nd Field Conference, San Luis Basin (Colorado), p. 141-163.

Dickinson, W.R., 2000, Geodynamic interpretation of Paleozoic tectonic trends oriented oblique to the Mesozoic Klamath-Sierran continental margin in Califronia, *in* Soreghan, M.J., and Gehrels, G.E., eds., Paleozoic and Triassic paleogeography and tectonics of western Nevada and northern California: Geological Society of America Special Paper 347, p. 209-245.

Dickinson, W.R. and Lawton, T.F., 2001, Carboniferous to Cretaceous assembly and fragmentation of Mexico: Geological Society of America Bulletin, v. 113, p. 1142-1160.

Dickinson, W.R. and Lawton, T.F., 2003, Sequential intercontinental suturing as the ultimate control for Pennsylvanian Ancestral Rocky Mountains deformation: Geology, v. 31, p. 609-612.

Fishbaugh, D.A., 1980, Depositional environment for the lower Fountain Formation in the Manitou embayment, Colorado: MA thesis, Indiana University, 136p.

Frahme, C.W. and Vaughn, E.B., 1983, Paleozoic geology and seismic stratigraphy of the northern Uncompahgre Front, Grant County, Utah: Rocky Mountain Association of Geologists Field Conference, p. 201-211.

Gradstein, F.M., Ogg, J.G., Smith, A.G., Bleeker, W. and Lourens, L.J., 2004. A new geologic time scale, with special reference to Precambrian and Neogene. Episodes, 27: 83-100.

Hampton, M.A., 1975, Competence of fine-grained debris flows: Journal of Sedimentary Petrology, v. 45, p. 834-844.

Hendrickson, D. M., 1986, Stratigraphy and Sedimentology of the Pennsylvanian and lower Permian Fountain Formation in Perry Park, Douglas County, Colorado: MA thesis Colorado School of Mines, 296 p.

Howard, J.D., 1966, Patterns of sediment dispersal in the Fountain Formation of Colorado: Mountain Geologist, v. 3, p. 147-153.

Hoy, R.G. and Ridgway, K.D., 2002, Syndepositional thrust-related deformation and sedimentation in an ancestral Rocky Mountains basin, Central Colorado trough, Colorado, USA: Geological Society of America Bulletin, vol. 114, p. 804-828.

Hubert, J.F., 1960, Petrology of the Fountain and Lyons Formations, Front Range, Colorado: Colorado School of Mines Quarterly, v. 55, p. 1-242.

Janitzky, P., 1986, Laboratory methods: citrate-bicarbonate-dithionite (CBD) extractable iron and aluminum, *in* Singer, M.J. and Janitzky, P. (eds.), Field and laboratory procedures used in a soil chronosequence study: U.S. Geological Survey Bulletin, Report: B 1648, p. 38-41.

Jennings, J.R., 1980, Fossil plants from the Fountain Formation (Pennsylvanian) of Colorado: Journal of Paleontology, v. 54, no. 1, p. 149-158.

Kairo, S., Suttner, L.J., and Dutta, P.K., 1993, Variability in sandstone composition as a function of depositional environment in coarse-grained delta systems: Geological Society of America Special Paper 284, p. 263-283.

Kluth, C.F., 1986, Plate tectonics of the Ancestral Rocky Mountains, *in* Peterson, J.A., eds., Paleotectonics and Sedimentation in the Rocky Mountain Region, United Sates: American Association of Petroleum Geologists Memoir 41, p. 353-369.

Kluth, C.F., 1997, Comparison of the location and structure of the late Paleozoic and Late Cretaceous-early Tertiary Front Range uplift, *in* Bolyard, D.W. and Sonnenberg, S.A. (eds.), Geologic History of the Front Range: Rocky Mountain Association of Geologists, Denver, Colorado, p. 31-42.

Kluth, C.F., 1998, Late Paleozoic deformation of interior North America; the greater ancestral Rocky Mountains; discussion: American Association of Petroleum Geologists, v. 82, p. 2272-2279.

Kluth, C.F., and Coney, P.J., 1981, Plate tectonics of the Ancestral Rocky Mountains: Geology, v. 9, p. 10-15.

Kluth, C.F., and McCreary, J.A., 2006, Reinterpretation of the geometry and orientation of the late Paleozoic Frontrange Uplift: Abstracts with Programs—Geological Society of America, v. 38, no. 6, p. 29.

Langford, R.P., 1982, Depositional systems and geologic history of the lower part of the Fountain Formation, Manitou embayment, Colorado: MA thesis, Indiana University, 199p.

Lawton, T.F. and Giles, K.A., 2002, Origin of the Orogrande basin by strike-slip faulting: evidence from subsidence patterns and facies distribution, *in* Late Paleozoic Tectonics and hydrocarbon Systems of Western North America—The Greater Ancestral Rocky Mountains: Tulsa, American Association of Petroleum Geologists Hedberg Research Conference, p. 33-34.

Lindsey, D.A., Clark, R.F., and Soulliere, S.J., 1986, Minturn and Sangre de cristo Formations of southern Colorado: A prograding fan-delta and alluvial fan sequence shed from the Ancestral Rocky Mountains, *in* Peterson, J.A., eds., Paleotectonics and Sedimentation in the Rocky Mountain Region, United Sates: American Association of Petroleum Geologists Memoir 41, p. 541-561.

Mack, G.H., James, W.C. and Monger, H.C., 1993. Classification of Paleosols. Geological Society of America Bulletin v. 105, p. 129-136.

Maher, J.C., 1953. Permian and Pennsylvanian rocks of southeastern Colorado. American Association of Petroleum Geologists, v. 37, p. 913-939.

Mallory, W.W., 1958, Pennsylvanian coarse arkosic redbeds and associated mountains in Colorado, *in* Symposium on Pennsylvanian Rocks of Colorado and adjacent areas: Rocky Mountain Association of Geologists, p. 17-20.

Mallory, W.W., 1972, Pennsylvanian System, *in*, Mallory, W.W. (ed.), Geologic Atlas of the Rocky Mountain Region, Rocky Mountain Association of Geologists, p. 131-132.

Maples, C.G. and Suttner, L.J., 1990, Trace fossils and marine-nonmarine cyclicity in the Fountain Formation (Pennsylvanian; Morrowan/Atokan) near Manitou Springs, Colorado: Journal of Paleontology, vol. 64, p.859-880.

Maughan, E.K., and Ahlbrandt, T.S., 1985. Pennsylvanian and Permian eolian sandstone facies, northern Colorado and southeastern Wyoming. In: Macke, D.L. and Maughan, E.K. (Eds.), Rocky Mountain Section Field Trip Guide Book. RMS-AAPG, RMS-SEPM, NEMD, RMAG, pp. 99-113.

Maughan, E.K. and Wilson, R.F., 1963, Permian and Pennsylvanian strata in southern Wyoming and northern Colorado, *in* Katich, P.J. and Bolyard, D.W. (eds.), Guidebook to the geology of the northern Denver basin and adjacent uplifts: Rocky Mountain Association of Geologists, p. 95-104.

McKee, E.D., 1975, Interpretation of Pennsylvanian history, *in* McKee, E.D. and Crosby, E.J., (eds.), Paleotectonic investigations of the Pennsylvanian system in the United States: U.S. Geological Survey Professional Paper 853, pt. 2, p. 1-21.

McPherson, J.G., Shanmugam, G. and Moiola, R.J., 1987, Fan-deltas and braid deltas: varieties of coarse-grained deltas: Geological Society of America Bulletin, v. 99, p. 331-340.

Mehra, O.P. and Jackson, M.L., 1960, Iron oxide removal from soils and clays by a citrate-dithionite system buffered by sodium carbonate: Clays and Clay Mineralogy, v. 7, p. 317-327.

Miall, A.D., 1977, A review of the braided-river depositional environment: Earth-Science Reviews, v. 13, p. 1-62.

Miall, A.D., 1978, Lithofacies types and vertical profile models in braided river deposits: a summary, *in* Miall, A.D., (ed.), Fluvial sedimentology: Canadian Society of Petroleum Geologists Memoir 5, p. 597-604.

Miall, A.D., 1996, The Geology of Fluvial Deposits: sedimentary facies, basin analysis, and petroleum geology: Springer-Verlag, Berlin, Germany, 582p.

Moore, K.D., Soreghan, G.S. and Sweet, D.E., 2008, Stratigraphic and structural relations in the Proximal Cutler Formation of the Paradox Basin: Implications for timing of movement on the Uncompahgre Front. The Mountain Geologist, v. 45, p. 49-68.

O'Connell, A.F., 1981, Origin of the Glen Eyrie Member of the Fountain Formation: MA thesis, Indiana University, 174 p.

Paola, C. and Mohrig, D., 1996, Palaeohydraulics revisited: palaeoslope estimation in coarse-grained braided rivers: Basin Research, v. 8, p. 243-254.

Schatz, B.A., 1986. Depositional environments of the Upper Fountain and Ingleside Formations between Lyons and Loveland, Colorado. MS thesis, University of Colorado, Boulder, Colorado.

Scotese, C.R., 1997, Paleogeographic Atlas, PALEOMAP Progress Report 90-0497, Department of Geology, University of Texas at Arlington, Arlington, Texas, 45 pp.

Scott, K.M., Pringle, P.T., and Vallance, J.W., 1992, Sedimentology, behavior, and hazards of debris flows at Mount Rainier, Washington. U.S. Geological Survey Open-File Report 90-385, 106 p.

Smith, G.A., 1986, Coarse-grained nonmarine volcaniclastic sediment: terminology and depositional process: Geological Society of America Bulletin, v. 97, p. 1-10.

Smith, G.A. and Lowe, D.R., 1991, Lahars: volcano-hydrologic events and deposition in the debris flow-hyperconcentrated flow continuum, *in* Fisher, R.V. and Smith, G.A. (eds.), Sedimentation in volcanic settings: Society for Sedimentary Geology Special Publication 45, p. 59-70.

Stevenson, G.M. and Baars, D.L., 1986, The Paradox: a pull-apart basin of Pennsylvanian age: *in* Peterson, J.A. (ed.), Paleotectonics and sedimentation in the Rocky Mountain region, United States: American Association of Petroleum Geologists Memoir 41, p. 513-539.

Suttner, L.J., Langford, R.P., and O'Connell, A.F., 1984. New interpretation of the stratigraphic relationship between the Fountain Formation and its Glen Eyrie Member. In: Suttner, L.J., (Ed), Sedimentology of the Fountain fan-delta complex near Manitou Springs and Canon City, Colorado. Society of Economic Paleontologists and Mineralogists field guidebook, pp. 31-61.

Sweet, D.E. and Soreghan, G.S., 2008, Polygonal cracking in coarse clastics records cold temperatures in the equatorial Fountain Formation (Pennsylvanian-Permian, Colorado): Palaeogeography, Palaeoclimatology, Palaeoecology, v. 268, no. 3-4, p. 193-204.

Tanner, J.H., 1967, Wrench fault movement along the Washita Valley fault, Arbuckle Mountains area, Oklahoma: American Association of Petroleum Geologists Bulletin, v. 51, p. 126-134.

Thomas, W.A., 2007, Pennsylvanian sinistral faults along the southwest boundary of the Uncompahgre uplift, Ancestral Rocky Mountains, Colorado: Geosphere, v. 3, p. 119-132.

Trimble, D.E. and Machette, M.N., 1979, Geologic map of the Colorado Springs-Castle Rock area, Front Range Urban Corridor, Colorado: U.S.G.S. Map I-857-F, 1:100,000.

Wawrzyniec, T.F., Ault, A.K., Geissman, J.W., Erslev, E.A., and Fankhauser, S.D., 2007, Paleomagnetic dating of fault slip in the Southern Rocky Mountains, USA, and its importance to an integrated Laramide foreland strain field: Geosphere, v. 3, p. 16-25.

Wilson, R.F., 1975, Eastern Colorado, *in* McKee, E.D. and Crosby, E.J. (eds.), Paleotectonic investigations of the Pennsylvanian System in the United States; Part I, Introduction and regional analyses of the Pennsylvanian System: U. S. Geological Survey Professional Paper, Report: P No. 853-M, p.245-264.

Ye, H., Royden, L., Burchfiel, C., and Schuepbach, M., 1996, Late Paleozoic deformation of interior North America: The greater Ancestral Rocky Mountains: American Association of Petroleum Bulletin, v. 80, p. 1397-1432.

Ye, H., Royden, L., Burchfiel, C., and Schuepbach, M., 1998, Late Paleozoic deformation of interior North America; the greater ancestral Rocky Mountains; reply: American Association of Petroleum Geologists, v. 82, p. 2272-2279.

3. POLYGONAL CRACKING IN COARSE CLASTICS RECORDS COLD TEMPERATURES IN THE EQUATORIAL FOUNTAIN FORMATION (PENNSYLVANIAN-PERMIAN, COLORADO)

Abstract

Sand- and granule-filled polygonal fractures are present on bedding surfaces within the equatorial Fountain Formation (Pennsylvanian-Permian, Colorado). The surfaces are areally extensive (> 120,000 m^2) and occur within inferred braided-river deposits. The fractures penetrate downward into coarse sandstone to granule conglomerate and range from 3-55 cm and 13- >220 cm in width and depth, respectively. At one locality (Manitou Springs), both fracture fill and polygon interiors display a grain-supported texture and contain <14% clay; additionally, the fracture fill is microbrecciated. At the other locality (Loveland), both the fracture fill and polygon interiors display a grain-supported texture and contain <3.5% clay.

The polygonal fractures are inferred to have formed as frozen ground experienced thermal contraction induced by repeated cooling events. Owing to the equatorial location of the Fountain Formation, we suggest that diurnal, rather than seasonal, temperature variations provided the repeated cooling mechanism. Alternative causes of polygonal fracturing, such as desiccation of clay-rich sediments or thermal contraction of evaporite minerals, are untenable because the hosting strata contain minimal clay (<14%) and are framework-supported, indicating that there was insufficient space for either clay or evaporite minerals. A thermal contraction origin for these features implies that the

equatorial Fountain Formation experienced at least two episodes of remarkably cold conditions. Furthermore, using maximum reasonable stream gradients (~0.02) between the polygonally fractured surfaces and the shoreline (gauged from shallow-marine deposits of the Denver basin), the fractures formed at relatively low elevation (≤ 1800 m).

Introduction

Polygonal cracking on bedding planes in mud-rich continental strata is common and typically attributed to desiccation. A desiccation origin for polygonal cracks in coarse clastics (>50% sand), however, is untenable because the framework grains lack the contractive and cohesive qualities necessary for formation of desiccation cracks (Fellows, 1951; Neal, 1978; Weinberger, 2001). Other processes implemented to account for polygonal fracturing in coarse-grained clastic strata include ice- and sand-wedge formation (e.g. Lachenbruch, 1962; Black, 1976; Johnson, 1990), seasonal frost cracking (e.g. Katasonov, 1973; Black, 1976; Seppälä, 2004; Vliet-Lanoë et al., 2004), diurnal thermal contraction cracking (e.g. Hastenrath, 1981, 1984; Maloof et al., 2002) and thermal contraction of evaporites (e.g. Goldberg, 1967; Evans et al., 1969; Watson, 1985; Kocurek and Hunter, 1986). These processes take place on a stable land surface that undergoes thermal contraction in the presence of a binding medium (i.e. frozen interstitial water, or salts) that maintains cohesion within the polygon.

Different mechanisms of polygonal cracking have different paleoclimatic implications. For example, polygonal fractures containing evaporite minerals indicates a deficit of effective moisture (e.g. Parrish, 1998), whereas modern polygonal fracturing at high latitudes is the result of seasonal temperature swings (e.g. Lachenbruch, 1962;

Black, 1976; Washburn, 1980a, 1980b). Additionally, fracture fill lithology and structure is different for a cold-humid (i.e. ice wedges) or a cold-arid (i.e. sand wedges) climate (Black, 1976).

In this paper, we describe polygonal fractures within coarse clastic strata of the Pennsylvanian-Permian Fountain Formation (western U.S.; Fig. 3.1). Our analysis indicates that these features formed as a result of repeated thermal contraction, reflecting discrete episodes of remarkably cold temperatures in this equatorial setting.

Geologic Setting

The Pennsylvanian-Permian Fountain Formation consists of coarse arkosic sandstone and conglomerate deposited on the east flank of the ancestral Front Range (Fig. 3.1), one of a series of uplifts within the Ancestral Rocky Mountains (ARM). The ARM were an intracontinental array of Precambrian-cored uplifts and intervening basins situated in western equatorial Pangaea (Kluth and Coney, 1981). Latitudinal position of the study site ranged from 0°- 5°N in the mid to late Pennsylvanian (Golonka et al., 1994; Scotese, 1999).

At Manitou Springs, Colorado (Fig. 3.1), the lower Fountain Formation is characterized by intertonguing of continental facies with lagoonal to shallow marine facies (Glen Eyrie Member; Langford and Fishbaugh, 1984; Suttner et al., 1984), whereas the upper Fountain Formation is entirely continental (Langford and Fishbaugh, 1984). Our interval of interest is within the upper "Balanced Rock interval" of Suttner et al. (1984) which they have interpreted as a braided fluvial succession. Here the lower Fountain Formation has been assigned a Morrowan-Atokan (Bashkirian) age on the basis

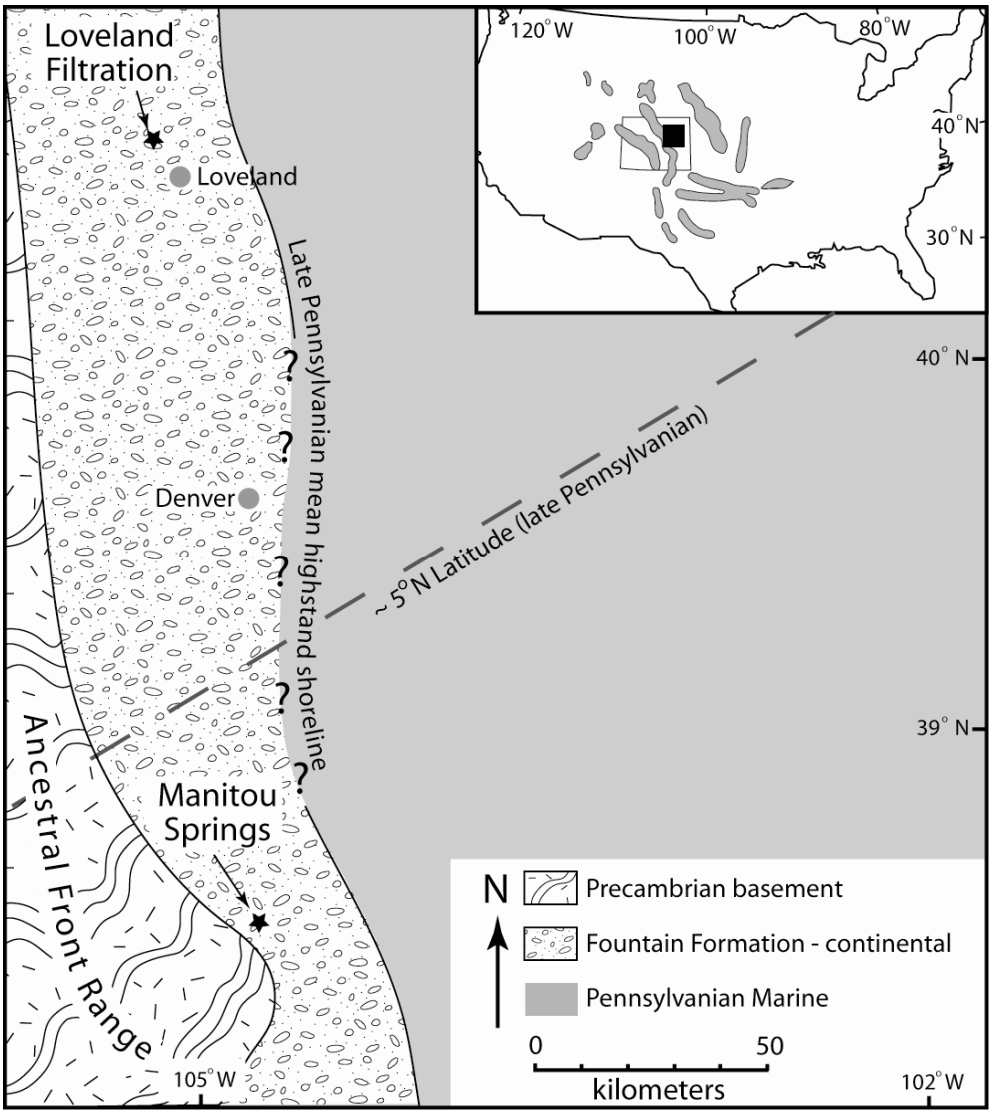

Figure 3.1: Late Pennsylvanian paleogeographic map along the east flank of the ancestral Front Range uplift. Manitou Springs and Loveland study sites are denoted by black stars. The average highstand shoreline is estimated from subsurface data of Maughan and Albrandt (1985) and Maher (1953). Latitudinal position estimated from Scotese (1999). Inset: Displays the outline of Colorado within the United States interior and location of ARM uplifts (*in* gray; modified from Kluth and Coney, 1981). Black box is the approximate area of enlarged view.

of marine invertebrate and plant fossils found in the Glen Eyrie Member (Chronic and Williams, 1978; Suttner et al., 1984), and the upper Fountain Formation is presumed to be of Wolfcampian (Asselian-Sakmarian) age as constrained by the overlying Lyons Formation of probable Wolfcampian to Leonardian (Sakmarian-Artinskian) age (Thompson, 1949; Fig. 3.2).

Near Loveland, Colorado (Fig. 3.1), the Fountain Formation consists of coarse arkosic sandstone and minor granule conglomerate interpreted as braidplain deposits (Hubert, 1960; Schatz, 1986). The upper Fountain Formation represents a transition zone between fluvial deposition below and eolian deposition of the overlying Ingleside Formation (Schatz, 1986). Our interval of interest occurs within the uppermost Fountain Formation (Fig. 3.2). North of Loveland, thin limestone beds containing Virgilian (Gzhelian) fusulinids interfinger with the upper Fountain Formation (Maughan and Albrandt, 1985) suggesting that the unit is entirely Pennsylvanian in the northern study site (Fig. 3.2).

Methods

Stratigraphic sections were measured with a Jacob Staff and Brunton compass and described at 1:25 scale. Fracture trends were measured with a Brunton compass on three-dimensional exposures. Samples of both the polygon interior and fracture fill were collected for sedimentary and x-ray diffraction (XRD) analyses.

Samples were disaggregated for grain-size and sand-microtextural analyses by immersion in a dilute sodium carbonate dispersant solution followed by gentle sonication for three hours. Calcite cement was then removed by submersion in 1N hydrochloric acid

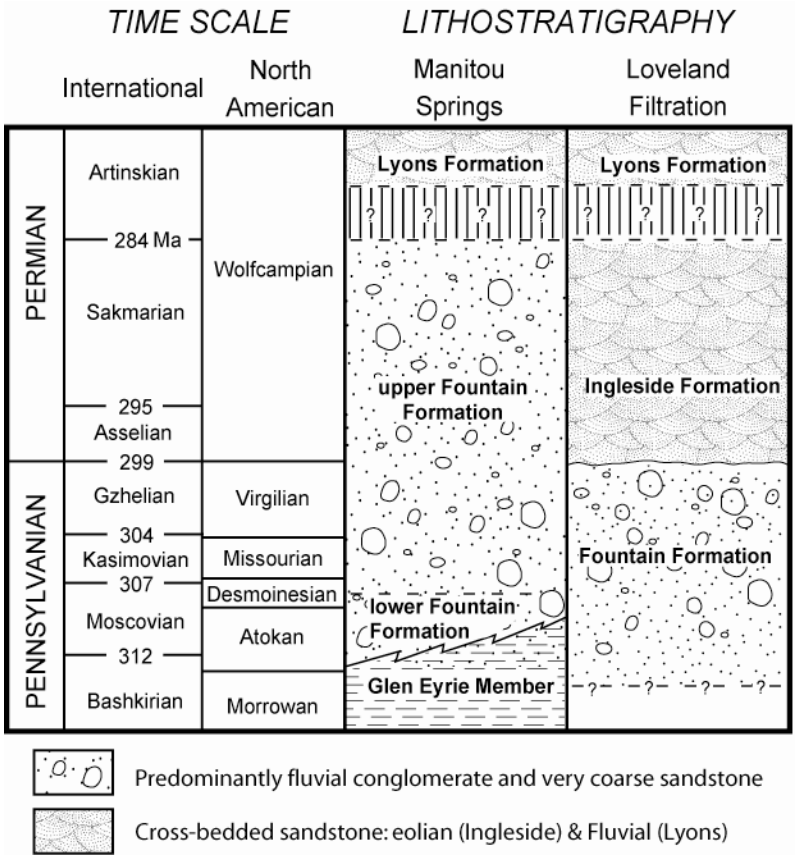

Figure 3.2: Late Pennsylvanian-Early Permian stratigraphy along the east flank of the ancestral Front Range uplift. Vertical black lines denote hiatuses. Location of stratigraphic columns shown on Figure 3.1 as black stars. Age of lithostratigraphic units at Manitou Springs from Chronic and Williams (1978), Trimble and Machette (1979) and Suttner et al. (1984). Ages of the lithostratigrapic units at Loveland, Colorado are from Maughan and Albrandt (1985). Timescale is from Gradstein et al., (2004).

at 50°C until effervescence ceased. Lastly, iron oxide cement was removed by the citrate-bicarbonate-diothionite (CBD) method (Mehra and Jackson, 1960; Janitzky, 1986). The resultant disaggregated sample was analyzed for grain-size distribution by wet-sieving with a 4 φ mesh (62.5 μm) to separate the sand + gravel from mud fractions. The mud fraction was analyzed with a Beckman-Coulter LS-230 laser particle-size analyzer. The sand + gravel fraction was dry-sieved into granule (>2000 μm), very coarse to coarse-sand (500-2000 μm), medium-sand (250-500 μm) and fine to very fine-sand (63-250 μm) fractions. Randomly selected quartz grains from the coarse- and medium-sand fractions were selected for scanning electron microscopy (SEM) analysis as outlined by Mahaney et al. (1988). The atlases of Krinsley and Doornkamp (1973) and Mahaney (2002) were used for identification of microtextures.

XRD analysis was undertaken to assess mineralogy of the clay fraction. Disaggregation for XRD analysis was completed by first crushing whole-rock samples with a ceramic mortar and pestle and wet sieving with a 4 φ mesh (62.5 μm). Next, the <62 μm fraction was subjected to gentle ultrasonic treatment in a dispersant solution (Calgon®) for 30 minutes. Lastly, the <2 μm fraction was captured by the pipette method described in Folk (1974). Smear mounts were made of the <2 μm fraction and analyses completed with a Rigaku automated wide angle x-ray diffractometer with a graphite monochromator and copper tube (CuK, 40 kV/30 mV) between 5-70°2θ with step size of 0.01°2θ and 1s count time. Data was analyzed with Jade Software version 3.1 and ICDD-PDF database.

Stratigraphic Intervals Containing Polygonal Fractures

Manitou Springs Study Area

At Manitou Springs, three stratigraphic horizons (MS1, MS2, and MS3) contain downwardly tapering, sand- and granule-filled fractures. These occur within a succession of predominantly crudely stratified granule conglomerate and sandstone with minor trough and planar cross-stratification and graded bedding interpreted to reflect alluvial deposition on a coarse-grained fan delta (e.g. Suttner et al., 1984; Fig. 3.3). The MS1 horizon comprises a 40 cm thick, massive, coarse-grained sandstone with scattered granules. The MS2 unit consists of 1 m of horizontally stratified fine-grained sandstone with 10 cm coarse-grained sandstone interbeds. Both the MS1 and MS2 horizons are overlain by crudely stratified granule conglomerate. The MS3 horizon (> 120, 000 m^2 exposure area) is composed of massive, poorly sorted, coarse- to very coarse-grained sandstone with abundant granules and is overlain by massive and laminated siltstone. All three horizons are laterally continuous throughout the exposed extent of the sand- and granule-filled fractured area.

Loveland Study Area

At Loveland, the Fountain Formation consists predominantly of massive, planar cross-stratified and trough cross-stratified coarse- to very coarse-grained arkosic sandstone interpreted to reflect braid-plain deposition (Schatz, 1986). The overlying Ingleside Formation consists of well-sorted, fine-grained sandstone with low-angle planar cross-stratification. Individual laminae composing the planar cross-stratification within the Ingleside Formation are graded and have been interpreted as eolian grain flows (Schatz, 1986).

Figure 3.3: Detailed measured column showing the stratigraphic location of the polygonal fractures (~8.75 meters above base) and clastic wedges (~2 and 3 meters above base) at Manitou Springs. Note the coarse nature of the hosting strata and fill.

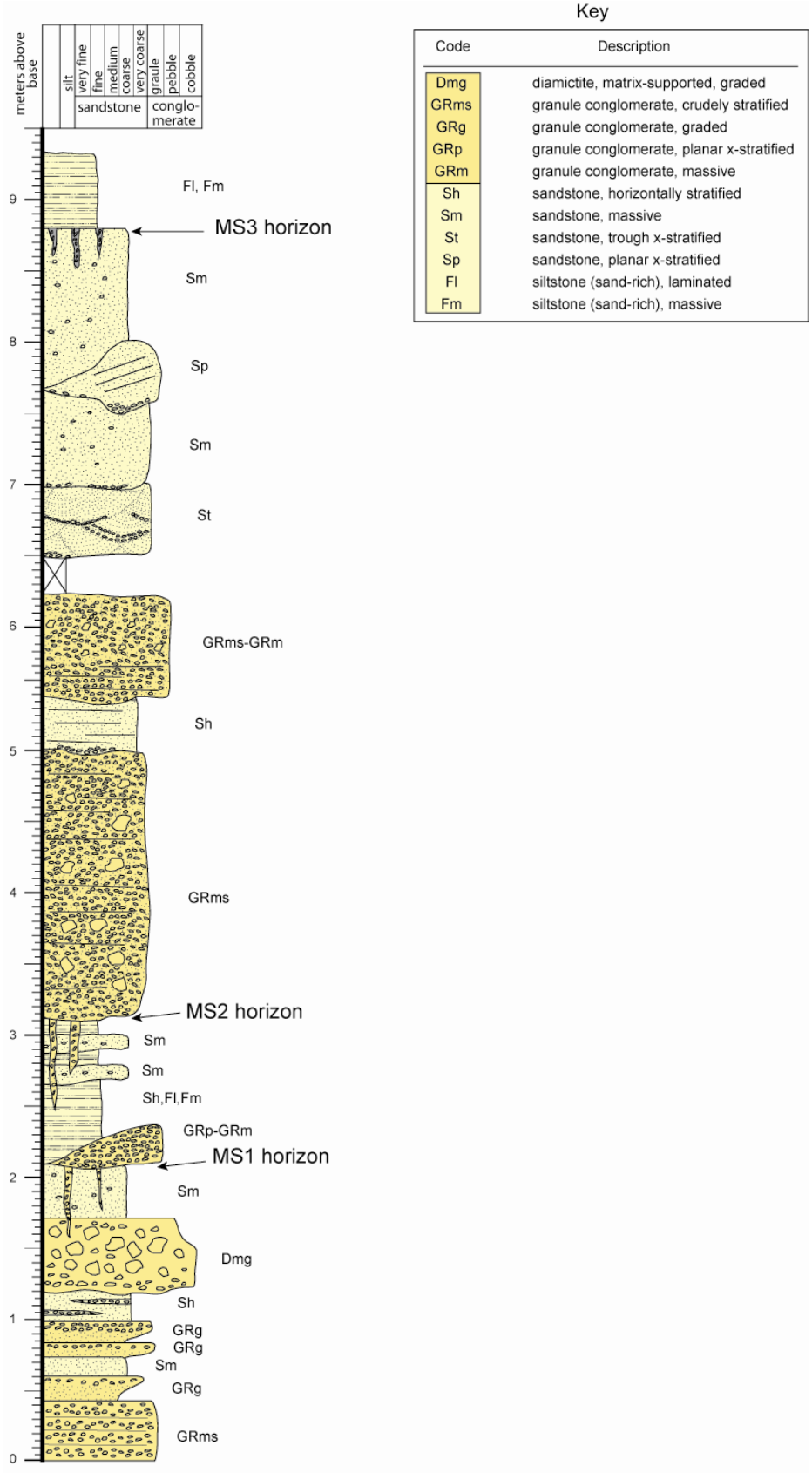
meters above base
silt
very fine
fine
medium
coarse
very coarse
granule
pebble
cobble
sandstone
conglo-merate
Fl, Fm
MS3 horizon
Sm
Sp
Sm
St
GRms-GRm
Sh
GRms
MS2 horizon
Sm
Sm
Sh,Fl,Fm
GRp-GRm
MS1 horizon
Sm
Dmg
Sh
GRg
GRg
Sm
GRg
GRms
0
1
2
3
4
5
6
7
8
9
Key
Code
Description
Dmg
diamictite, matrix-supported, graded
GRms
granule conglomerate, crudely stratified
GRg
granule conglomerate, graded
GRp
granule conglomerate, planar x-stratified
GRm
granule conglomerate, massive
Sh
sandstone, horizontally stratified
Sm
sandstone, massive
St
sandstone, trough x-stratified
Sp
sandstone, planar x-stratified
Fl
siltstone (sand-rich), laminated
Fm
siltstone (sand-rich), massive

We recognize a paleosol along the Fountain-Ingleside contact by the presence of downwardly bifurcating root traces, discrete clay and carbonate horizons, bleaching and a blocky ped structure. The pedogenic horizon is 50-75 cm thick where well developed, but the horizon is discontinuous, forming lentils approximately 70-150 m long that abut unaltered Fountain Formation (Fig. 3.4). The dominate pedogenic features are an illuviated clay horizon (10 cm thick), clay coatings on blocky peds and quartz grains, and abundant clay- and dolomite-filled veins. Secondary pedogenic features include rare dolomite- and clay-filled downwardly bifurcating casts (inferred as root casts), mottling, and small (<1 cm) dolomite nodules. Locally, relict bedding and original depositional texture is readily observable. In thin section, framework grains within pedogenic horizons are commonly supported by dolomite (Fig. 3.5), suggesting that displacive growth of carbonate occurred during pedogenesis. XRD analysis of the <2 μm fraction shows a dominance of muscovite, but chlorite is also present. We interpret this paleosol as a Calcic Protosol (classification of Mack et al., 1993).

Calcic protosol lentils abutting unaltered Fountain Formation (Fig. 3.4) is interpreted to represent original microtopography rather than erosional truncation because the unaltered Fountain Formation sits topographically higher and contains polygonal fractures. If the lentils were erosional remnants of a once through going paleosol, then the fractures should have been eroded as well, and the overlying Ingleside Formation should truncate the paleosol horizon instead of truncating the unaltered Fountain Formation (Fig. 3.4).

We focus on sand- and granule-filled fractures that occur at the Fountain-Ingleside contact and taper downward into the Fountain Formation. Fractures occur

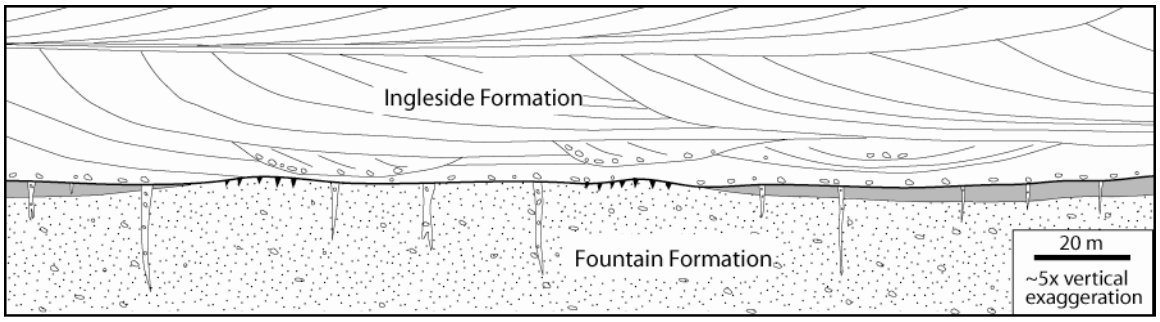

Figure 3.4: Schematic sketch of the Fountain-Ingleside contact at Loveland filtration showing the relationship between polygonal fractures (small black triangles), clastic wedges (large wedges) and pedogenic horizons (lenticular gray bodies). Note that the polygonal fractures occur only on unaltered Fountain Formation, whereas the clastic wedges penetrate both the pedogenic horizons and unaltered Fountain Formation. In addition, note that the paleosol is laterally juxtaposed on the Fountain Formation.

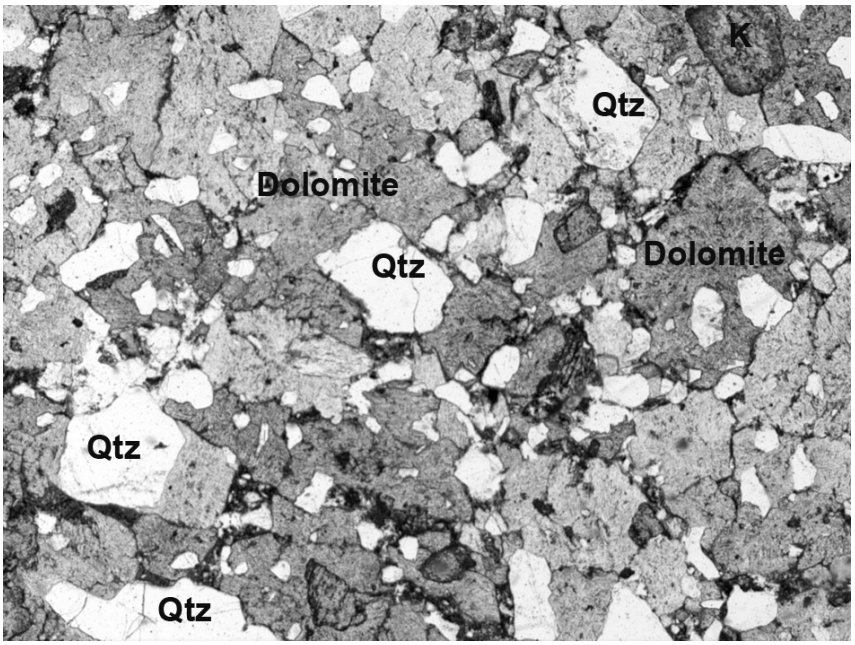

Figure 3.5: Photomicrograph of the paleosol located at the top of the Fountain Formation. Note that the clasts are supported by carbonate (dolomite). Qtz = quartz, K = Potassium feldspar. Photomicrograph is in plane-polarized light. Field of view is 3 mm.

within both the pedogenic horizon and unaltered Fountain Formation (Fig. 3.4). These fractures persist laterally along the Fountain-Ingleside contact for the length of the exposure (5 km).

Descriptions of Polygons and Wedges

Polygonal Fractures

Description—At the Manitou Springs and Loveland localities, downwardly tapering, bedding-discordant, sand- and granule-filled fractures form a polygonal pattern

on a bedding surface (Fig. 3.6). Pentagons predominate, with most dimensions in the 10^1 cm scale (Table 3.1). At both localities, grain-size distributions show abundant sand and gravel (>70%) with minor silt (<16%) and clay (<14%) (Fig. 3.7). At Manitou Springs, XRD analysis of the <2 μm fraction of both polygon interior and fracture fill shows a dominance of kaolinite with minor muscovite and chlorite. At both localities, petrographic observations indicate that both fracture fill and polygon interiors are grain supported with a framework mineralogy of quartz, feldspar and minor mica. Silica, clay and iron oxide cement is common and dolomite cement is present locally at the Loveland locality. At Manitou Springs, the fracture fill displays a microbrecciated texture which contrasts with the relatively loose packing and subangular clast shapes within the polygon interiors (Fig. 3.8a, b, c). At Loveland, the fracture fill is predominantly fine sand whereas the polygon interior is coarse to very coarse sand (Fig. 3.8d, e). At both localities, the fracture fill is poorly sorted, typically massive, and comprises material that resembles the overlying and/or adjacent strata.

At Manitou Springs, SEM analysis of surfaces of sand grains extracted from polygon fracture fill show the presence of high- to medium-relief subparallel linear fractures, linear steps, very angular features, conchoidal fracture faces and v-shaped percussion scars (as defined by Mahaney, 2002 and Krinsley and Doornkamp, 1973) (Fig. 3.9). These features are overprinted by dissolution etching, likely induced by later Fountain Formation diagenesis, as described by Hubert (1960) and/or Walker (1967).

Interpretation—The polygonal fractures described above are interpreted to be synsedimentary features because they: 1) are confined to discrete bedding planes, 2) form

Figure 3.6: Photographs of polygonal fractures. A) Sand- and granule-filled fractures forming a polygonal net on a bedding-plane surface within the Fountain Formation at Manitou Springs. B) Cross-sectional and plan view of polygonal fractures at Manitou Springs. C) Close-up of polygonal fracturing shown in A and B. Note pencil (13 cm long) for scale. D) Plan view of polygonal fractures at Loveland. E) Cross-sectional view of polygonal fracture fill at Loveland. Image taken at the same horizon as polygons displayed in D. F) Cross-sectional view of polygonal fractures at Loveland. Image taken from same horizon as D and E.

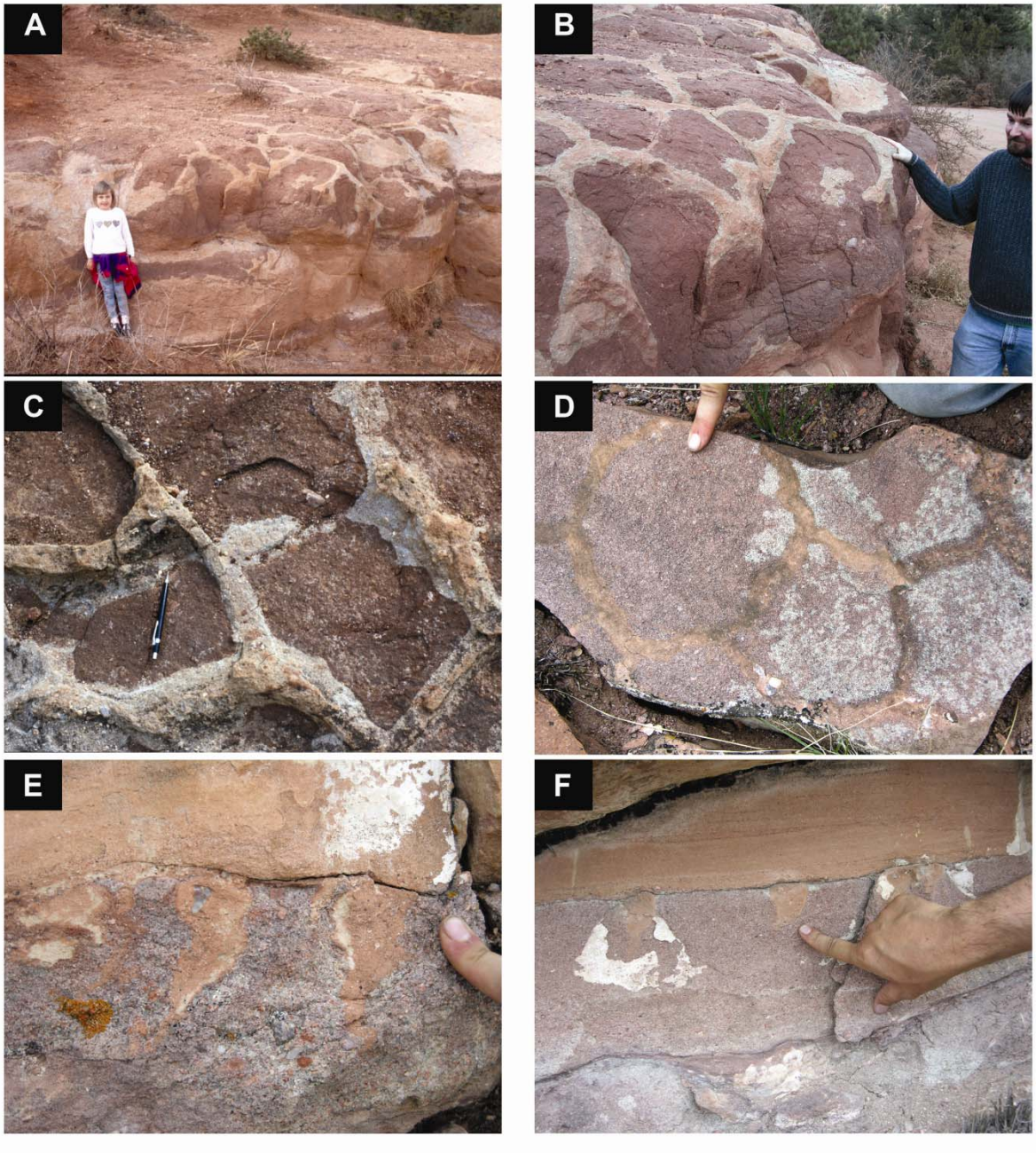
A
B
C
D
E
F

downwardly tapering wedges that originate at these discrete bedding planes, and 3) are filled with sediment derived from adjacent and suprajacent strata. At Loveland,

Table 3.1. Geometric relationships of polygons and clastic wedges

Feature	Plan view				Cross-sectional view								
	Polygon	Polygon width (cm)			Fracture depth (cm)			Fracture width (cm)			Depth/width ratio		
	n	Range	Mean	N	Range	Mean	N	Range	Mean	N	Range	Mean	N
Manitou Springs													
polygon wedges	4-6 sided	15-76	45	28	13-61	37	15	3-22	9	15	2-16	5.6	15
clastic wedges	N/A	N/A	N/A	N/A	63->220	123	6	10-55	24	7	6-7	6.5	6
Loveland Filtration													
polygon wedges	4-6 sided	7-25	16	23	2-10	6	27	1-8	5	25	9-3	1.4	25
clastic wedges	N/A	N/A	N/A	N/A	40->395	96	20	6-35	14	20	2-15	7.5	16
Other studies													
evaporite polygons *(Kocurek & Hunter, 1986)*	4 sided	60-590	180	58	10-150	60	36	10-180	10	38	0.1-14	3.4	35
ice-wedge polygons *(Johnson, 1990)*	4-6 sided	10^3->10^4	N/A	N/A	<250	150-200	N/A	<200	N/A	N/A	2-15	1.5-4	N/A
large dessication polygons *(Loope and Haverland, 1988)*	4 sided	$\geq 10^3$	N/A	N/A	≤200-570	N/A	N/A	1-18	N/A	N/A	45*	N/A	N/A
seasonal frost-crack polygons *(Maruszczak, 1987)*	4-6 sided	100	N/A	N/A	≤200	N/A	N/A	<50	N/A	N/A	>4*	N/A	N/A

* Calculations estimated by using the median fracture width and depth values of corresponding author(s)
N = number of measurments
Note: most values have been rounded to nearest whole number

petrographic comparison of the Ingleside Formation and polygonal fracture fill indicates that both contain abundant sub-rounded and well-sorted fine-grained sand, suggesting that the majority of the fill came from the overlying Ingleside Formation. Local granules likely were either sourced from the fracture walls or from the basal Ingleside Formation.

At Manitou Springs, the fracture fill is much coarser than the overlying unit (Fig. 3.3), and thus likely was sourced from the fracture wall. Furthermore, the angularity and

shattered texture of the fracture fill implies brecciation penecontemporaneous with the fracture-filling process. The linear steps, conchoidal fracture faces and subparallel linear

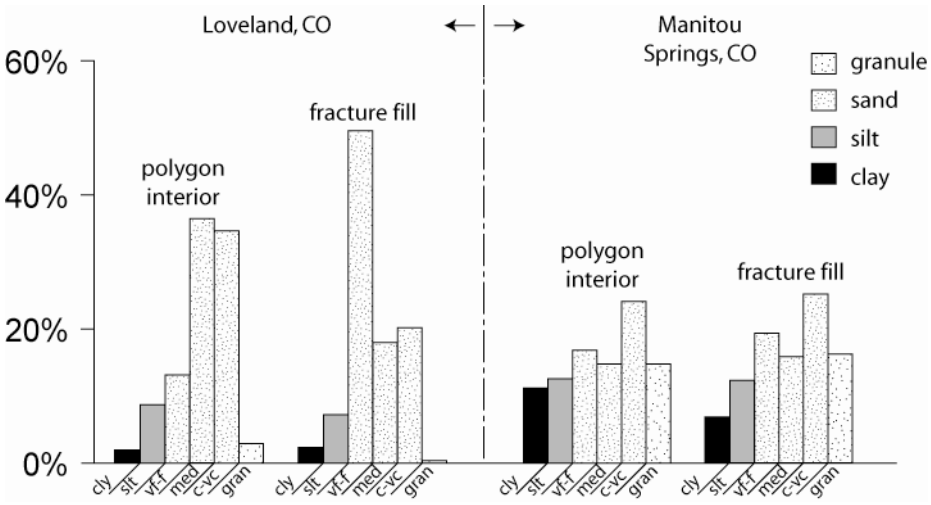

Figure 3.7: Sand-silt-clay percentages of polygon interiors and sand-filled fractures at Manitou Springs and Loveland. cly = clay, slt = silt, vf-f = very fine to fine sand, med = medium sand, c-vc = coarse to very coarse sand, gran = granule

Figure 3.8: A) Photomicrograph of polygonal fracture fill at Manitou Springs study site. Note the angular and shattered clasts. Photomicrograph is in plane light. Horizontal field of view is 3 mm. B) Magnification of fracture fill at the Manitou Springs study site. Note the comminuted quartz comprising the groundmass. Horizontal field of view is 1.2 mm. C) Photomicrograph of polygonal interior at Manitou Springs study site. Photomicrograph is in plane light. Horizontal field of view is 3 mm. D) Photomicrograph of polygonal fracture fill at the Loveland study site. Photomicrograph is in plane light. Horizontal field of view is 3 mm. E) Photomicrograph of the contact between clastic wedge fill (fine-grained, well-sorted material to lower right) and the hosting strata at the Loveland study site. Note the framework-supported grains within the hosting strata (lower right). Photomicrograph is in plane light. Horizontal field of view is 3 mm. F) Photomicrograph of the Ingleside Formation. Note the well-sorted and rounded material similar to Figure 9D and 9E. Photomicrograph is in plane light. Field of view is 3 mm. Note for all photomicrographs, Qtz = quartz, P = plagioclase, K = potassium feldspar.

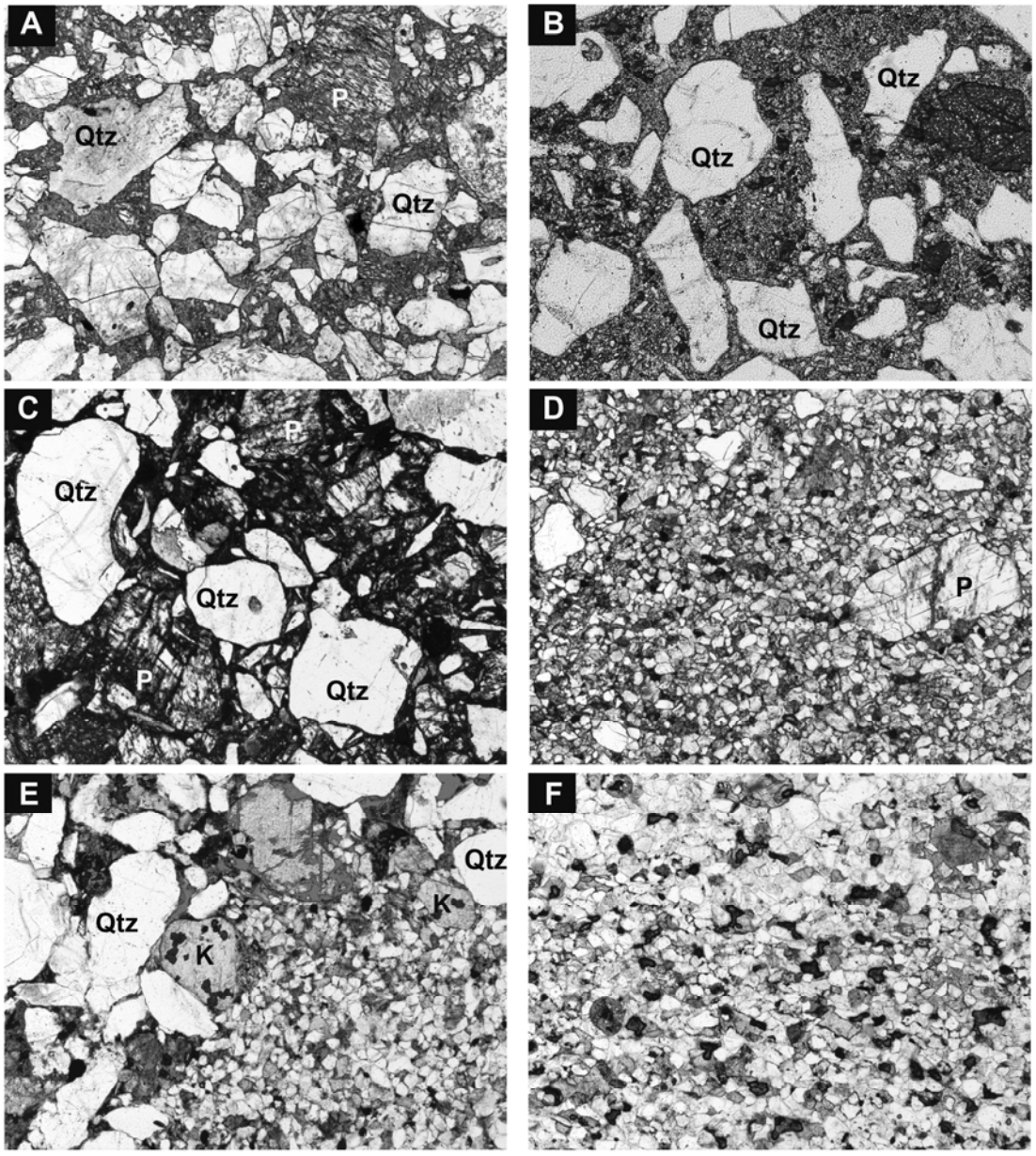
A
Qtz
P
Qtz
B
Qtz
Qtz
Qtz
C
P
Qtz
Qtz
P
Qtz
D
P
E
Qtz
Qtz
K
K
F

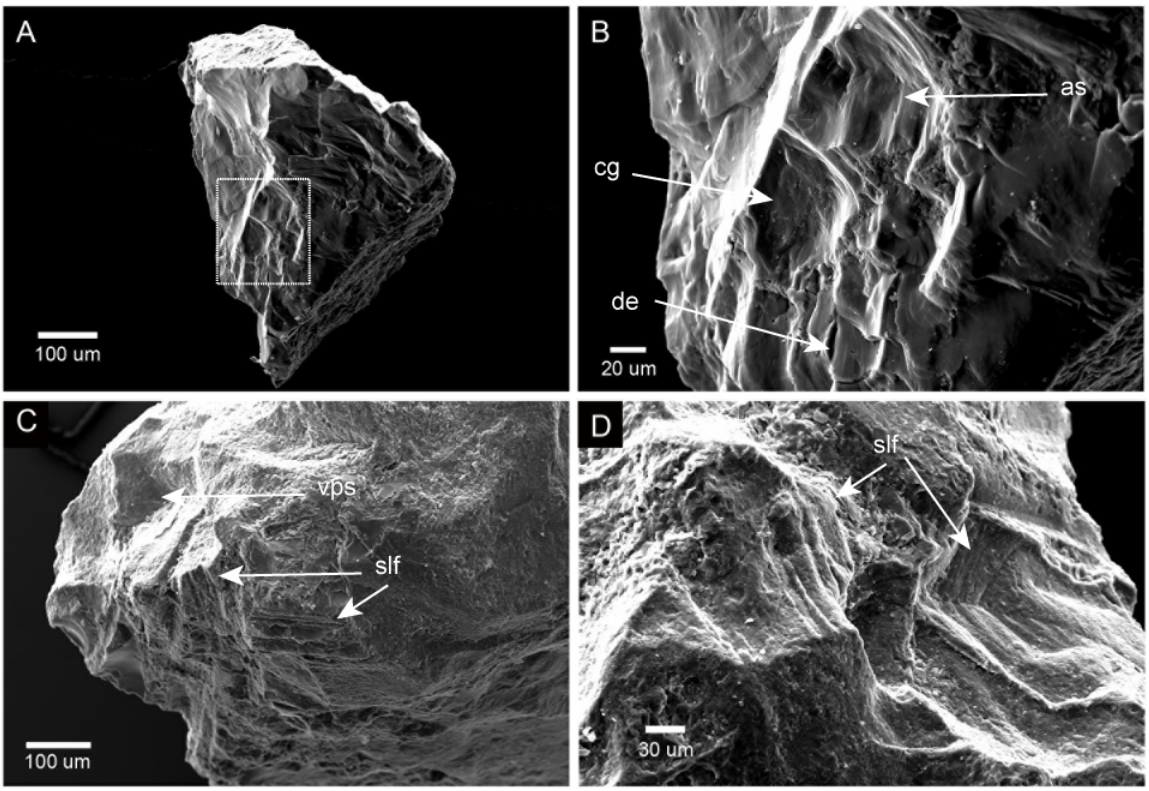

Figure 3.9: SEM image of a quartz sand grain from polygonal fracture fill. A) Very angular grain displaying conchoidal fracturing on the left face. B) Close-up of the conchoidally fractured face in A. The image displays crescentic gouges (cg) and linear or arc-shaped steps (as) at center and center-top, respectively. Note the dissolution and mineral precipitation on these structures indicating they were formed before dissolution occurred. C) Medium relief, sub-parallel linear fractures (slf) and v-shaped percussion scars (vps) overprinted by dissolution. D) Sub-parallel linear fractures (slf) and linear steps overprinted by dissolution.

fractures observed on sand-grain surfaces are consistent, but not exclusive to, textures formed by frost shattering (Coudé-Gaussen and Lautridou, 1987) and/or crushing (e.g. Krinsley and Doornkamp, 1973; Mahaney, 2002). The v-shaped percussion scars and sub-rounded edges are most consistent with a fluvial environment (Mahaney, 2002). The presence of dissolution features on fracture surfaces suggests that these features are indeed a primary product and not induced by sample preparation.

Clastic Wedges

Description—In addition to the polygonal fractures described above, a larger-scale set of sand and granule-filled fractures, here termed clastic wedges, occur at both study sites and are observable only in cross-section (Fig. 3.10). The clastic wedges originate at the same stratigraphic horizon or are confined to nearby stratigraphic horizons (Fig. 3.3, 3.4). At both localities, the wedges are oriented at a high angle to bedding, taper downward into both single and multiple vertices, and have nearly parallel fracture walls. Dimensions of the wedges range from 10^1-10^2 cm scale (Table 3.1). In most cases, the deeper the wedge, the farther the spacing between wedges. Fracture fill closely resembles the overlying strata and is poorly sorted and typically massive; rarely however, a weak foliation is visible subparallel to fracture walls. Laminae within host strata are rare, but where present they commonly are truncated and rarely bent upward at wedge walls (Fig. 3.10d, g). At Loveland, grain-size distribution of the hosting Fountain Formation and wedge fill are similar with >80% sand and gravel and <3.5% clay (Fig. 3.7). Wedge trends at both study localities show a wide range of orientations (Fig. 3.11). At Loveland, wedges locally intersect on bedding plane surfaces at angles ranging from 90-120°. At Loveland, thin-section analyses indicate that both the fracture fill and

hosting strata are framework supported (Fig. 3.8d, e). In addition, the fracture fill contains abundant subrounded, fine-grained sand, whereas the host stratum is predominantly medium to very coarse-grained sand (Fig. 3.7). Dolomite, clay and hematite cements are present.

Interpretation— The clastic wedges likely are genetically related to the smaller polygonal patterns because both features are: 1) confined to the same horizon or nearby stratigraphic horizons (Fig. 3.3,3.4), 2) filled with sediment that resembles adjacent and/or suprajacent strata (compare Fig. 3.8d, f) and 3) arranged in a similar polygonal pattern because intersections of individual fractures were observed locally and measured trends show a wide scatter in fracture orientations. The actual shape of these polygons is unclear because measured trends suggest a rectangular shape (Fig. 3.11), but observed intersections were often >90°, suggesting a pentagonal or hexagonal shape.

Fracturing Mechanism

In general, polygonal cracking results from volume reduction related to thermal contraction or desiccation. Within continental clastic environments such features form related to 1) periodic temperature drops of already frozen ground (either seasonal or diurnal) resulting in ice-wedge, sand-wedge or frost-crack polygons (e.g Lachenbruch, 1962; Péwé et al., 1969; Black, 1976; Washburn, 1980a, 1980b; Hastenrath, 1981, 1984; Williams, 1986, 2001; Maloof et al., 2002), 2) desiccation resulting in mudcracks (e.g. Neal et al., 1968; Neal, 1978), and 3) thermal contraction and expansion of interstitial evaporite minerals (e.g. Evans et al., 1969; Watson, 1985).

Figure 3.10: Photographs of clastic wedges. A) Clastic wedge along the MS1 horizon at Manitou Springs. B) Clastic wedges at Manitou Springs. Host strata is a muddy stratified conglomerate laterally correlative to the MS1 horizon shown on Figure 3.3. C) Clastic wedge at Manitou Springs along the MS2 horizon. Clastic wedge is hosted within massive sandstone and conglomerate. Note lens cap for scale. D) Clastic wedge at Manitou Springs along the MS1 horizon. Note the slight upturning of bedding along wedge edge indicated by white arrow. E) Clastic wedge penetrating Fountain Formation at the Loveland study site. Hammer is ~ 30 cm. F) Close-up of wedge shown in D. Note that the wedge fill consists of granules and pebbles floating in fine sand. G) Clastic wedge at Loveland study site showing truncations of host strata laminae against wedge edge. H) Clastic wedge penetrating the Calcic Protosol at the Loveland study site.

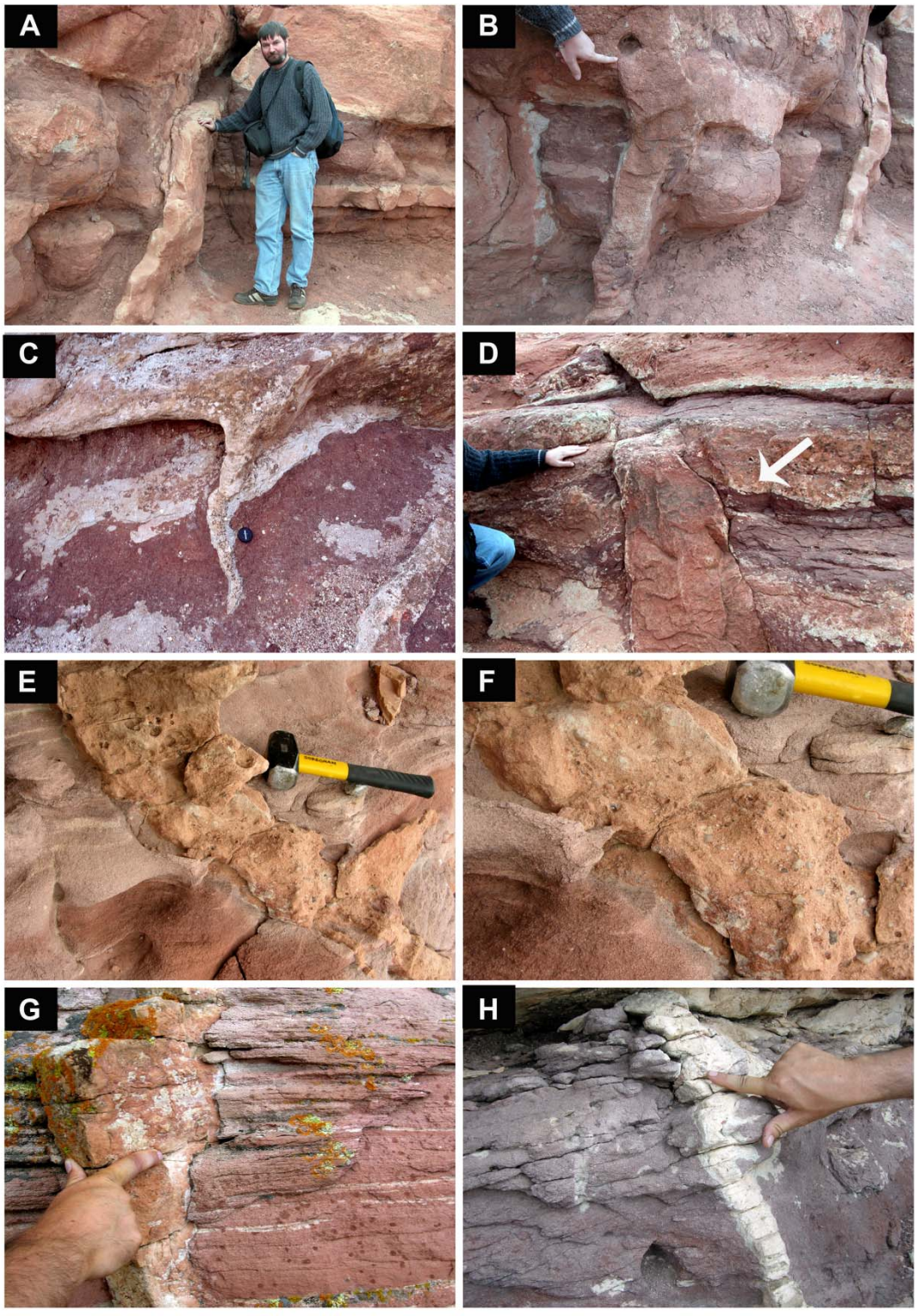
A
B
C
D
E
F
G
H

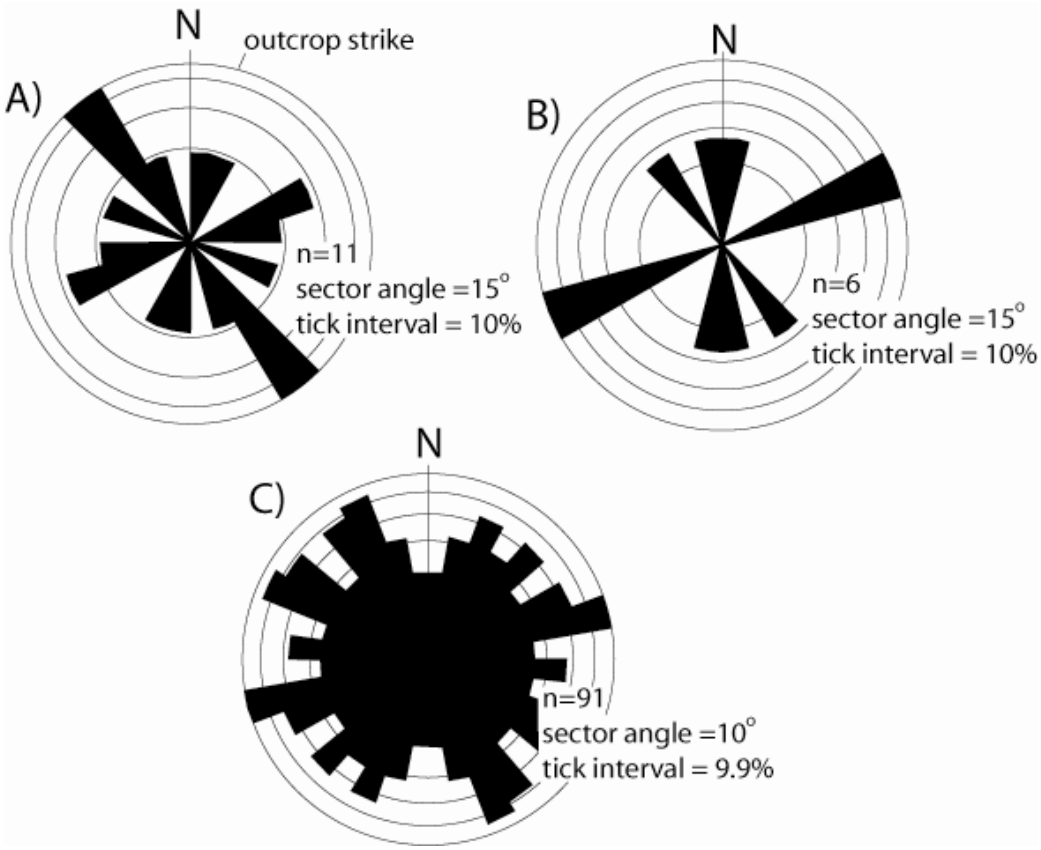

Figure 3.11: Area-weighted rose diagrams of fracture trends. A) Clastic wedges at Loveland. Note the relative paucity of measured trends subparallel to outcrop strike. B) Clastic wedges at Manitou Springs. C) Polygonal fractures at Manitou Springs.

Desiccation is typically inferred for polygonal fracturing in clay-rich strata because clay minerals undergo volume reduction upon desiccation and provide the cohesion necessary to maintain the polygonal shape. In experiments on desiccation cracking, the addition of > 50% of sand- to gravel-sized sediment precludes desiccation cracking (Kindle, 1917; Fellows, 1951) because clasts (e.g. quartz, feldspar, lithics) provide a rigid framework strong enough to withstand tensional stresses created through desiccation. Additionally, natural mudcracks terminate at deeper, sandy substrates (Weinberger, 2001). Thus, a desiccation mechanism is untenable for the polygonal fracturing reported here because all localities contain ≥ 70% sand and gravel and are framework supported.

Polygonal cracking in evaporite-rich sediment is often attributed to thermal strain because the coefficients of volume expansion of evaporite minerals (e.g. ≥ 72.6 x 10^{-6}/°C) are sufficient to produce cracks at typical surface temperatures (Kocurek and Hunter, 1986). This mechanism requires that evaporite minerals form a sufficient volume of the sediment to enable framework grains to float in an evaporite matrix (e.g. Kocurek and Hunter, 1986 and Loope and Haverland, 1988). As noted above, however, fracture fill and hosting strata reported here are all framework-grain supported, show no evidence of diagenetic leaching of grains and contain no evaporite minerals nor pseudomorphs. In addition, evaporites have not been reported anywhere within the Fountain Formation. Thus, thermal expansion and contraction of evaporitic minerals is not a likely method of fracturing for this system.

At high- and moderate latitudes today, polygonal cracking occurs as a result of rapid seasonal (winter) cooling of already frozen ground (Lachenbruch, 1962, 1966;

Mackay, 1974). However, seasonal temperature variations at low latitudes are minimal under the Earth's current obliquity configuration. Thus, temperature variations at low latitudes could result only from diurnal change, or a high obliquity orbit (≥ 54° compared to 22-24.5° today; Maloof et al., 2002; Williams and Schmidt, 2004). *A priori* it seems unlikely for the Earth to tilt to high obliquity and then realign to modern configurations on a time frame consistent with the formation of polygonal cracking on a discrete surface. However, Maloof et al. (2002) predicted that diurnal temperature variations are sufficient to enable crack penetration of >0.5 m if the ground remains continuously frozen. Today, polygonal contraction cracks occur in sandy material at high altitudes in equatorial regions as a result of diurnal temperature fluctuations of ~20°C and mean annual temperature of ~2°C (Hastenrath, 1981, 1984).

We interpret the sand- and granule-filled polygonal fractures reported here as the result of repeated cooling under a strong diurnal cycle (10-25°C day/night variation) and low ground temperatures (<0°C). We infer that the microbrecciated texture of the fracture-fill material at Manitou Springs reflects repeated movement within cracks, consistent with repeated fracturing. Furthermore, SEM microtextural analysis of surfaces of quartz sand from fracture fills show a prevalence of shattered and/or crushed textures suggesting frost shattering (Coudé-Gaussen and Lautridou, 1987) and/or localized ice-segregation fracturing (Murton et al., 2006). The original microtopography observed in the paleosol along the Fountain-Ingleside contact at the Loveland locality is consistent with frost heaving. Modern frost-heaved regions generate microtopography in soils by channeling surface and near-surface water towards topographic lows, thereby enhancing pedogenesis (e.g. Johnson, 1990; Engstrom et al., 2005). Other polygonal fractures

contained in coarse-clastic, quartzose strata of Precambrian age lacking in calcareous or evaporite cement have also been interpreted as freeze-thaw cracks (e.g. Deynoux, 1985, Williams, 2001; Spencer, 1971; Edwards, 1975)

Elevation and Duration of Polygonally Fractured Surfaces

At Manitou Springs, the polygonally fractured surfaces occur within an inferred braided-river succession. Suttner et al. (1984) indicated that correlative marine strata occur a few kilometers away and marine strata are present ≤ 25 m stratigraphically below these surfaces. Accordingly, barring significant uplift in the time recorded by the intervening strata, these surfaces may have formed very near sea level. Maximum reasonable stream gradients (~0.02, Boothroyd and Ashley, 1973) between the polygonally fractured surfaces and the estimated shoreline (gauged from shallow-marine deposits of the Denver basin; Rascoe and Baars, 1972) suggest an absolute maximum elevation of 1800 m. Thus, the fracturing occurred on surfaces located at <1800 m elevation. By comparison, Quaternary ice at the equator reached elevations as low as 2850 m and corresponding periglacial environments at even lower elevations (Downie and Wilkinson, 1972; Mahaney, 1990; Porter, 2001).

Seasonal thermal-contraction cracks are relatively small (<2 cm) upon formation and only 8-75% will crack the subsequent year (Mackay, 1974). Fracture growth up to meters wide occurs from recurrent fracturing along previously formed fractures in subsequent winters and infilling of those fractures in subsequent summers (e.g. Lachenbruch, 1962; Black, 1976). Rates of growth are quite variable, but 1 mm/year is a conservative number based on modern seasonal cracking (Washburn, 1980a). Employing

estimates from data on seasonal cracking, the polygonal fractures reported here record surfaces that were stable on the order of $\leq 10^3$-10^5 years, however diurnal cracking should require less time. These are rough estimates and show that it is unlikely the polygonal fractures were forming over more than a 10^5 year time-frame.

Paleoclimatic Implications

Most analytical and field studies demonstrate that thermal cracking occurs when already frozen ground (<0°C) experiences further cooling (e.g. Lachenbruch, 1962, 1966; Péwé, et al., 1969; Mackay, 1974; Maloof et al., 2002). Modern high-latitude cracks arrest downward in deeper layers that retain heat from the previous summer (Lachenbruch, 1962). With diurnal temperature swings of 10-25°C, stress is restricted to the upper 16 cm and cracks would penetrate no farther if the soil profile was not completely frozen (Maloof et al., 2002). However, if the ground is completely frozen, then fractures can propagate ≥ 0.5 m deep (Maloof et al., 2002). Thus, we infer that ground temperatures, during the formation of the polygonally fractured surfaces reported here, were <0°C to depths of 2-4 m because most crack depths are >16 cm and <4 m (Table 3.1). Curiously, the Fountain Formation lacks undulation and/or slumping, a common feature formed by melting of frozen ground (e.g. Black, 1976; Vliet-Lanoë et al., 2004). The simplest explanation for this is that the hosting stratum was massive and/or lacked high water content (Fig. 3.3, 3.4).

Comparison of the two localities suggests that conditions during the formation of the polygonal fractures at Manitou Springs were wetter than those that prevailed at Loveland. At Loveland, the fracture fill consists of subrounded fine sand (Fig. 3.7, 3.8d)

from the overlying eolian Ingleside Formation. Furthermore, the polygonally fractured horizon is stratigraphically associated with a Calcic Protosol (Fig. 3.4, 3.5). These data suggest that the soil profile at the Loveland locality was not saturated and surface conditions were sufficiently dry to enable eolian transport. At the Manitou locality, however, SEM textures of sand grain surfaces suggest shattering. Recently, Murton et al. (2006) have shown experimentally that films of water occur between growing ice lenses and rock surfaces that obtain pressure sufficient to fracture rocks; however for this to occur, a supply of water must be available in the soil profile, consistent with a wet profile at the Manitou locality.

These differences in fracture fill reflect different paleoclimatic conditions and, thus probably different ages for these strata. The relative age of the two localities cannot be determined with confidence (Fig. 3.2, 3.12), but it is likely that the polygonal surfaces at the Manitou Springs are latest Atokan-Missourian because of the close stratigraphic association with Glen Eyrie member (Chronic and Williams, 1978; Suttner et al., 1984); whereas, the polygonal fractures at the Loveland locality are likely Virgilian because of the close stratigraphic association with the Ingleside Formation (Maughan and Albrandt, 1985). The polygonally fractured surfaces reported here occurred during a time when temperatures at this low latitude site were remarkably cold at relatively low elevation and possibly correlative with a maximum in ice development during the late Paleozoic icehouse (Veevers and Powell, 1987; Frakes et al., 1992; Gonzalez and Eyles, 1995; Crowell, 1999; Mii et al., 1999, 2001; Isbell et al., 2003; Fig. 3.12). Thus, better age constraints on these polygonally fractured surfaces may provide constraints on timing of ice development during the late Paloezoic icehouse.

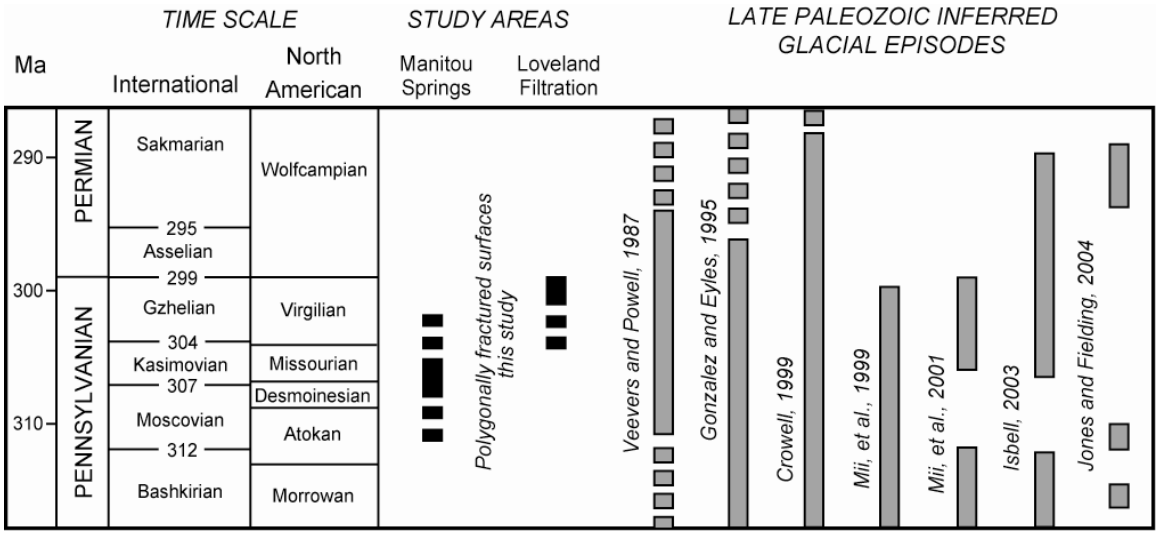

Figure 3.12: Correlation chart of possible timing of formation of thermally contracted polygonal surfaces reported in this paper, denoted by vertical black bars, and inferred glacial maximums from various workers, denoted by vertical gray bars. Timescale is from Gradstein et al., 2004.

Conclusions

Sand- and gravel-filled polygonal fractures described from the Pennsylvanian-Permian Fountain Formation are the result of low ground temperatures (<0°C) subjected to diurnal temperature swings of 10-25°C. These fractures occurred on surfaces stable for 10^3-10^5 years and at elevations ≤ 1800 m. The geometry, fill, and textural characteristics indicate that the Loveland locality formed polygonal fractures under conditions that were drier than those that prevailed at the Manitou Springs locality and most likely formed at

different times. Thus, the east flank of the ancestral Front Range experienced at least two discrete episodes of remarkably cold temperatures in this equatorial lowland environment.

Acknowledgments

This research was supported by National Science Foundation grant EAR-0230332 (to Lynn Soreghan), Sigma Xi Grants-in-Aid of Research, and Geological Society of America student grant. I thank George Morgan, Robert Conlon and Margaret Landis of the University of Oklahoma for electron microprobe, X-ray diffraction and scanning electron microscopy, respectively. Discussions with Ze'ev Reches and Charles Gilbert of the University of Oklahoma helped with many of the ideas presented here. Lastly, I am grateful to Kurt Schroeder (City of Colorado Springs Parks Department) and Johhny Tuxhorn (City of Loveland, Colorado) for access and sampling permission in the study sites.

References

Black, R.F., 1976. Periglacial features indicative of permafrost: ice and soil wedges. Quaternary Research, 6: 3-26.

Boothroyd, J.C. and Ashley, G.M., 1975. Process, bar morphology, and sedimentary structures on braided outwash fans, northeastern Gulf of Alaska. In: Jopling, A.V. and McDonald, B.C. (eds.), Glacio-fluvial and glaciolacustrine sedimentation. Society of Economic Paleontologists and Mineralogists Special Paper 23, pp. 193-222.

Chronic, B.J. and Williams, C.A., 1978. The Glen Eyrie Formation (Carboniferous) near Colorado Springs. In: Pruitt, J.D. and Coffin, P.E. (Eds.), Energy Resources of the Denver Basin: Rocky Mountain Association of Geologists field conference guidebook, pp. 199-206.

Coudé-Gaussen, G. and Lautridou, J.P., 1987. SEM characterization of microfeatures on frost shattered quartz grains. In: Pécsi, M. and French, H.M. (Eds.), Loess and periglacial phenomena. Akadémiai Kiadó, Budapest, pp. 253-261.

Crowell, J.C., 1999. Pre-Mesozoic ice ages: their bearing on understanding the climate system. Geological Society of America Memoir 192, 106 pp.

Deynoux, M., 1985. Periglacial polygonal structures and sand wedges in the late Precambrian glacial formations of the Taoudeni Basin in Adrar of Mauretania (West Africa). Palaeogeography, Palaeoclimatology, Palaeoecology, 39: 55-70.

Downie, C. and Wilkinson, P., 1972. The Geology of Kilamanjaro. University of Sheffield, U.K., 253 pp.

Edwards, M., 1975. Glacial retreat sedimentation in the Smalfjord Formation, late Precambrian, North Norway. Sedimentology, 22: 75-94.

Engstrom, R., Hope, A., Kwon, H., Stow, D. and Zamolodchikov, D., 2005. Spatial distribution of near surface soil moisture and its relationship to microtopography in the Alaskan Arctic Coastal Plain. Nordic Hydrology, 36: 219-234.

Evans, G., Schmidt, V., Bush, P., and Nelson, H., 1969. Stratigraphy and geologic history of the sabkha, Abu Dhabi, Persian Gulf. Sedimentology, 12: 145-159.

Fellows, R.H. Jr., 1951. Experiments in the formation of desiccation cracks sediments. M.S. Thesis, Southern Methodist University, Dallas, Texas, 67 pp.

Folk, R.L., 1974. Petrology of sedimentary rocks. Hemphill Publishing, Austin, Texas, 184 pp.

Frakes, L.A., Francis, J.E., and Syktus, J.I., 1992. Climate Modes of the Phanerozoic. Cambridge University Press, Cambridge, U.K., 274 pp.

Golonka, J., Ross., M.I. and Scotese, C.R., 1994. Phanerozoic paleogeographic and paleoclimatic modeling maps. In: Embry, A.F., Beauchamp, B., and Glass, D.J. (Eds.), Global Environments and Resources. Canadian Society of Petroleum Geologists Memoir 17, pp. 1-47.

Goldberg, M., 1967. Supratidal dolomitization and dedolomitization in Jurassic rocks of Hamakhtesh Haqatan, Israel. Journal of Sedimentary Petrology, 37: 760-773.

Gonzalez-Bonorino, G. and Eyles, N. 1995. Inverse relation between ice extent and the late Paleozoic glacial record of Gondwana. Geology, 23: 1015-1018.

Gradstein, F.M., Ogg, J.G., Smith, A.G., Bleeker, W. and Lourens, L.J., 2004. A new geologic time scale, with special reference to Precambrian and Neogene. Episodes, 27: 83-100.

Hastenrath, S.H., 1981. The Glaciation of the Ecuadorain Andes. A.A. Balkema, Rotterdam, Netherlands, 159 pp.

Hastenrath, S.H., 1984. The Glaciers of Equatorial East Africa. D Reidel Publishing, Dordrecht, Netherlands, 353 pp.

Hubert, J.F., 1960. Petrology of the Fountain and Lyons Formations, Front Range, Colorado. Colorado School of Mines Quarterly, 55: 1-242.

Isbell, J.L., Miller, M.F., Wolfe, K.L., and Lenaker, P.A., 2003. Timing of Late Paleozoic glaciation in Gondwana: was glaciation responsible for the development of northern hemisphere cyclothems? In: Chan, M.A. and Archer, A.W. (eds.),

Extreme depositional environments: mega end members in geologic time. Geological Society of America Special Paper 370, pp. 5-24.

Janitzky, P., 1986. Laboratory methods: citrate-bicarbonate-dithionite (CBD) extractable iron and aluminum. In: Singer, M.J. and Janitzky, P. (eds.), Field and Laboratory Procedures used in a Soil Chronosequence Study. U.S. Geological Survey Bulletin, Report: B 1648, pp. 38-41.

Johnson, W.H., 1990. Ice-wedge casts and relict patterned ground in central Illinois and their environmental significance. Quaternary Research, 33: 51-72.

Jones, A.T. and Fielding, C.R., 2004. Sedimentological record of the late Paleozoic glaciation in Queensland, Australia. Geology, 32: 153-156.

Katasonov, E.M., 1973. Classification of frost-caused phenomena with references to the genesis of the sediments in central Yakutia. Biuletyn Peryglacjalny, 21: 71-80.

Kindle, E.M., 1917. Some factors affecting the development of mud-cracks. Journal of Geology, 25: 135-144.

Kluth, C.F. and Coney, P.J., 1981. Plate tectonics of the Ancestral Rocky Mountains. Geology, 9: 10-15.

Kocurek, G. and Hunter, R.E., 1986. Origin of polygonal fractures in sand, uppermost Navajo and Page sandstones, Page, Arizona. Journal of Sedimentary Petrology, 56: 895-904.

Krinsley, D.H. and Doornkamp, J.C., 1973. Atlas of sand grain surface textures. Cambridge University Press, Cambridge, U.K., 91 pp.

Lachenbruch, A.H., 1962. Mechanics of thermal contraction cracks and ice-wedge polygons in permafrost. Geological Society of America Special Paper 7, 69 pp.

Lachenbruch, A.H., 1966. Contraction theory of ice-wedge polygons: A qualitative discussion. Permafrost Internation Conference Proceedings, National Academy of Science/national Research Council Publication 1287, pp. 63-71.

Langford, R.P. and Fishbaugh, D.A., 1984. Sedimentology of the Fountain fan-delta complex near Manitou Springs, Colorado. In: Suttner, L.J., (ed.), Sedimentology of the Fountain Fan-delta Complex near Manitou Springs and Canon City, Colorado. Society of Economic Paleontologists and Mineralogists field guidebook, pp. 1-30.

Loope, D.B. and Haverland, Z.E., 1988. Giant desiccation fissures filled with calcareous eolian sand, Hermosa Formation (Pennsylvanian), southeastern Utah. Sedimentary Geology, 56: 403-413.

Mack, G.H., James, W.C. and Monger, H.C., 1993. Classification of Paleosols. Geological Society of America Bulletin 105: 129-136.

Mackay, J., 1974. Ice-wedge cracks, Garry Island, Northwest Territories. Canadian Journal of Earth Science, 11: 1366-1383.

Mahaney, W.C., 1990. Ice on the Equator: Quaternary Geology of Mount Kenya, East Africa. Wm Caxton, Sister Bay, Wisconsin, 386 pp.

Mahaney, W.C., 2002. Atlas of Sand Grain Surface Textures and Applications. Oxford University Press, Oxford, U.K, 256 pp.

Mahaney, W.C., Vortsich, W. and Julig, P.J., 1988. Relative differences between glacially crushed quartz transported by mountain and continental ice, some examples from North America and East Africa. American Journal of Science, 288: 810-826.

Maher, J.C., 1953. Permian and Pennsylvanian rocks of southeastern Colorado. American Association of Petroleum Geologists, 37: 913-939.

Maloof, A.C., Kellogg, J.B., and Anders, A.M., 2002. Neoproterozoic sand wedges: crack formation in frozen soils under diurnal forcing during a snowball Earth. Earth and Planetary Science Letters, 204: 1-15.

Maruszczak, H., 1987. Problems of paleogeographic interpretation of ice wedge casts in European loesses. In. Pécsi, M. and French, H.M. (Eds.), Loess and periglacial phenomena. Akadémiai Kiadó, Budapest, pp. 285-302.

Maughan, E.K., and Ahlbrandt, T.S., 1985. Pennsylvanian and Permian eolian sandstone facies, northern Colorado and southeastern Wyoming. In: Macke, D.L. and Maughan, E.K. (Eds.), Rocky Mountain Section Field Trip Guide Book. RMS-AAPG, RMS-SEPM, NEMD, RMAG, pp. 99-113.

Mehra, O.P. and Jackson, M.L., 1960. Iron oxide removal from soils and clays by a citrate-dithionite system buffered by sodium carbonate. Clays and Clay Mineralogy, 7: 317-327.

Mii , H. Grossman, E.L. and Yancey, T.E., 1999. Carboniferous isotope stratigraphies of North America: implications for Carboniferous paleooceanography and Mississippian glaciation. Geological Society of America Bulletin, 111: 960-973.

Mii , H. Grossman, E.L., Yancey, T.E., Chuvashov, B. and Egorov, A., 2001. Isotopic records of brachiopod shells from the Russian Platform: evidence for the onset of Mid-Carboniferous glaciation. Chemical Geology, 175: 133-147.

Murton, J.B., Peterson, R. and Ozouf, J.C., 2006. Bedrock fracture in ice segregation in cold regions. Science, 314, 1127-1129.

Neal, J.T., 1978. Mudcracks (contractional polygons). In: Fairbridge, R.W. and Bourgeois, J. (Eds.), Encyclopedia of Sedimentology. Dowden, Hutchinson and Ross, Stroudsberg, Pennsylvania., pp. 486-488.

Neal, J.T., Langer, A.M., and Kerr, P.F., 1968. Giant desiccation polygons of Great Basin playas. Geological Society of America Bulletin, 79: 69-90.

Parrish, J.T., 1998. Interpreting the pre-Quaternary climate from the geologic record. Columbia University Press, New York, NY, 338 pp.

Péwé, T.L., Church, R.E. and Andresen, M.J., 1969. Origin and paleoclimatic significance of large-scale patterned ground in the Donnelly Dome area, Alaska. Geological Society of America Special Paper 103, 87 pp.

Porter, S.C., 2001. Snowline depression in the tropics during the last glaciation. Quaternary Science Reviews, 20: 1067-1091.

Rascoe, B.R. Jr. and Baars, D.L., 1972. Permian System. In: Mallory, W.W. (ed.), Geologic Atlas of the Rocky Mountain Region. Rocky Mountain Association of Geologists, pp. 143-165.

Schatz, B.A., 1986. Depositional environments of the Upper Fountain and Ingleside Formations between Lyons and Loveland, Colorado. Master's Thesis, University of Colorado, Boulder, Colorado.

Scotese, C.R., 1999. *PALEOMAP* Animations 'Paleogeography', PALEOMAP Project. Department of Geology, University of Texas at Arlington, Arlington, Texas.

Seppälä, M., 2004. Wind as a geomorphic agent in cold climates. Studies in Polar Research, Cambridge University Press, Cambridge, UK., 385 pp.

Spencer, A., 1971. Late Precambrian glaciation in Scotland. Geologic Society of London Memoir 6, 100 pp.

Suttner, L.J., Langford, R.P., and O'Connell, A.F., 1984. New interpretation of the stratigraphic relationship between the Fountain Formation and its Glen Eyrie Member. In: Suttner, L.J., (Ed), Sedimentology of the Fountain fan-delta complex near Manitou Springs and Canon City, Colorado. Society of Economic Paleontologists and Mineralogists field guidebook, pp. 31-61.

Thompson, W.O., 1949. Lyons sandstone of Colorado Front Range. American Association of Petroleum Geologists Bulletin, 33: 52-72.

Trimble, D.E. and Machette, M.N., 1979. Geologic map of the Colorado Springs-Castle Rock area, Front Range urban corridor, Colorado. USGS Map I-857-F, 1:100,000.

Veevers, J.J. and Powell, C.McA., 1987. Late Paleozoic glacial episodes in Gondwanaland reflected in transgressive-regressive depositional sequences in Euramerica. Geological Society of America Bulletin, 98: 475-487.

Vliet-Lanoë, B.v., Magyari, A., and Meilliez, F., 2004. Distinguishing between tectonic and periglacial deformations of Quaternary continental deposits in Europe. Global and Planetary Change, 43: 103-127.

Walker, T.R., 1967. Formation of red beds in modern and ancient deserts. Geological Society of America Bulletin, 78: 353-368.

Washburn, A.L., 1980a. Permafrost features as evidence of climatic change. Earth-Science Reviews, 15: 327-402.

Washburn, A.L., 1980b. Geocryology. John Wiley & Son, New York, NY, 406 pp.

Watson, A., 1985, Structure, chemistry and origins of gypsum crusts in southern Tunisia and the central Namib Desert. Sedimentology, 32: 855-875.

Weinberger, R., 2001. Evolution of polygonal patterns in stratified mud during desiccation: The role of flaw distribution and layer boundaries. Geological Society of America Bulletin, 113: 20-31.

Williams, G.E., 1986.Precambrian permafrost horizons as indicators of paleoclimate. Precambrian Research, 32: 233-242.

Williams, G.E., 2001. Late Neoproterozoic periglacial aeolian sand sheet, Stuart Shelf, South Australia. Australian Journal of Earth Sciences, 45: 733-741.

Williams, G.E. and Schmidt, P.W., 2004. Neoproterozoic Glaciation: reconciling low paleolatitudes and the geologic record. The Extreme Proterozoic: Geology, Geochemistry, and Climate, Geophysical Monograph Series 146, pp. 145-159.

4. APPLICATION OF QUARTZ SAND MICROTEXTURAL ANALYSIS TO INFER COLD-CLIMATE WEATHERING IN THE EQUATORIAL FOUNTAIN FORMATION (PENNSYLVANIAN-PERMIAN, COLORADO)

Abstract

Scanning Electron Microscopy (SEM) of first-cycle quartz grains from the equatorial, Pennsylvanian-early Permian Fountain Formation reveals microtextures that resulted from fracturing during depositional transport, even after diagenetic overprinting occurred under moderate burial conditions (up to 3.5 km depth and 100°C). Depositional transport microtextures can be grouped based on fracture process into: 1) high-stress fractures, consisting of fractures created through sustained high-shear stress, such as grooves, deep troughs, and gouges, and are inferred to occur predominantly during glacial transport; 2) percussion fractures, consisting of fractures created by grain-to-grain contact during saltation or traction flow, such as randomly oriented v-shaped cracks and edge rounding, and are inferred to occur predominantly during saltation and/or traction flow; and 3) polygenetic fractures, such as conchoidal fractures, arc-shaped steps, linear steps and linear fractures, occur under a wide range of transport processes and thus indicate no environmental significance. Using a ternary diagram that distinguishes high-stress, percussion, and polygenetic fracture types, data from this study demonstrate that quartz grains from the Fountain Formation exhibit microtextures similar to both Quaternary till and glaciofluvial deposits, suggesting that periods of upland glaciation occurred in the Fountain Formation provenance region (Ute Pass uplift).

The frequency of high-stress fractures versus stratigraphic level shows three peak intervals (I, II, & III). These intervals are inferred to record the presence of ice within the Ute Pass uplift and are correlative with polygonally fractured bedding paleosurfaces within the Fountain Formation inferred to reflect cold-temperature weathering. Moreover, the peak intervals are roughly coeval to inferred episodes of ice maxima from high-latitude localities. Employing geologically reasonable stream gradients and estimated transport distance, elevation of the ice terminus is constrained to <1500 m. These data suggest that upland glaciers episodically existed within this equatorial setting and further use of this technique may reveal more evidence of ice in other proximal deposits of the ancestral Rocky Mountains, as well as other systems of various geologic ages.

Introduction

Scanning Electron Microscopy (SEM) analysis of microtextures on quartz grains has long been used to attempt interpretation of depositional environments within Neogene deposits (e.g. Krinsley and Takahashi, 1962; Krinsley and Donahue, 1968; Krinsley and Doornkamp, 1973); however, a variety of processes in a wide range of depositional environments have been found to produce similar types of microtextures, which is the concept of equifinality. Recent work, however, indicates that glacial environments tend to produce a unique suite of microtextures as a result of the extraordinary stress imparted to grains in a subglacial environment (e.g. Mahaney, 2002; Mahaney and Kalm, 2000). Despite the advancement of SEM microtextural identification in glacial environments, such analysis is typically not applied to pre-Neogene strata owing in part to the overprinting effects of diagenesis and/or recycling.

Recently, Soreghan et al. (2008) have proposed episodic and widespread cold conditions including glaciation, within the Ancestral Rocky Mountains (ARM) of Pennsylvanian-Permian tropical Pangaea. Additionally, Sweet and Soreghan (2008) have proposed a cold-weathering origin for paleosurfaces exhibiting polygonal fractures within the Fountain Formation of the ARM. Here we present SEM microtextural analysis of quartz grains recovered from the Pennsylvanian-early Permian Fountain Formation deposited on the east flank of the Front Range uplift of the ARM to assess: 1) the application of SEM microtextural analysis to ancient strata and 2) the hypothesis of low-latitude glaciation within western equatorial Pangaea. Our data indicate that primary (i.e. non-diagenetic) microtextures are recognizable and indicate episodic influxes of glacially induced microtextures.

Geologic Background

The ARM were an intraplate collage of basement-cored uplifts and intervening sedimentary basins (Fig. 4.1; Kluth and Coney, 1981) that developed within western equatorial Pangaea in Late Paleozoic time. Mantling the basement-cored uplifts are coarse, clastic wedges of first-cycle arkosic sediments. In the study area, the coarse clastic wedge that was shed eastward off the Front Range uplift is represented by the Fountain Formation (Fig. 4.1; e.g. Hubert, 1960; Mallory, 1972; 1975). The Fountain Formation records coarse-grained fan-delta and braided river deposition (Chapter 2; Suttner et al., 1984; Maples and Suttner, 1990; Sweet and Soreghan, in review).

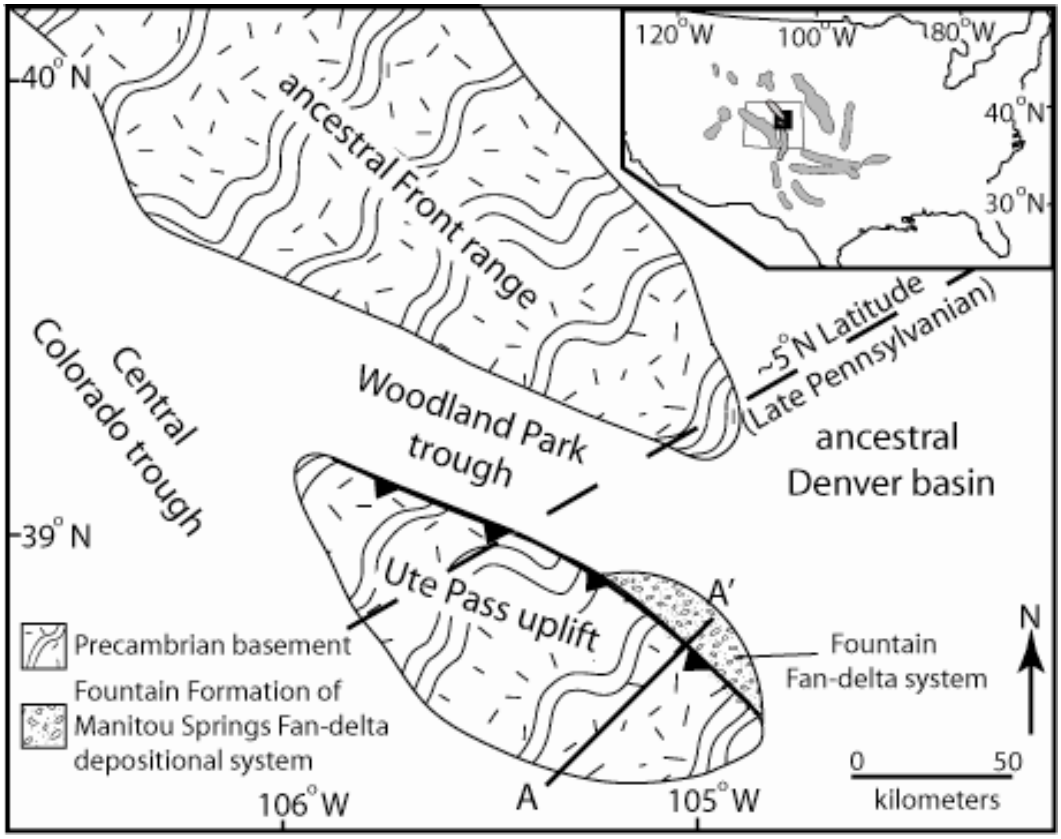

Figure 4.1: Late Pennsylvanian paleogeography of the southern ancestral Front Range and Ute Pass uplifts. Woodland Park trough and Precambrian uplift paleogeography modified from Kluth and McCreary, 2006. Latitudinal position is estimated from Scotese (1997). Inset: Displays outline of Colorado within the United States interior and location of ARM uplifts (*in* gray; modified from Kluth and Coney, 1981). The black box is the approximate area of the enlarged view.

Despite numerous studies of the Fountain Formation, interpretations of the climate that prevailed during deposition are conflicting. Early workers interpreted a warm-humid climate on the basis of an inferred lateritic paleosol, local coaly layers and scattered plant fragments (Wahlstrom, 1948; Hubert, 1960), all restricted to the lower 150 m of the 900 m-thick Fountain Formation. Mack and Suttner (1977) demonstrated that the compositional maturity of first-cycle sediments within the lower Fountain Formation exceeds that of first-cycle sediments from modern drainages in the region, and used these results to advocate warm-humid (tropical) conditions for the lower Fountain Formation. Conversely, Raup (1966) and Walker (1967) cited the interstitial clay composition and hematite content of the Fountain Formation as evidence for a warm-arid climate. More recently, Suttner and Dutta (1986) and Dutta and Suttner (1986) suggested that an upward increase in mineralogical immaturity, together with the decrease in inferred neoformed kaolinite upward within the Fountain Formation reflect a change from warm-humid to warm semi-arid conditions.

All previous researchers favor a warm climate; yet none of the indicators used bear solely on temperature. For instance, coal reflects high effective moisture under a wide range of temperatures (Parrish, 1998; Begossi and Della Fávera, 2002; Barber et al., 2003). Additionally, Suttner and Dutta (1986) noted that compositional immaturity characterizes both cold and warm-arid climates. The only proxies that bear exclusively on temperature conditions during deposition of the Fountain Formation are those of Dutta and Suttner (δO^{18} values of neoformed clays; 1986) and Sweet and Soreghan (2008), both of which indicate anomalously cool equatorial temperatures.

The Fountain Formation consists of three tectonostratigraphic units (lower, middle and upper) separated by unconformities of varied duration (Fig. 4.2; Sweet and Soreghan, in review). Morrowan-Atokan (Bashkirian) marine invertebrate and plant fossils were recovered from the basal Glen Eyrie Member of the lower Fountain Formation (Chronic and Williams, 1978; Suttner et al., 1984). The middle Fountain Formation composes the same depositional system as the lower unit and thus is only slightly younger. The upper Fountain Formation has no age control in the study area except through relative stratigraphic position. In northern Colorado, the uppermost Fountain contact is tightly constrained by Virgilian fusulinids recovered 4 m below the contact and Wolfcampian fusulinids recovered from the overlying Ingleside Formation (Maughan and Ahlbrandt, 1985). Sweet and Soreghan (in review) provide an overview of the age of the upper Fountain Formation and propose that it is latest Pennsylvanian to possibly earliest Permian in age, and the unconformity separating the upper and middle units represents a substantial amount of time (i.e. 5-10 Ma).

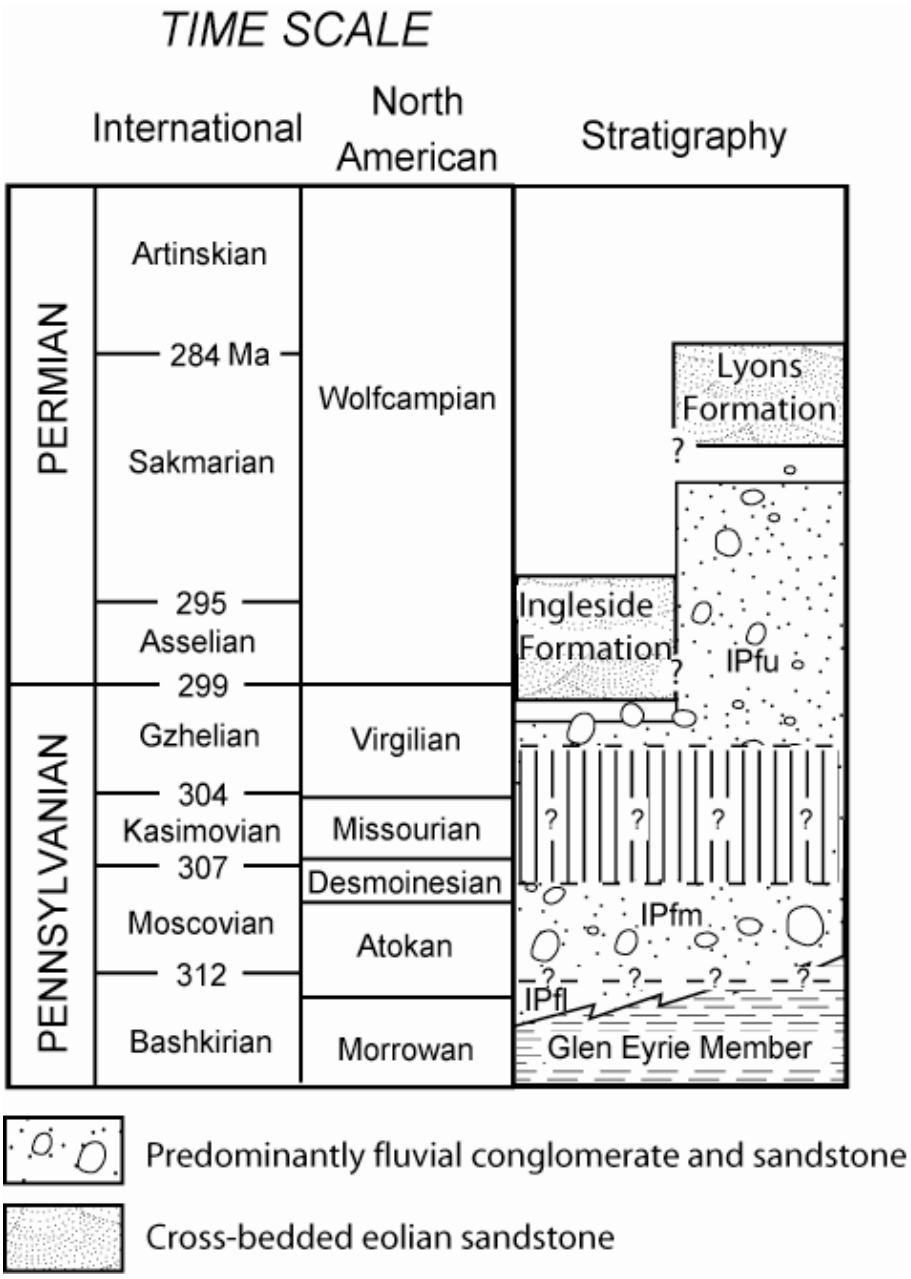

Figure 4.2: Fountain Formation stratigraphy of the Manitou Springs region after Sweet and Soreghan (in review). Note that the upper Fountain Formation is gradational with either the Lyons or Ingleside Formations. Time scale is from Gradstein et al. (2004). IPlf = lower Fountain Formation; IPmf = middle Fountain Formation; IPuf = upper Fountain Formation.

Methods

Samples were collected from 3 facies—fluvial, debris flow and marine shoreface—in conjunction with description of the measured section presented in Sweet and Soreghan (in review). Fifteen samples were collected and 10-55 individual quartz grains from each sample were analyzed by SEM.

Samples were disaggregated for microtextural analyses by removing iron oxide cement with the citrate-bicarbonate-dithionite (CBD) method (Mehra and Jackson, 1960; Janitzky, 1986). The sand + gravel fraction was wet-sieved and the 3-1.5 mm, 1.5-0.7 mm and 0.7-0.3 mm fractions were analyzed. No sonication was used during the disaggregation process. Quartz grains were randomly selected with a binocular microscope for SEM analysis as outlined by Mahaney et al. (1988).

Individual grains were placed on an aluminum SEM stub and sputter coated with a gold-palladium mixture. Grains were examined with a Zeiss 960 SEM, tungsten filament and 15 Kv. All grains were individually verified as quartz by energy dispersive spectrum (EDS) analysis.

The atlases of Krinsley and Doornkamp (1973) and Mahaney (2002) were used for identification of microtextures. Each microtexture evaluated was noted as either present or not present following the methods of Mahaney (2002); no attempt was made to estimate percentage of grain covered or relative importance of certain microtextures. Quantitative summary analyses were plotted similarly to methods outlined in Mahaney and Kalm (2000) and Mahaney et al. (2001).

Diagenesis and Antiquity of Microtextures

The Fountain Formation is a first-cycle arkose as indicated by textural and compositional immaturity. Burial depth is constrained to <3.5 km based on results of vitrinite reflectance analysis (R_o = 0.61%, h_vB_b = 100°C, written communication, B. Cardott, 2008) on coal recovered from the lower Fountain Formation and employing a modern geothermal gradient of 30°C/ km for the Denver Basin (Raynolds et al., 2001). The Fountain Formation was exhumed at Manitou Springs during Laramide-age shortening, thus maximum burial and temperature conditions most likely occurred in the latest Cretaceous. Primary diagenetic products formed during burial consist of authigenic clay, quartz overgrowths and "turtle-skin" quartz as described by Folk (1978) (Fig. 4.3). At least one of these precipitation features are found on each quartz grain analyzed, and commonly precipitation completely obscures the grain surface. However, of the 542 quartz grains analyzed, 330 or 61% exhibit fracture surfaces that pre-date diagenesis because: 1) precipitation of "turtle-skin" quartz is present on the fracture surface, 2) quartz overgrowths partially encroach onto fracture surfaces, and/or 3) dissolution pits are present on fracture surfaces. Thus, the pre-diagenetic fractures must have formed during the late Paleozoic, as that was the last time these sediments were present at the Earth's surface, and the fractures were imparted during sedimentary transport. On a few grains pristine fracture surfaces cut across precipitation features indicating new fracturing induced during either the disaggregation or sampling process.

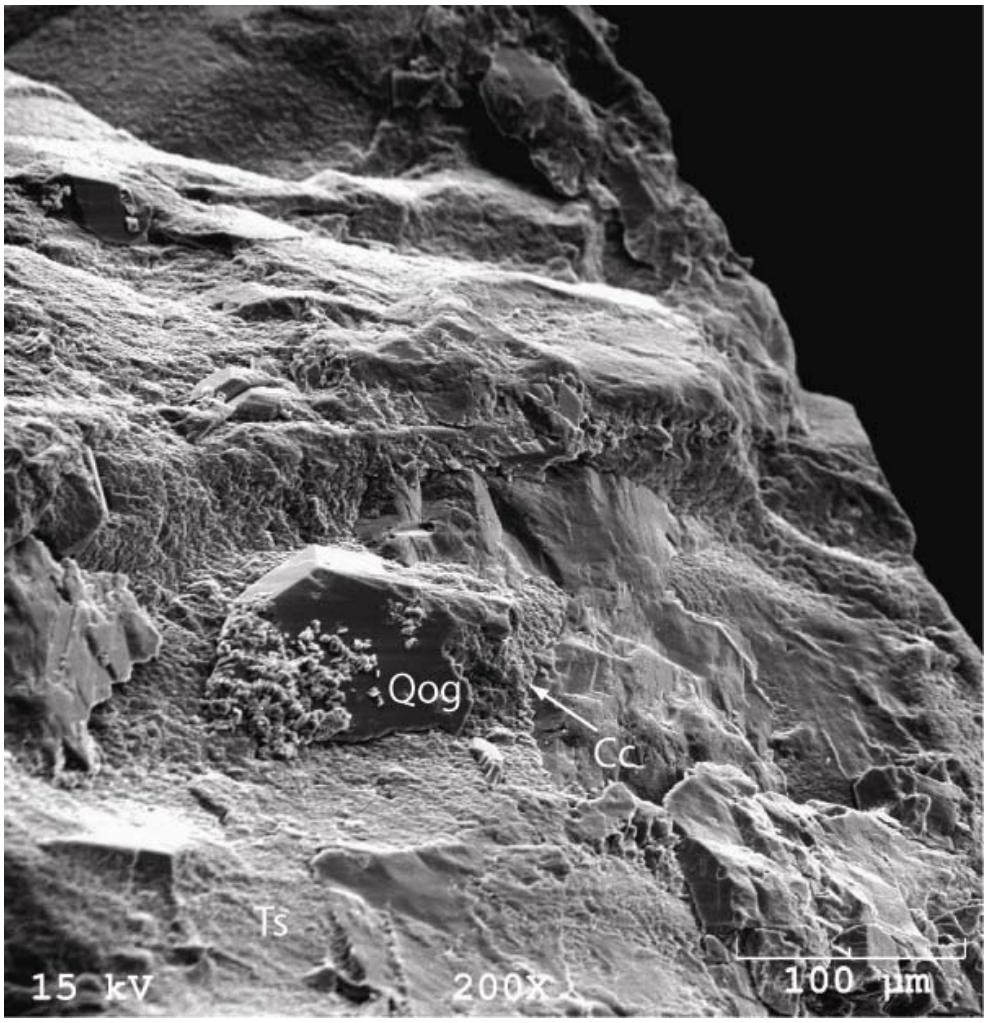

Figure 4.3: SEM image showing common diagenetic features exhibited on Fountain Formation quartz grains. Qog = quartz overgrowth; Cc = clay coating; Ts = turtle skin silica coating

Summary of Microtextures

Disaggregated material is composed predominantly of quartz and feldspar with varying amounts of muscovite and biotite. Grain texture ranges widely from angular to well-rounded. Overall, the most abundant microtextures observed are conchoidal fractures, sub-parallel linear fractures and edge-rounding fractures (Fig. 4.4 & 4.5). Because the samples represent various facies, it is useful to examine and compare data both from similar facies and similar stratigraphic levels. Microtextural variance based on grain size was not observed in this study.

Facies trends

Marine shoreface facies typically exhibit more mineralogical and textural maturity than the other facies; this maturity enhancement has been interpreted as an environmental effect attributable to wave action in the shoreface (Hood, 1987; Kairo et al., 1993). SEM analysis indicates that nearly 60% of the grains contain edge rounding and low relief (Fig. 4.5a), which probably records this shoreface environmental effect. Breakage blocks, randomly oriented v-shaped cracks, arc-shaped steps, conchoidal fractures and sub-parallel linear fractures occur on 20-30% of the grains (Fig. 4.4 & 4.5a). Grooves, gouges and troughs are relatively rare but present locally, and are probably relicts of nonmarine transport because those microtextures are inferred to require considerable and sustained pressure (e.g. Mahaney and Kalm, 2000; Mahaney 2002), conditions atypical of the marine realm.

Quartz grains from debris flow facies are often partially encased by clay minerals that were not removed by the CBD process, and exhibit the precipitated quartz common to other facies. These two factors resulted in a low population of grains with observable

Figure 4.4: SEM images of quartz sand grains from the Fountain Formation exhibiting a variety of microtextures inferred to be created during grain transport due to the presence of diagenetic features on the fractured surface. A) Well-rounded quartz grain recovered from marine shoreface facies. This grain displays randomly oriented v-shape cracks (vc) and is coated with turtle skin silica and local authigenic clay minerals. B) Angular quartz grain displaying high-relief, subparallel linear fractures (lf), deep trough (dt) and edge rounding (er). C) Straight grooves (sg) on a fracture face. D) Straight grooves (sg) and linear steps (ls). A euhedral quartz overgrowth (ov) has formed at the terminus of the grooves. E) Irregularly shaped grain displaying high-relief and arc-shaped steps (as). Grain surface is coated with turtle skin silica, local clay minerals and mica grain. F) Well-rounded grain recovered from marine shoreface facies showing a remnant curved groove (cg). G) Fracture face (ff) on grain surface shows evidence for edge rounding (er) fracturing. H) Mechanically-upturned plate (mup) on grain surface with local pockets of quartz precipitation (qp) on upturned-plate. I) Well-rounded grain recovered from marine shoreface facies showing randomly oriented v-shaped cracks (vc).

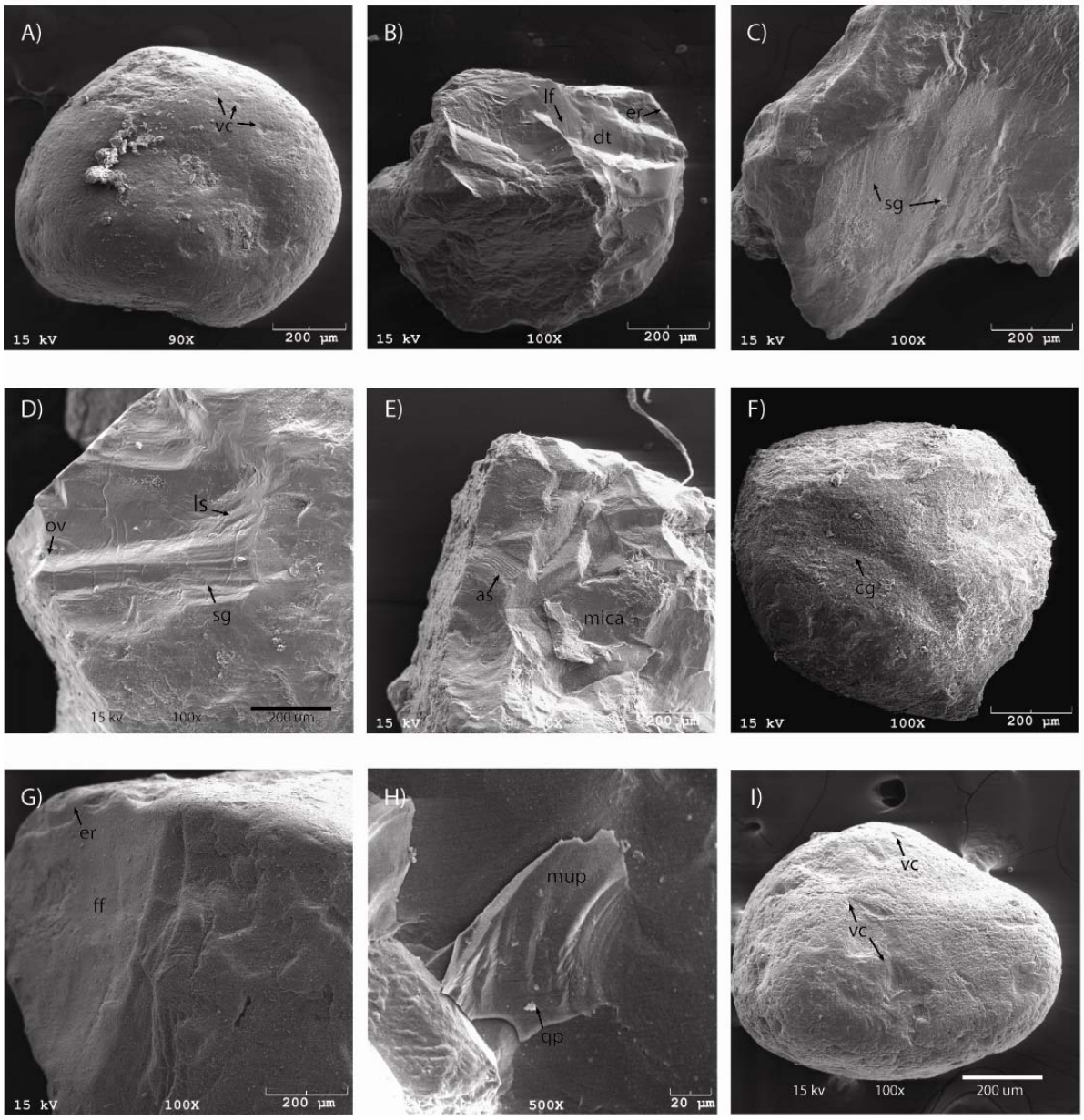
A)
vc
15 kV
90X
200 µm
B)
lf
er
dt
15 kV
100X
200 µm
C)
sg
15 kV
100X
200 µm
D)
ls
ov
sg
15 kV
100x
200 um
E)
as
mica
15 kV
200 µm
F)
cg
15 kV
100X
200 µm
G)
er
ff
15 kV
100X
200 µm
H)
mup
qp
500X
20 µm
I)
vc
vc
15 kv
100x
200 um

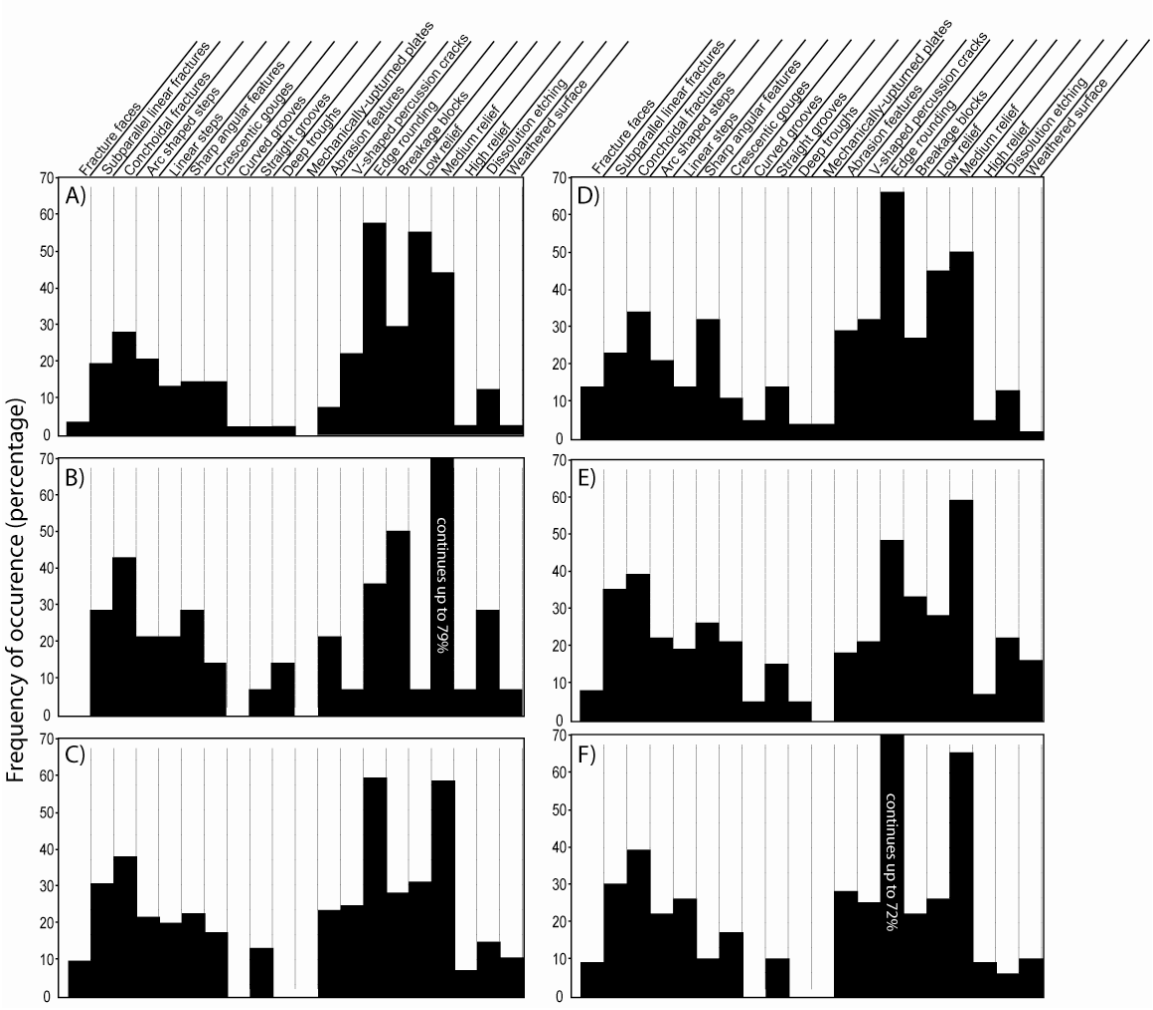

Figure 4.5: SEM microtexture frequency of occurrence comparison of: A) quartz grains from marine facies; B) quartz grains from debris flow facies; C) quartz grains from fluvial facies; D) quartz grains from the lower Fountain Formation; E) quartz grains from the middle Fountain Formation; F) quartz grains from the upper Fountain Formation.

ancient microtextures. Of the grains with ancient features, 30-50% exhibit breakage blocks, conchoidal fractures and edge rounding (Fig. 4.5b), whereas 15-25% of the grains show sub-parallel linear fractures, arc-shaped steps and linear steps, ultimately resulting in more grain angularity (Fig. 4.4). Grains are characterized predominantly as having medium relief often with sharp angular features associated. Gouges, grooves and troughs are rare in this facies.

Quartz grains from the fluvial facies display the widest variation in microtextures. Edge-rounding fractures are the most abundant and found on nearly 60% of the grains examined (Fig. 5c). Other prominent microtextures are conchoidal and sub-parallel linear fractures, arc-shaped and linear steps, randomly oriented v-shaped cracks and breakage blocks. Relative to debris-flow and shoreface facies, grooves, troughs and gouges occur in highest abundance within the fluvial facies. Mechanically-upturned plates were only observed in this facies (Fig. 4.4h). Similar to the debris-flow facies, grains are characterized best as medium relief, however, a higher percentage of grains display high relief in the fluvial facies.

Overall, the microtextural variation in facies is subtle, suggesting that environment of deposition did not impart a dramatic signal in overall microtextural character. However, the lack of v-shaped cracks on grains from the debris-flow facies and the wide diversity of fractures observed on the grains from fluvial facies probably reflect processes intrinsic to those environments that partially controlled for those microtextures. For example, randomly oriented, v-shaped cracks are thought to record percussion (Campbell and Thomspon, 1991; Jackson, 1996; Mahaney and Kalm, 2000; Mahaney, 2002), a process that is absent or limited in debris flows owing to minimal intragranular

collisions (e.g. Costa, 1988). In contrast, percussion is an important process in both streams and shoreface environments and the relative abundance of v-shaped cracks in those facies probably reflects that difference.

Stratigraphic trends

Each sample was taken from a different bed within the stratigraphic section, thus each sample represents a different time such that grouping facies essentially time-averages the textural data. The Fountain Formation has poor age control, but the tectonostratigraphic units proposed by Sweet and Soreghan (in review) provide a relative chronostratigraphic framework for our samples (Fig. 4.2). Fluvial facies are the only samples to occur in all three tectonostratigraphic units; hence we examined only fluvial samples within this chronostratigraphic framework to attempt to isolate age-specific processes.

Microtextural frequency plots from fluvial facies of the lower, middle and upper Fountain Formation (Fig. 4.5d, e, and f) all show a predominance of medium-relief grains and edge-rounding fracturing. Conchoidal and sub-parallel linear fractures are also relatively important features, present on 20-40% of the grains. A notable inter-sample difference is the higher percentage of gouges, grooves and troughs observed on grains of the middle Fountain tectonostratigraphic unit relative to those of the other units. A high frequency of edge-rounding fracturing (50-70%) and randomly oriented, v-shaped cracks (20-30%) throughout the section, both thought to record percussion (Mahaney and Kalm, 2000; Mahaney, 2002), presumably reflect intragranular collision during fluvial transport. However, the stratigraphic variation in frequency of grooves, troughs, and gouges—all reflecting considerable and sustained pressure (Mahaney and Kalm, 2000)—are unlikely

to be a result of fluvial processes. Hence, we infer the influence of process(es) within a different environment that affected grain microtextures previous to fluvial entrainment, as discussed below.

Discussion of Data

Historically, microtextural frequency data have been displayed as shown in Figure 4.5 (Campbell and Thompson, 1991; Mahaney et al., 1991; Mahaney, 1995; Mahaney and Kalm, 1995; Mahaney and Kalm, 2000; Mahaney, 2002). Comparison of different data sets using these plots, however, is difficult unless there are very large contrasts in frequency data, such as those data shown in Mahaney and Kalm (2000). The histograms all appear similar, rendering comparison between plots difficult. Therefore, comparison of data to assess possible differences that reflect transport process would be better served by grouping microtextures created by similar fracturing processes. While the majority of microtextures are created in different environments through a variety of processes, some are thought to record specific transport processes. Notably, randomly oriented, v-shaped cracks and edge-rounding fracturing are commonly interpreted to reflect percussion (saltation) transport (e.g. Campbell and Thompson, 1991; Mahaney and Kalm, 2000; Mahaney, 2002). In contrast, straight and curved grooves, deep troughs and crescentic gouges are thought to reflect sustained high shear stress (e.g. Mahaney and Kalm, 2000; Mahaney, 2000). Building upon these findings, we distinguish three basic groupings for mechanically fractured microtextures: (1) high-stress fractures, (2) percussion fractures and (3) polygenetic fractures, or those created through a variety of processes. These

groups can then be plotted on a ternary diagram for quantitative inter-sample comparison (Fig. 4.6).

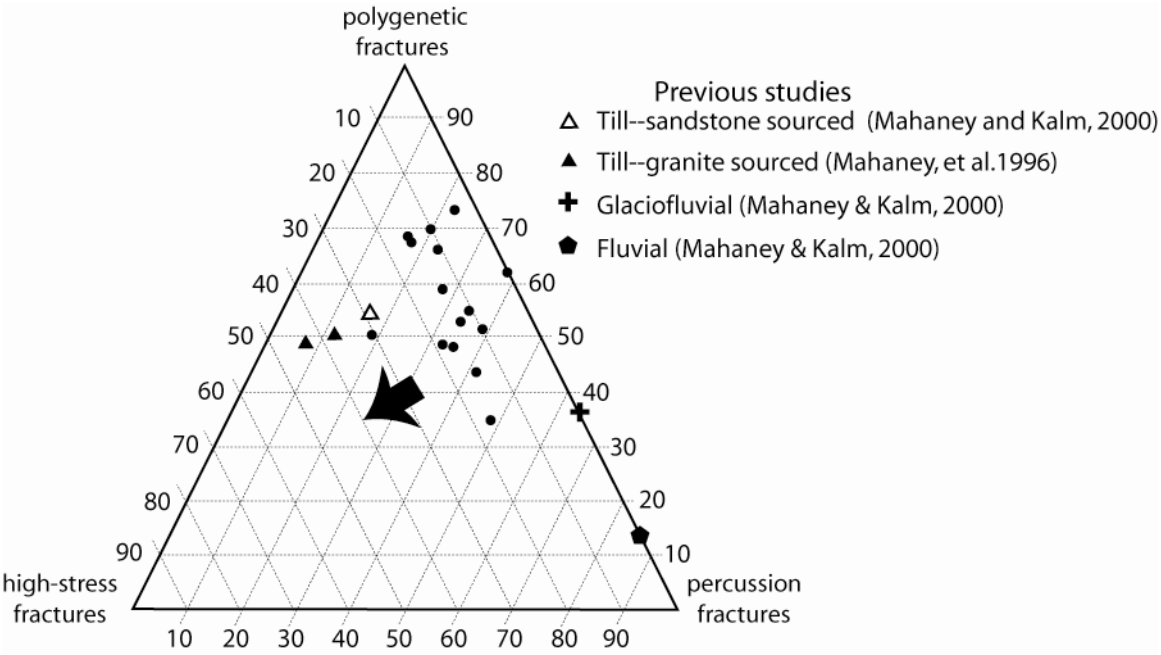

Figure 4.6: Polygenetic-high stress-percussion fractures ternary diagram. Solid black dots are data from this study. Polygenetic fracture apex includes fracture faces, subparallel linear fractures, conchoidal fractures, arc-shaped steps, linear steps and breakage blocks. High-stress fracture apex includes curved grooves, straight grooves, deep troughs, and mechanically-upturned plates. Percussion fracture apex includes randomly oriented v-shaped cracks and edge rounding. Note that the data from this study (black circles) are deviate off the polygenetic-percussion join towards the high-stress apex as denoted by large black arrow.

When the Manitou Springs samples are plotted on a high stress-percussion-polygenetic fracture ternary diagram, a first-order trend of the data shows that all samples except one deviate from the polygenetic-percussion join and trend toward the high-stress apex (Fig. 4.6). This trend indicates that the majority of the grains experienced sustained high-stress at some point during transport. A second data trend forms parallel to the polygenetic-percussion join indicating that grains experienced varying amounts of grain-to-grain collision that resulted in the v-shaped cracks and edge rounding defining the percussion apex. Furthermore, most of the Fountain Formation data plots in between published data from glacially influenced Quaternary sediments (i.e. till and glacio-fluvial) and Devonian fluvial sandstone as recorded by Mahaney and Kalm (2000). This indicates that the majority of the Fountain Formation samples exhibit microtextures similar to glacially influenced sediments (Fig. 4.6). Accordingly, we suggest that these high-stress fractures were created during glacial transport, most likely from upland glaciation within the ancestral Ute Pass uplift. However, the samples also exhibit percussion fracturing suggesting that grains were entrained fluvially, and in some cases transported to the marine environment, after initial glacial deposition and as indicated by their facies context. Because the majority of samples exhibit a frequency of high-stress fractures that is elevated relative to Quaternary glaciofluvial sediments, it is possible that the Fountain Formation grains were transported a relatively short distance such that high-stress fractures survived complete overprinting by the fluvial environment. However, data to assess this supposition are not preserved.

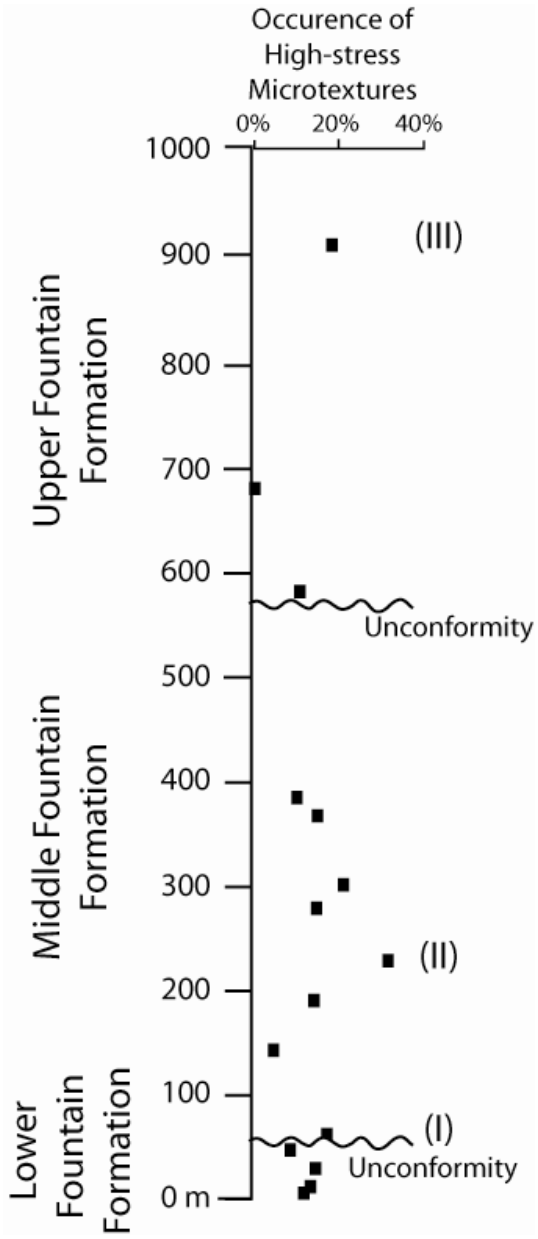

Figure 4.7: Occurrence of high-stress fracture plotted by stratigraphic depth of sample recovery. I, II, and III indicate maxima in frequency of occurrence of high-stress fractures. Lower, middle and upper Fountain Formation are tectonostratigraphic units separated by intraformational unconformities (wavy lines) as defined by Sweet and Soreghan (in review) and Chapter 2.

The frequency occurrence of high-stress fractures plotted with respect to stratigraphic level shows three maxima of 17-31% with intervening minima and 4% (Fig. 4.7). Because we infer these features as glacial in origin, we hypothesize that the maxima record peaks in glaciation. The majority of samples exhibit high-stress microtextures which could be interpreted to reflect nearly constant presence of ice atop the Ute Pass uplift during deposition of the Fountain Formation. However, given the episodic nature of glaciation, alternative likely scenarios are possible and treated in detail below.

Transport Distance and Constraints on Ice-Terminus Elevation

Glacial meltwater streams should contain a significant component of grains with high-stress fractures imparted during previous glacial transport. Indeed, Jackson (1996) has recognized that, under conditions of low discharge, low velocity, and short transport distances (< 1 km), v-shaped cracks were developed atop high-stress microtextures that formed during earlier glacial transport. Thus, fluvial transport will overprint high-stress glacial fractures, but no systematic studies have been done to assess the fluvial transport distance necessary to completely obliterate any glacially induced microtextures. The Ute Pass uplift was ~ 70 km wide, which constrains the maximum transport distance for the Fountain Formation depositional system. However, because the Ute Pass uplift was structurally bounded on only its northeast margin (Kluth and McCreary, 2006; Sweet and Soreghan, in review), the uplift was likely asymmetric, with the topographic crest closer to the faulted margin; hence, transport distances were likely <35 km (Fig. 4.1 & 4.8).

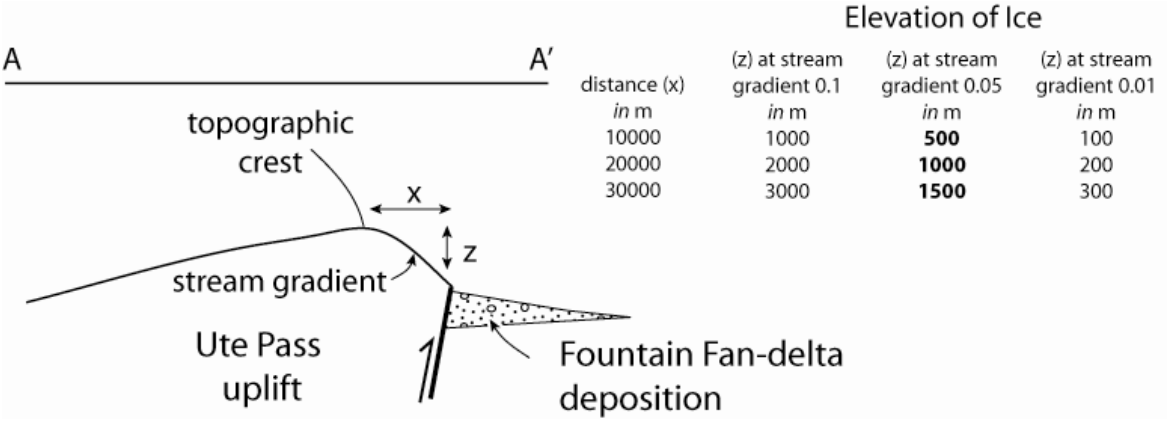

Elevation of Ice

distance (x) *in* m	(z) at stream gradient 0.1 *in* m	(z) at stream gradient 0.05 *in* m	(z) at stream gradient 0.01 *in* m
10000	1000	**500**	100
20000	2000	**1000**	200
30000	3000	**1500**	300

Figure 4.8: Diagram showing the general structural relationship of the Ute Pass uplift and fan-delta depositional wedge during lower and middle Fountain time. Location of cross-section (A-A') is shown in Figure 4.1. Variable x defines the distance from the Ute Pass crest to the northeastern structural margin and essentially estimates proglacial transport distance. Variable z is the elevation of ice as a function of x and stream gradient. Note that the Ute Pass uplift is ~70 km wide (Kluth and McCreary, 2006; Sweet and Soreghan, in review). Inset: Estimates of ice elevation (z) as a function of a variety of x values and stream gradients. Values in bold are inferred as most likely as discussed in text.

Table 4.1: Proglacial stream gradients of various upland glaciers

Glacier Name	Bedrock type	Location	Average stream gradient from ice terminus to 10 km	Average stream gradient from ice terminus to 20 km	Average stream gradient from ice terminus to 20 km
Nisqually	volcanic	Washington, USA	0.1	0.03	0.02
Soule'	granite	Alaska, USA	0.06	n/a	n/a
Franz Josef	schist, gneiss and volcanics	New Zealand	0.12	0.08	n/a
Agassiz	carbonate	Montana, USA	0.09	0.05	n/a
Scott	granite, volcanic and sedimentary	Alaska, USA	0.02	0.01	n/a
Herron	granite and sedimentary	Alaska, USA	0.02	0.01	0.01
Unnamed	volcanic	Peru	0.08	0.06	0.05
		Average	0.07	0.04	0.03

Stream gradients in glacial systems are quite variable. Exceptionally high gradients commonly prevail proximal to ice hosted on crystalline bedrock, but decrease abruptly downstream to gradients of 0.1-0.01, however, most upland systems typically approach 0.05 within 20 km (Table 4.1). These admittedly broad constraints on stream gradients and transport distances provide a means to estimate the elevation of the ice terminus (Fig. 4.8). Using a stream gradient of 0.05 and maximum transport distance of 30 km, we estimate that ice elevation was < 1500 m (Fig. 4.8) above sea level because the lower and middle Fountain Formation were deposited essentially at sea level, as evidenced by intercalated marine strata (Suttner et al., 1984; Maples and Suttner, 1990). The upper Fountain Formation, however, lacks intercalated marine strata proximally to the Ute Pass uplift such that elevational arguments relying on stream gradient and

transport distance only constrain relief above the elevation of the Fountain depositional slope.

Stratigraphic Distribution of Inferred Cold Pulses

Constraining the temporal context of these data precisely is difficult owing to lack of absolute dates and the generally nonfossiliferous character of the strata. Age constraints consist of numerous conodonts recovered from marine beds housed in the lower Fountain Formation including *Idiognathoides sinuatus* (Suttner et al., 1984), which indicates an early Pennsylvanian conodont zone ranging from ~315-317 Ma (Davydov et al., 2004). These conodont-bearing strata occur approximately 75-100 meters above base and were correlated using a series of unpublished measured sections (Fig. 4.7; Suttner, unpublished data). Using the conodont age constraint, the first peak (I) in high-stress fractures occurs in the latest Morrowan-early Atokan (Fig. 4.9).

The middle peak (II) in high-stress fractures is separated from the lower peak by an intraformational unconformity of likely minimal duration (Fig. 4.9; Sweet and Soreghan, in review). This peak is coeval with paleosurfaces that contain polygonal fractures attributed to cold-weathering phenomena (Fig. 4.9; Sweet and Soreghan, 2008). The estimated age for this interval is middle to late Atokan.

The upper Fountain Formation is late Virgilian to early Wolfcampian(?) in age (Sweet and Soreghan, in review) and houses the third (III) maximum in high-stress fractures. This uppermost maximum is approximately coeval to cold-weathering polygonal fractures reported by Sweet and Soreghan (2008; Fig. 4.9).

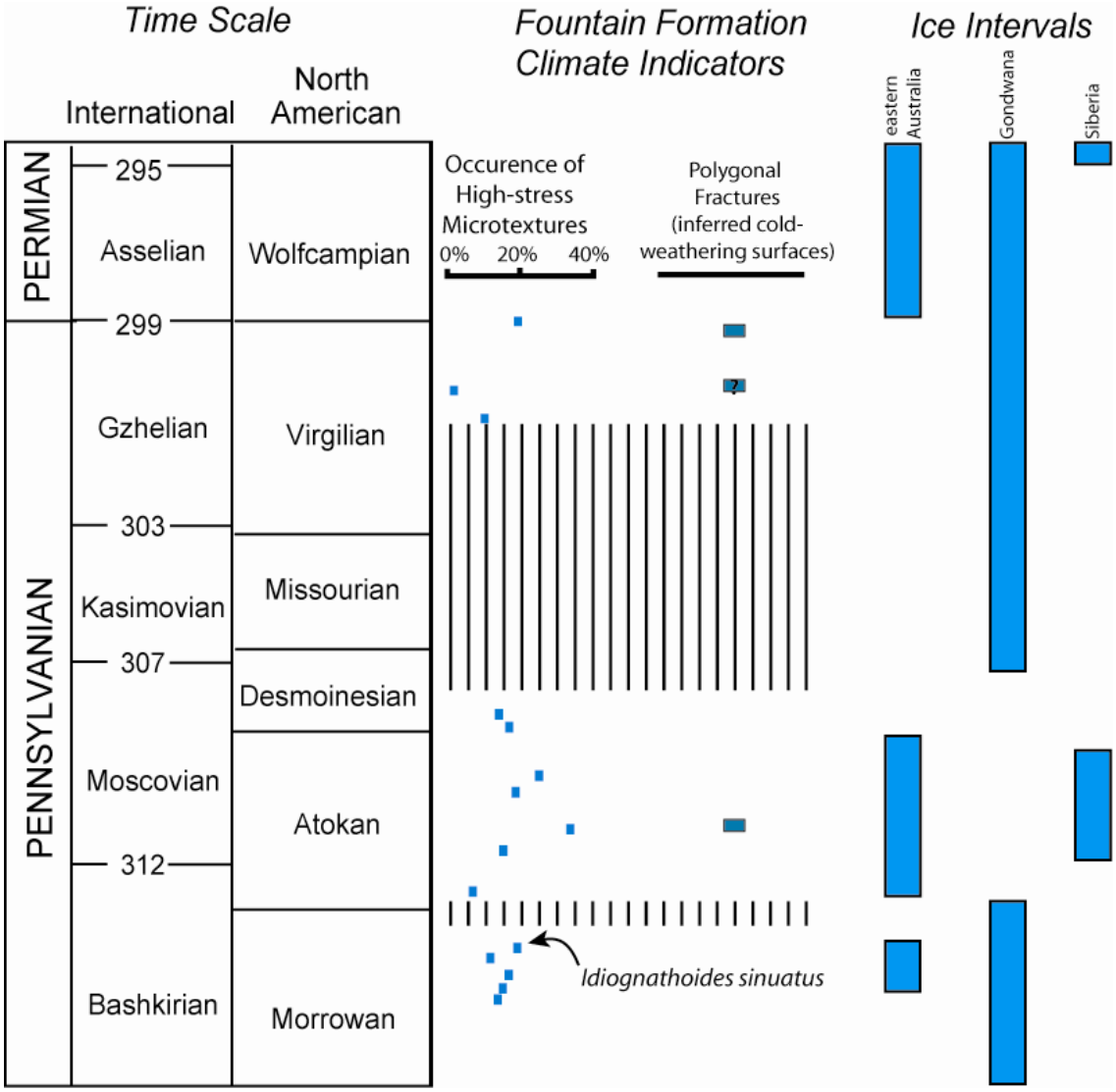

Figure 4.9: Fountain Formation climatic indicator chart compared to late Paleozoic glacial episodes. Glacial episodes of: eastern Australia from Fielding et al. (2008); Gondwana from Isbell et al. (2003); and Siberia from Epshtyn (1981a, 1981b) and Chumakov (1994). Vertical lines denote time represented by intraformational unconformities. Time scale is from Gradstein et al. (2004).

The correspondence of peaks in high-stress fractures with other indicators of cold temperatures within the Fountain depositional system (Fig. 4.9) reinforces the interpretation of possible upland glaciation. Owing to the low-latitude paleoposition of the Fountain system, episodes of upland glaciation likely correlate to globally cold intervals. Recent work within late Paleozoic strata of Gondwanan region has demonstrated pulses of glacially influenced sediments separated by inferred nonglacial sediments (Isbell et al., 2003; Fielding et al., 2008). The high-stress maxima (I, II, and III) are broadly coeval to individual glacial episodes from high-latitude Pangaea (Fig. 4.9) suggesting that anomalously cool episodes within equatorial Pangaea may correspond with Gondwanan ice growth maxima.

The Utility of Microtextural Analysis

Soreghan et al. (2008) suggested that glaciers existed at relatively low-elevation within the ARM. However, in the absence of ice-contact deposits, glacially influenced sediments can be indistinguishable from other coarse-grained depositional systems. If SEM microtextures can be used to infer glacially imparted fracturing (e.g. Mahaney and Kalm, 2000, Mahaney, 2002, Van Hoesen and Orndorff, 2004), and if glacially produced fractures can survive burial diagenesis, then this technique opens the possibility to infer a glacial influence in systems of varying age and tectonic histories. Moreover, the ternary plot developed here provides an improved approach for semi-quantitative comparison of microtextural data.

Conclusions

1. SEM analysis of quartz grains recovered from the Pennsylvanian-early Permian (?) Fountain Formation demonstrates that transport- related fracturing is observable even through the mask of diagenetic overprinting that occurred at depths of up to 3.5 km and 100°C. Transport-created microtextures can be grouped into three categories based upon fracture mechanism: 1) high-stress fractures, such as troughs, grooves and gouges obtained through sustained high-shear stress; 2) percussion fractures, such as random oriented v-shaped cracks and edge rounding fracturing obtained through saltation and/or traction flow; and 3) polygenetic fractures, such as steps, conchoidal surfaces, and lineaments obtained in a variety of depositional environments and fracture processes. These microtextural data can be quantitatively assessed by plotting on a high stress-percussion-polygenetic ternary diagram.
2. Fountain Formation microtextural data show similarities to Quaternary till and glaciofluvial SEM microtextural data when plotted on the aforementioned ternary diagram, suggesting that the high-stress fractures developed through sustained grain-to-grain shear-stress in a glacial environment. The glacially imprinted quartz grains subsequently entered the proglacial environment and were subjected to predominantly percussion-related fracturing.
3. The high-stress (inferred glacial) fractures form three peaks in frequency of occurrence when plotted stratigraphically. We infer that each peak records an interval of upland glaciation within the Ute Pass uplift. Residence time within the drainage basin (i.e. temporary moraine deposition), however, effectively time-averages the high-stress data such that samples may exhibit high-stress fractures even during times

of no highland ice. Owing to crude age constraints within the Fountain Formation and the residence time of the sediments within the drainage basin, we cannot posit any durations for existence of upland glaciers. Constraints on transport distance and proglacial stream gradient constrain elevation of ice to <1500 m.

4. The occurrence peaks of high-stress fractures correlate with polygonally fractured bedding paleosurfaces within the Fountain Formation inferred to reflect cold-temperature weathering. Age models for the Fountain Formation are crude, but reasonable geologic arguments allow the possibility that the maxima in high-stress fractures correlate with peak Gondwanan glaciations. Hence, these data support the hypothesis that equatorial Pangaea was punctuated by anomalously cool conditions, as suggested by Soreghan et al. (2008) and Sweet and Soreghan (2008).
5. SEM microtextural analysis may be useful to assess a glacial influence where ice-contact facies are lacking, even in strata that have undergone moderate burial. The ternary plot developed here provides an improved quantitative approach to microtextural analysis.

Acknowledgments

This work was funded in part by GSA graduate student research grants, Sigma Xi Grants-in-Aid of Research, Colorado Scientific Society Research Grant, J.D. Love Field Geology Fellowship, SEPM Presidential Fund—student grant and NSF grant # EAR-0230332 awarded to Lynn Soreghan. I thank Preston Larson of the Sam Noble Electron Laboratory for Scanning Electron Microscopy technologic training. Ze'ev Reches and Mike Soreghan of the University of Oklahoma for numerous discussions. Brian Cardott

of the University of Oklahoma for vitrinite reflectance. Lastly, I thank Kurt Schroeder of the Colorado Springs Parks Department for access and sampling permission of the study area.

References

Barber, K.E., Chambers, F.M., Maddy, D., 2003, Holocene paleoclimates from peat stratigraphy: macrofossil proxy climate records from three oceanic raised bogs in England and Ireland: Quaternary Science Reviews, v. 22, p. 521-539.

Begossi, R. and Della Fávera, J.C., 2002, Catastrophic floods as a possible cause for organic matter accumulation giving rise to coal, Parana Basin, Brazil: International Journal of Coal Geology, v. 52, p. 83-89.

Campbell, S. and Thompson, I.C., 1991, The palaeoenvironmental history of Late Pleistocene deposits at Moel Tryfan, North Wales: evidence from Scanning Electron Microscopy (SEM): Proceedings of the Geological Association, v. 102, no. 2, p. 123-134.

Chronic, B.J. and Williams, C.A., 1978, The Glen Eyrie Formation (Carboniferous) near Colorado Springs, *in* Pruitt, J.D. and Coffin, P.E. (eds.), Energy Resources of the Denver Basin: Rocky Mountain Association of Geologists field conference guidebook, p. 199-206.

Chumakov, N.M., 1994, Evidence of late Permian glaciation in the Kolyma River basin: a repercussion of the Gondwana glaciations in northeast Asia?: Stratigraphy and Geological Correlation 2, p. 426-444.

Costa, J.E., 1988, Rheologic, geomorphic, and sedimentologic differentiation of water floods, hyperconcentrated flows, and debris flows, *in* Baker, V.R., Kochel, C.R., and Patton, P.C., Flood Geomorphology: John Wiley & Sons, New York, NY, United States (USA), p. 113-122.

Davydov, V., Wardlaw, B.R., and Gradstein, F.M., 2004, The Carboniferous Period, *in* Gradstein, F.M., Ogg, J.G., and Smith, A.G., (eds.), A Geologic Time Scale 2004: New York, Cambridge University Press, p. 222-248.

Dutta, P.K. and Suttner, L.J., 1986, Alluvial sandstone composition and paleoclimate, II. Authigenic mineralogy: Journal of Sedimentary Research, v. 56, p. 346-358.

Epshteyn, O.G., 1981a, Middle Carboniferous ice-marine deposits of northeastern U.S.S.R., *in* Hambrey, M.J. and Harland, W.B. (eds.), Earth's pre-Pleistocene glacial record. Cambridge University Press, Cambridge, UK, p. 268-269.

Epshteyn, O.G., 1981b, Late Permian ice-marine deposits of the Atkan Formation in the Kolyma river headwaters region, U.S.S.R., *in* Hambrey, M.J. and Harland, W.B.

(eds.), Earth's pre-Pleistocene glacial record. Cambridge University Press, Cambridge, UK, p. 270-273.

Fielding, C.R., Frank, T.D., Birgenheier, L.P., Rygel, M.C., Jones, A.T. and Roberts, J., 2008, Stratigraphic imprint of the Late Paleozoic Ice Age in eastern Australia: a record of alternating glacial and non-glacial climate regime: Journal of the Geological Society of London, v. 165, p. 129-140.

Folk, R.L., 1978, Angularity and silica coatings of Simpson Desert sand grains, Northern Territory, Australia: Journal of Sedimentary Petrology, v. 48, no. 2, p. 611-624.

Gradstein, F.M., Ogg, J.G., Smith, A.G., Bleeker, W. and Lourens, L.J., 2004, A new geologic time scale, with special reference to Precambrian and Neogene: Episodes, v. 27, p. 83-100.

Hood, L.A., 1987, The effect of depositional environment on framework mineralogy and diagenesis within a nonmarine-marine transition zone: the lower Fountain fan-delta (Pennsylvanian), Manitou Springs, Colorado: unpublished MS thesis, Indiana University, 104 p.

Hubert, J.F., 1960, Petrology of the Fountain and Lyons Formations, Front Range, Colorado: Colorado School of Mines Quarterly, v. 55, p. 1-242.

Isbell, J.L., Miller, M.F., Wolfe, K.L., and Lenaker, P.A., 2003, Timing of Late Paleozoic glaciation in Gondwana: was glaciation responsible for the development of northern hemisphere cyclothems? *in* Chan, M.A. and Archer, A.W. (eds.), Extreme depositional environments: mega end members in geologic time: Geological Society of America Special Paper 370, p. 5-24.

Jackson, G., 1996, Stratigraphy and paleohydraulic analysis of glacial and meltwater sediments in the Mesa del Caballo area, Sierra de Santo Domingo, Venezuelan Andes, *in* Mahaney, W.C. and Kalm, V. (eds.), Field guide for the International Conference on Quaternary Glaciation and Paleoclimate in the Andes Mountains: Quaternary Surveys, Toronto, Ontario.

Janitsky, P., 1986, Laboratory methods: citrate-bicarbonate-dithionite (CBD) extractable iron and aluminum, *in* Singer, M.J. and Janitzky, P. (eds.), Field and laboratory procedures used in a soil chronosequence study: U.S. Geological Survey Bulletin, Report: B 1648, p. 38-41.

Kairo, S., Suttner, L.J., and Dutta, P.K., 1993, Variability in sandstone composition as a function of depositional environment in coarse-grained delta systems: Geological Society of America Special Paper 284, p. 263-283.

Kluth, C.F., and Coney, P.J., 1981, Plate tectonics of the Ancestral Rocky Mountains: Geology, v. 9, p. 10-15.

Kluth, C.F., and McCreary, J.A., 2006, Reinterpretation of the geometry and orientation of the late Paleozoic Frontrange Uplift: Abstracts with Programs—Geological Society of America, v. 38, no. 6, p. 29.

Krinsley, D.H. and Donahue, J., 1968, Environmental interpretation of sand grain surface textures by electron microscopy: Geological Society of America Bulletin, v. 79, p. 743-748.

Krinsley, D.H. and Doornkamp, J.C., 1973, Atlas of sand grain surface textures: Cambridge University Press, Cambridge, U.K., 91pp.

Krinsley, D. and Takahashi, T., 1962, Applications of electron microscopy to geology: New York Academy of Science Transactions, v. 25, p. 3-22.

Mack, G.H. and Suttner, L.J., 1977, Paleoclimate interpretation from petrographic comparison of Holocene sands and the Fountain Formation (Pennsylvanian) in the Colorado Front Range: Journal of Sedimentary Petrology, v. 47, p. 89-100.

Mahaney, W.C., 1995, Pleistocene and Holocene glacier thickness, transport histories and dynamics inferred from SEM microtextures on quartz particles: Boreas, v. 24, p. 293-304.

Mahaney, W.C., 2002, Atlas of Sand Grain Surface Textures and Applications: Oxford University Press, Oxford, U.K., 256 pp.

Mahaney, W.C. and Kalm, V., 1995, Scanning electron microscopy of Pleistocene tills in Estonia: Boreas, v. 24, p. 13-29.

Mahaney, W.C. and Kalm, V., 2000, Comparative SEM study of oriented till blocks, glacial grains and Devonian sands in Estonia and Latvia: Boreas, v. 29, p. 35-51.

Mahaney, W.C., Vortsich, W., Julig, P.J., 1988, Relative differences between glacially crushed quartz transported by mountain and continental ice, some examples from North America and East Africa: American Journal of Science, v. 288, p. 810-826.

Mahaney, W.C., Vaikmae, R., and Vares, K., 1991, Scanning electron microscopy of quartz grains in supraglacial debris, Adishy Glacier, Caucasus Mountains, USSR: Boreas, v. 20, p. 395-404.

Mahaney, W.C., Stewart, A., Kalm, V., 2001, Quantification of SEM microtextures useful in sedimentary environmental discrimination: Boreas, vol.30, p.165-171.

Mallory, W.W., 1972, Pennsylvanian System, *in*, Mallory, W.W. (ed.), Geologic Atlas of the Rocky Mountain Region: Rocky Mountain Association of Geologists, p. 131-132.

Mallory, W.W., 1975, Middle and southern Rocky Mountains, northern Colorado Plateau, and eastern Great Basin region, *in* McKee, E.D. and Crosby, E.J., (eds.), Paleotectonic investigations of the Pennsylvanian system in the United States: U.S. Geological Survey Professional Paper 853-N, p. 265-278.

Maples, C.G. and Suttner, L.J., 1990, Trace fossils and marine-nonmarine cyclicity in the Fountain Formation (Pennsylvanian; Morrowan/Atokan) near Manitou Springs, Colorado: Journal of Paleontology, v. 64, p. 859-880.

Maughan, E.K., and Ahlbrandt, T.S., 1985. Pennsylvanian and Permian eolian sandstone facies, northern Colorado and southeastern Wyoming. In: Macke, D.L. and

Maughan, E.K. (Eds.), Rocky Mountain Section Field Trip Guide Book. RMS-AAPG, RMS-SEPM, NEMD, RMAG, pp. 99-113.

Mehra, O.P. and Jackson, M.L., 1960, Iron oxide removal from soils and clays by a citrate-dithionite system buffered by sodium carbonate: Clays and Clay Mineralogy, v. 7, p. 317-327.

Parrish, J.T., 1998, Interpreting the pre-Quaternary climate from the geologic record: Columbia University Press, New York, NY, 338p.

Raup, O.B., 1966, Clay mineralogy of Pennsylvanian redbeds and associated rocks flanking ancestral Front Range of central Colorado: American Association of Petroleum Geologists Bulletin, v. 50, p. 251-268.

Raynolds, R.G.H., Johnson, K.R., Arnold, L.R., Farnham, T.M., Fleming, F., Hicks, J.F., Kelley, S.A., Lapey, L. A., Nichols, D.J., Obradovich, J.D. and Wilson, M.D., 2001, The Kiowa Core, a Continuous Drill Core Through the Denver Basin Bedrock Aquifers at Kiowa, Elbert County, Colorado: U.S. Geological Survey open-file report 01-0185, p. 26.

Scotese, C.R., 1997, Paleogeographic Atlas, PALEOMAP Progress Report 90-0497, Department of Geology, University of Texas at Arlington, Arlington, Texas, 45 pp.

Soreghan, G.S., Soreghan, M.J., Poulsen, C.J., Young, R.A, Sweet, D.E. and Davogustto, O.C., 2008, Anomalous cold in Pangaean tropics: Geology, v. 36, no. 8, p. 659-662.

Suttner, L.J., and Dutta, P.K., 1986, Alluvial sandstone composition and paleoclimate, I. Framework mineralogy: Journal of Sedimentary Research, v. 56, p. 329-345.

Suttner, L.J., Langford, R.P., and O'Connell, A.F., 1984, New interpretation of the stratigraphic relationship between the Fountain Formation and its Glen Eyrie Member, *in* Suttner, L.J., (ed), Sedimentology of the Fountain fan-delta complex near Manitou Springs and Canon City, Colorado: Society of Economic Paleontologists and Mineralogists field guidebook.

Sweet, D.E. and Soreghan, G.S., 2008, Polygonal cracking in coarse clastics records cold temperatures in the equatorial Fountain Formation (Pennsylvanian-Permian, Colorado): Palaeogeography, Palaeoclimatology, Palaeoecology, v. 268, no. 3-4, p. 193-204.

Sweet, D.E. and Soreghan, G.S., in review, Late Paleozoic tectonics and paleogeography of the Ancestral Front Range: Structural, stratigraphic and sedimentological evidence from the Fountain Formation (Manitou Springs, Colorado): [submitted GSA Bulletin, September 2008]

Van Hoesen, J.G. and Orndorff, R.L., 2004, A comparative SEM study on the micromorphology of glacial and nonglacial clasts with varying age and lithology: Canadian Journal of Earth Sciences, v. 41, p. 1123-1139.

Wahlstrom, E.E., 1948, Pre-Fountain and recent weathering on Flagstaff Mountain near Boulder, Colorado: Geological Society of America Bulletin, v. 59, p. 1173-1190.

Walker, T.R., 1967, Formation of red beds in modern and ancient deserts: Geological Society of America Bulletin, v. 78, p. 353-368.

5. MAGNITUDE OF EARLY PENNSYLVANIAN SEA-LEVEL CHANGE: CONSTRAINTS FROM A FAN DELTA SETTING

Abstract

At Manitou Springs, Colorado, the lower ~ 240 meters of the Fountain Formation is composed of successive continental-marine cycles. Each cycle is characterized by alluvial-fan deposits overlain by a marine progradational package. A thin cobble conglomerate marks the base of marine strata and is inferred to represent a transgressive lag. Furthermore, each of these lags can be traced down depositional dip throughout the study area. The above field relationships allow for a minimum calculation of the magnitude of sea-level change because: 1) a minimum horizontal distance of transgression can be measured from the mapped transgressive lag deposits; and 2) the slope of the surface over which transgression progressed can be estimated through paleohydraulic analysis of the fluvial deposits.

Magnitudes of sea level change over six successive cycles were calculated using an estimated depositional slope of 0.005; results suggest a minimum of 10-18 m of change. A large eustatic component is inferred for these six cycles because each marine package is separated throughout the study area by alluvial packages; conversely, inferred autogenic cycles of the Fountain Formation have alluvial components that grade laterally into marine strata. Tectonic pulses occur over too long a time frame to have produced these higher-frequency cycles.

Marine strata of the lower Fountain Formation have yielded Morrowan-Atokan conodonts (*Idiognathoides sinuatus*). Few estimates of the magnitude of sea-level change

exist for this time period, but incised valley depths suggest 20-45 m of eustatic sea-level change and modeling of ice-volume and facies models suggest 40-60 m of sea-level change. Our estimates are absolute minimums and the method does reflect some sensitivity to variations in slope, such that an order-of-magnitude change in slope results in ~100 m of sea-level change. Nevertheless, the range given by our method approaches other estimates and provides a new method for estimating magnitudes of sea-level change.

Glacio-eustasy is the result of ice growth and ice melt due to cyclical climate change. The data presented here indicate low levels of interglacial ice melt when compared to other times in the late Paleozoic. However, high- and low-latitude records indicate that cold conditions may have prevailed during the Morrowan-Atokan possibly suggesting that the estimates may reflect cooler interglacials with high-volume ice that experienced reduced melt.

Introduction

Estimating magnitudes of sea level change is difficult. The most reliable estimates involve the burying of paleotopography during sea level rise (e.g. Goldstein and Franseen, 1995). However, other methods involve: 1) oxygen isotopic records that attempt to reconcile global ocean conditions (e.g. Bates and Lyons, 2006; Joachimski et al., 2006); 2) modeling of ice volume fluctuations (e.g. Crowley and Baum, 1991; Isbell et al., 2003); 3) estimates of the depth of deposition of juxtaposed sedimentary facies (e.g. Heckel, 1994) or 4) estimates of strata thickness corrected for subsidence and compaction (e.g. Klein, 1994). Accuracy of each approach is dependent upon the

assumptions and caveats specific to each method. Nevertheless, magnitudes of sea-level change are useful in high-frequency cyclical successions because they provide the data necessary to infer the mechanism of sea-level change (Plint, et al., 1992).

The Late Paleozoic is characterized by Gondwanan glaciation (e.g. Crowley, 1983; Crowell, 1999) and northern hemisphere cyclothems resulting from the waxing and waning of ice sheets (e.g. Wanless and Shepard, 1936; Veevers and Powell, 1987). Thus, estimates of late Paleozoic sea level variation provide estimates on the volume change of coeval ice sheets. Characterization of sea-level change throughout the late Paleozoic provides significant data to further our understanding of glaciation (e.g. Isbell et al., 2003; Rygel et al., 2008). However, specific time periods have significantly better and more abundant estimates of sea-level change than others (Rygel et al., 2008).

The Late Paleozoic of western equatorial Pangaea is characterized by Precambrian-cored mountains, the Ancestral Rocky mountains, and adjacent coarse clastic sedimentation mantling those uplifts (Fig. 5.1; e.g. Kluth and Coney, 1981). The alluvial coarse-grained systems typically grade down dip into marine deltaic systems, such that sea-level fluctuations produced an assemblage of marine-continental progradational packages (Suttner et al., 1984; Maples and Suttner, 1990; Kairo et al., 1993; Houck 1997). Estimations of the magnitude of sea-level fluctuation have not been attempted on these strata presumably because constraints from which to measure magnitudes have not been recognized. Here we present a novel method for determining magnitude of sea-level change, as demonstrated by the example of the Morrowan-Atokan (mid-Bashkirian to mid-Moscovian) lower Fountain Formation at Manitou Springs,

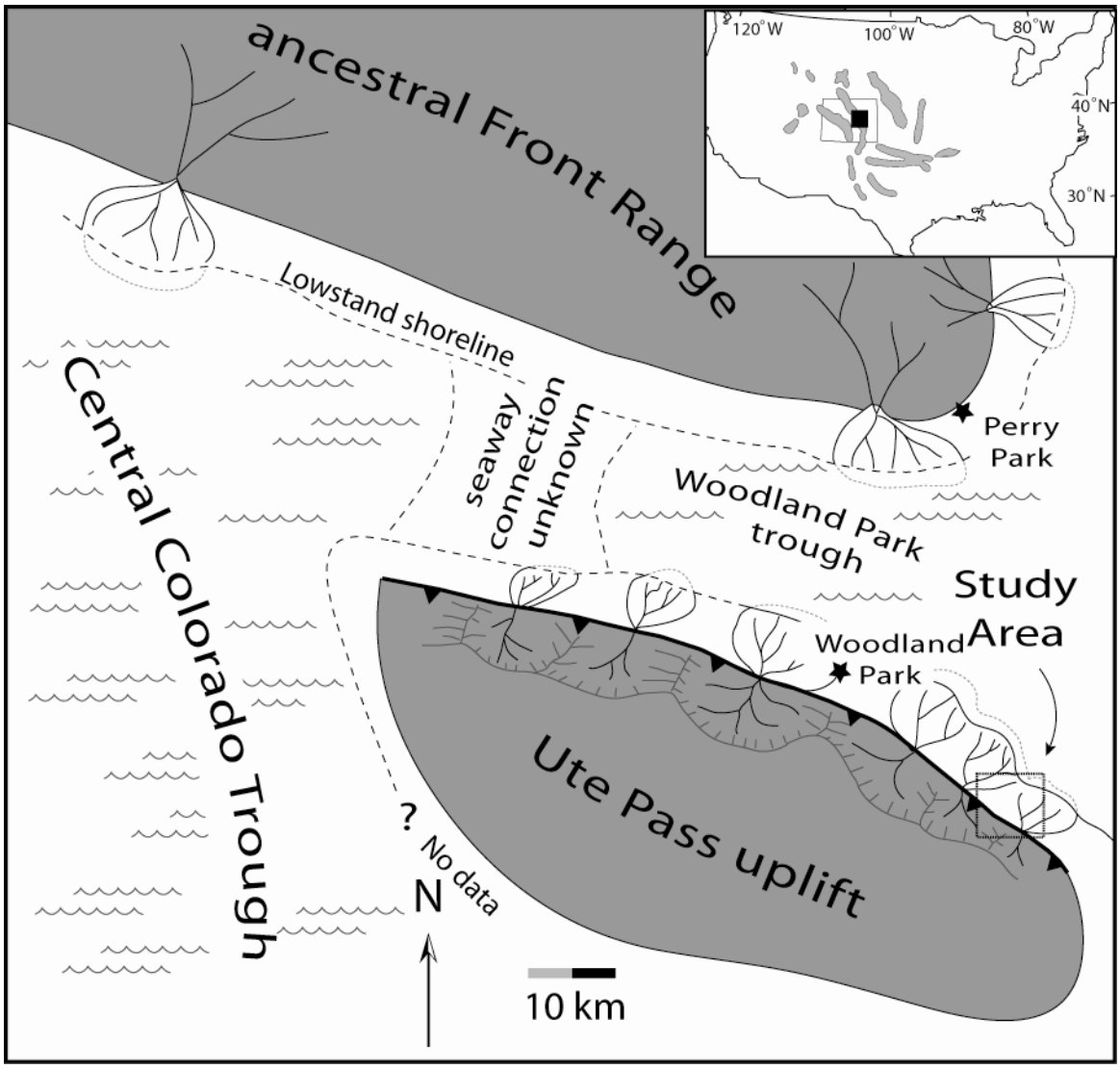

Figure 5.1: Early Pennsylvanian paleogeography of the southern ancestral Front Range during deposition of the lower and middle Fountain Formation. Data for the Central Colorado trough is from Hoy and Ridgway (2002). Data from Perry Park region is from Hendrickson (1986) and Trimble and Machette (1979). Inset: Location of ancestral Rocky Mountains (in gray; modified from Kluth and Coney, 1981) and state outline of Colorado within the United States. Black box denotes the approximate area shown by the larger paleogeographic map.

Colorado. The method utilizes the mapped extents of individual transgressive-lag deposits and slope estimates—calculated through paleohydraulic analysis—of the surface over which transgression occurred.

Geologic Setting of the Lower Fountain Formation

In the study area, the Fountain Formation was shed from the Ute Pass uplift across the ancestral Ute Pass fault and deposited within the Woodland Park trough (Fig. 5.1 & 5.2A; Suttner et al., 1984; Kluth and McCreary, 2006; Sweet and Soreghan, in review). Deposition consisted of interfingering alluvial and marine environments, such that the lower ~ 200 m is composed of marine-alluvial progradational cycles bounded by unconformities (Fig. 5.2B; Suttner et al., 1984; Maples and Suttner, 1990). The base of each cycle is marked by an unconformable, commonly scoured, surface overlain by alluvial sediments deposited in an alluvial-fan setting (Suttner et al., 1984; Sweet and Soreghan, in review). Overlying the alluvial strata is a progradational marine package typically consisting, from base to top, of a distinctive thin basal conglomerate, off-shore mudstone, hummocky cross-stratified sandstone, shoreface sandstone and a foreshore sandstone cap (Fig. 5.3; Suttner et al., 1984; Maples and Suttner, 1990). The distinctive basal conglomerates are persistent throughout the study for most of the marine packages and are invariably atop alluvial strata, indicating an origin as a transgressive lag.

Figure 5.2: A) Geologic map of the study area displaying the locations of measured sections used in B. Transgressive surfaces extend farther south of the anticline located south of the line A-A';however, individual surfaces cannot be traced across the anticline so they were not used in construction of B (see text for details). sxn I = measured section I from Sweet and Soreghan (in review). White hexagons indicate measured sections from Suttner (unpublished data) and Maples and Suttner (1990). B) Stratigraphic cross-section illustrating the vertical and lateral relationships of seven alluvial-marine cycles within the Fountain Formation. Note that the base of each alluvial package denotes a sequence boundary, whereas the top of the alluvial package indicates a transgressive surface (heavier black line). Black triangles indicate "pinning points" in the terminology of Goldstein and Franseen (1995). Vertical dashed gray lines indicate the vertical extent of measured columns used in constructing the cross-section and were used to represent a floating datum, rather than one single datum.

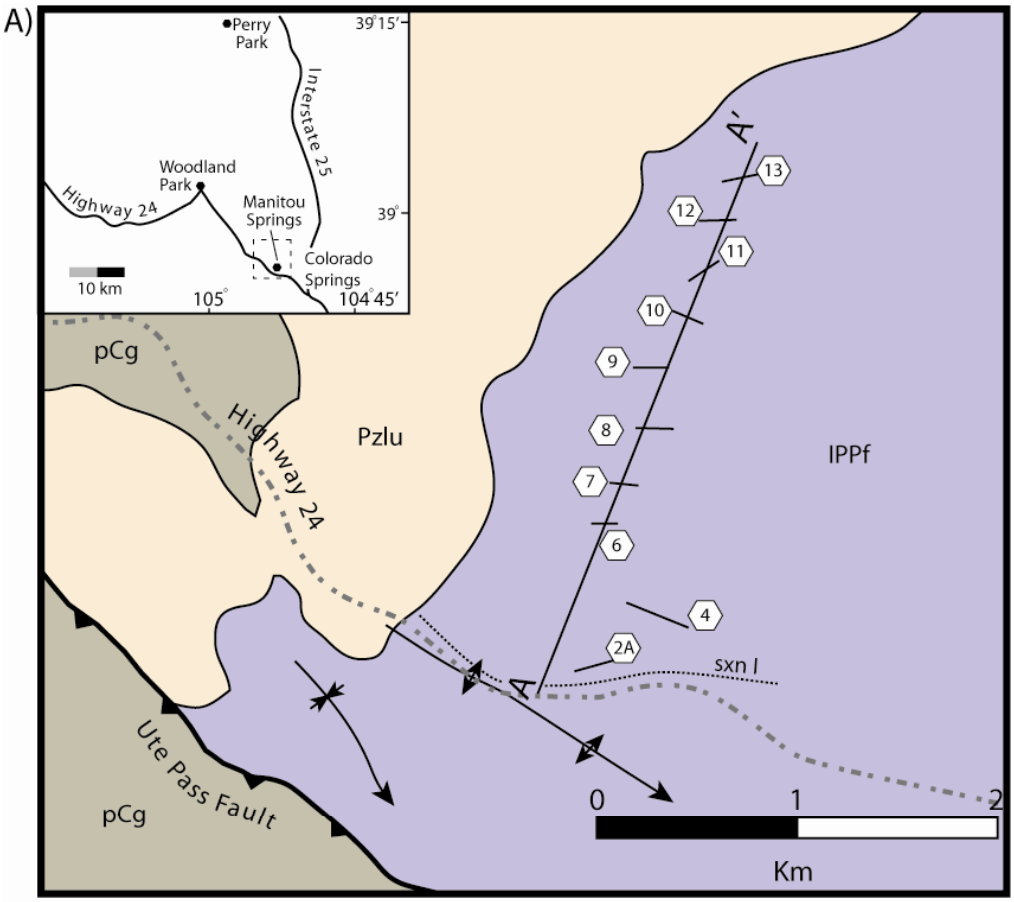
A)
Perry Park
39°15′
Interstate 25
Woodland Park
Highway 24
Manitou Springs
39°
Colorado Springs
10 km
105°
104°45′
pCg
Highway 24
Pzlu
IPPf
A′
13
12
11
10
9
8
7
6
4
2A
sxn I
A
Ute Pass Fault
pCg
0
1
2
Km

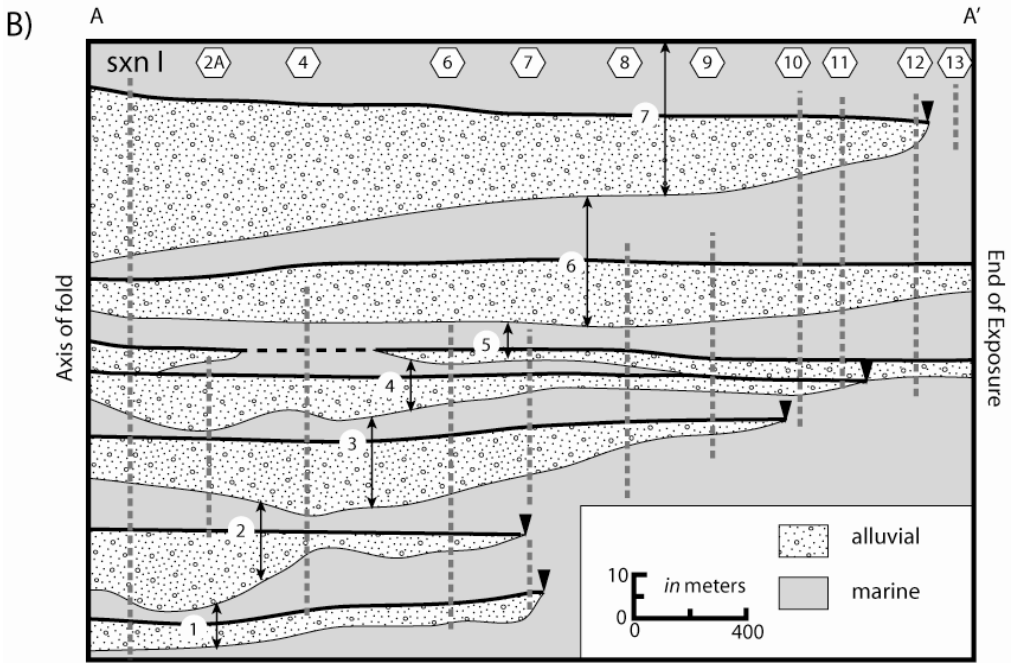
B)
A
A′
sxn I
2A
4
6
7
8
9
10
11
12
13
Axis of fold
End of Exposure
1
2
3
4
5
6
7
alluvial
marine
10
0
in meters
0
400

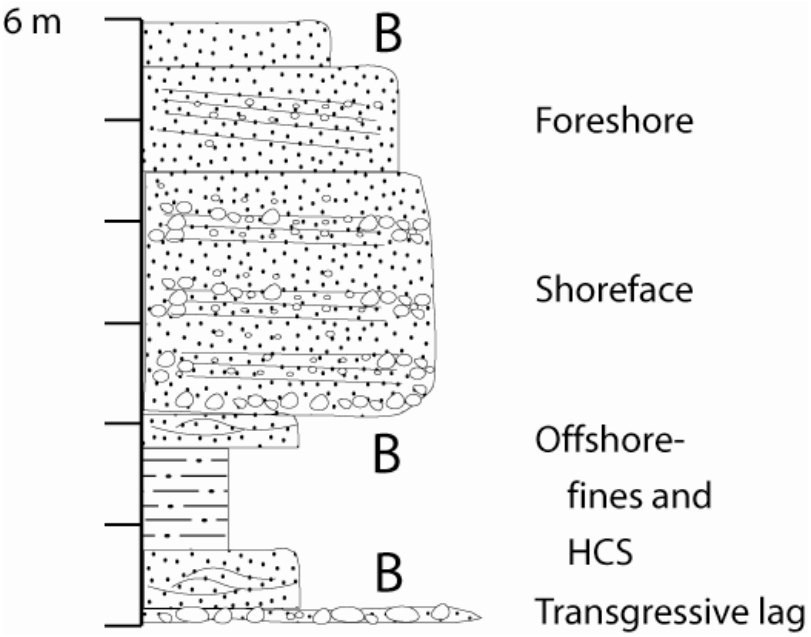

Figure 5.3: Typical marine progradational cycle originally defined by Suttner et al. (1984). HCS = hummocky cross-stratification. B = bioturbation

Sea-level calculation methodology and results

The conglomerate lags at the bases of marine progradational packages provide a means to calculate the minimum horizontal distance of transgression because individual lag deposits can be traced throughout the study area (Fig. 5.2; Suttner et al., 1984). Thus, if the slope of the depositional surface can be estimated, then the amount of relative sea-level rise can be calculated by:

$$X = \Delta D \quad (1)$$

where Δ is the slope of the surface over which transgression occurred (depositional slope of the alluvial section), D is the horizontal distance of the transgressive-lag deposits as traced from outcrop and X is the amount of relative sea rise (Fig. 5.4).

Paola and Mohrig (1996) have shown that slope relates to mean grain size and flow depth by:

$$S = 0.094D^{*}H^{-1} \quad (2)$$

where S = depositional slope, D = mean grain size (D50), and H = mean water depth. Minimum water depth for the upper and middle sections of the Fountain Formation are estimated (Table 5.1) using thicknesses of upwardly fining inferred channel-fill units. These estimates were corroborated from nearby trough cross-stratified and planar cross-stratified beds by estimating water depth from the relationship of ripple height to water depth shown by Allen (1968). D50 was obtained by previously discussed methods. Depositional slope of the intercalated alluvial strata calculated from Eq. (2) is ~0.005.

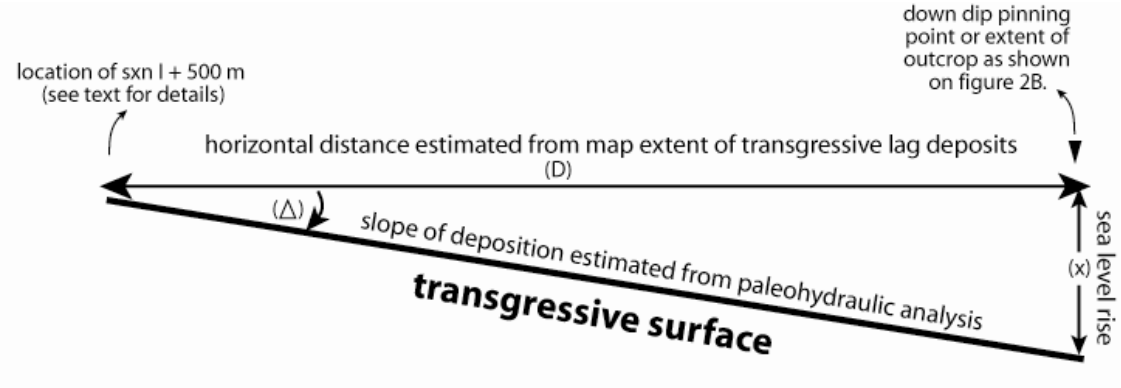

Figure 5.4: Diagram illustrating conceptual methodology of calculating magnitude of sea-level rise.

Table 5.1. Parameters and slope estimations of the middle and upper Fountain Formation

Middle Fountain	D50 (cm)	Water Depth (cm)
	8	160
	5	203
	8	229
	20	177
		195
Average	10.25	192.8
Upper Fountain		
	1.7	109
	0.5	126
	1.6	116
	0.2	137
		131
Average	1.00	122

Four key assumptions in using this method are quasi-steady state flows, noncohesive channel banks, bedform-free beds and dominantly bedload transport. Thus, application is best applied to deposits that: 1) lack signs of rapid deposition, plant roots and muddy overbank deposits, and 2) contain massive to crudely bedded channel deposits. Intervals of cobble conglomerate and crudely stratified fluvial sandstone facies within the alluvial strata below each marine-progradational package meet all criteria with the exception of quasi-steady flow and possible "backwater effects" from close proximity to shoreline. Because the system was relatively steep (Chapter 2; Sweet and Soreghan, in review), the "backwater effect" likely had little effect on the system. The Fountain depositional system was likely intermittent due to the fan depositional setting inferred for the lower Fountain Formation (Chapter 2; Sweet and Soreghan, in review), thus quasi steady-state flow conditions were not met for the entire depositional history of the fan, but may have approached steady state during individual flow events. Nonetheless, the

slope estimate is geologically reasonable compared to modern fan settings (Blair and McPherson, 1994).

Magnitude of sea-level rise for six individual cycles was calculated using Eq. (1), and varies from ~10-18 m (Table 5.2). Each estimate is an absolute minimum because the exposure of a few transgressive lags projected into the subsurface in the northern part of the study area and individual lag deposits could not be traced over the axis of a fold proximal to the Ute Pass fault (Fig. 5.2A). For the latter reason, an additional 500 m of horizontal distance was added to each cycle because transgressive lag deposits extend at least that far to the south—across the fold axis (Fig. 5.2A)—but could not be correlated to specific lag deposits used in the study.

Slope calculations used in this method are estimates, and constitute the most unknown part of the equation; thus the sensitivity of the results (from Eq. 1) to changes in depositional slope estimates (from Eq. 2) is important. An order-of-magnitude change in depositional slope increases the magnitude of sea level change by ~ 100 m (Table 5.2). However, an order-of-magnitude change in depositional slope, from 0.005 to 0.05 is geologically unreasonable, as the latter is too steep. In fact, a slope of 0.01 is extremely steep for a depositional setting, yet, using this slope, the estimated magnitudes in this study are only approximately doubled (Table 5.2). Thus, this method does show sensitivity to changes in depositional slope if the change is an order of magnitude, but reasonable geological arguments preclude the use of slopes that large.

Table 5.2. Early Pennsylvanian relative sea level changes calculated with a variety of slopes

	Geologically reasonable depositional slopes							Unreasonable depositional slopes				
Slope	0.003	0.004	0.005	0.006	0.007	0.008	0.009	0.01	0.02	0.03	0.04	0.05
Trangressive lag 1	6.1	8.1	**10.2**	12.2	14.3	16.3	18.3	20.4	40.7	61.1	81.5	101.9
Transgressive lag 2	8.8	11.8	**14.7**	17.7	20.6	23.5	26.5	29.4	58.8	88.3	117.7	147.1
Transgressive lag 3	9.9	13.2	**16.5**	19.8	23.1	26.4	29.7	33.0	66.0	99.0	132.0	165.0
Transgressive lag 4	10.8	14.4	**18.0**	21.6	25.2	28.8	32.4	36.0	71.9	107.9	143.8	179.8
Transgressive lag 5	10.8	14.4	**18.0**	21.6	25.2	28.8	32.4	36.0	71.9	107.9	143.8	179.8
Transgressive lag 6	10.3	13.8	**17.2**	20.7	24.1	27.6	31.0	34.5	68.9	103.4	137.9	172.4

note: bold numbers indicate magnitude of sea level change calculated with the depositional slope estimated by equation 2 in text

Discussion of relative versus eustatic sea-level change

Suttner et al., 1984 has inferred two types of marine-alluvial cycles within the Fountain Formation. The first type is characterized by relatively thin (<2 m) often abbreviated marine progradational cycles that grade laterally into alluvial facies over 10^2 m distance and is inferred to represent delta-lobe switching. The second type is characterized by thick (~5-20 m), complete, laterally persistent marine-progradational facies traceable throughout the study area and inferred to record allocyclic variations in sea level. Overall the system progrades upward through the section (Fig. 5.2B) which indicates that sediment supply exceeded accommodation space owing to either climate, drainage evolution, or uplift. The marine progradational cycles are commonly incised by overlying alluvial facies indicating a sea level drop, however, each alluvial portion is overlain by marine deposits indicating transgression and sea level rise. Thus, the most likely control for the marine-alluvial cycles was global eustatic change because each cycle indicates both a sea-level drop and sea-level rise. Since the Late Paleozoic is a well-known icehouse period (e.g. Veevers and Powell, 1987; Crowell, 1999) and contains abundant similar cyclic deposits inferred to represent the waxing and waning of ice sheets

(e.g. Wanless and Shephard, 1936), we infer that the Fountain Formation marine-alluvial cycles used in this study are the result of glacio-eustasy, similar to other studies (e.g. Maples and Suttner, 1990).

Age models for comparison

Conodonts were recovered from marine strata a few tens of meters below the first cycle shown on Figure 2B, among which was *Idiognathoides Sinuatus* (Suttner et al., 1984) indicating an early Pennsylvanian (Morrowan) conodont zone ranging from ~315-317 Ma (Davydov et al., 2004). Given the high frequency glacio-eustatic inference for the marine-alluvial cycles, it is likely that all six cycles studied are Morrowan-Atokan. Glacio-eustatic magnitudes inferred by other workers for this time period range from 20-60 m with a mean value of ~ 40 m (Rygel et al., 2008, references therein). Furthermore, using only those glacio-eustatic estimates recovered by inferred buried topography—the method closest to the one we employ here—the mean value is ~36 m. The estimates in magnitude of glacio-eustatic change estimated in this paper (~10-18 m) fall below the means and ranges stated above; however, we stress that the values reported here are absolute minimums and compare well to the lower ranges of others estimates. Thus, we argue that this technique for estimating magnitude of sea-level change has value for inferring a quantitative minimum value.

Estimates of sea-level change have often been used to infer the state of Gondwanan glaciation; i.e., large fluctuations are equated to the waxing and waning of large ice sheets and small fluctuations to the waxing and waning of small ice sheets (Veevers and Powell, 1987; Isbell et al., 2003; Rygel et al., 2008). The estimates of sea

level change in this paper and other estimates for the Morrowan-Atokan are of lower magnitude than other estimates throughout the late Paleozoic (e.g. Rygel et al., 2008, references therein). From this, the small sea-level fluctuations have been assumed to record times of little ice (Isbell et al., 2003; Rygel et al., 2008); however, small sea-level fluctuations indicate only minimal amounts of ice melt. That is, large ice sheets could have waxed and waned slightly, or smaller regional ice came and went. Sweet and Soreghan (2008; in review) have shown that cold conditions likely occurred at the low-latitude site of Fountain Formation deposition during the Morrowan-Atokan, as indicated by periglacial polygonal fracturing and glacial striations and grooves preserved on individual quartz grains. Thus, if cold temperatures existed at low latitudes, then the volume of ice buildup in Gondwana was likely large. Indeed, glacial deposits of equivalent Morrowan-Atokan age are documented in eastern Australia (Fielding et al, 2008) and from Siberia (Epshtyn, 1981a, 1981b). Therefore, although the Morrowan-Atokan appears to be a time of low-magnitude, sea-level change relative to the rest of the late Paleozoic, it was likely to have been a globally cold time marked by episodic glacial maximums and cooler interglacial periods at both high- and low-latitudes.

Acknowledgements

This work was funded in part by GSA graduate student research grants, Sigma Xi Grants-in-Aid of Research, Colorado Scientific Society Research Grant, J.D. Love Field Geology Fellowship, SEPM Presidential Fund—student grant and NSF grant # EAR-0230332 awarded to Lynn Soreghan. I thank Lee Suttner , emeritus University of Indiana, for use of unpublished data and discussions. I also thank Evan Franseen of the University

of Kansas and Kansas Geological Survey for discussions on the use of pinning points. Lastly, I thank Kurt Schroeder of the Colorado Springs Parks Department for access to portions of the study area.

References

Allen, J.R.L., 1968, Current Ripples, their relation to Patterns of Water and Sediment Motion. North Holland Publishing Co., Amsterdam. 433 p.

Bates, S.M. and Lyons, T.W., 2006, A coupled oxygen isotope and trace metal record of glacioeustatic sea level variation and enhanced water column productivity: Geological Society of America, Abstracts with Programs, v. 38, p. 183.

Blair, T.C. and McPherson, J.G., 1994, Alluvial fans and their natural distinction from rivers based on morphology, hydraulic processes, sedimentary processes, and facies assemblages: Journal of Sedimentary Research, v. A64, p. 450-489.

Crowell, J.C., 1999, Pre-Mesozoic ice ages: their bearing on understanding the climate system: Geological Society of America Memoir, v. 192, 106 p.

Crowley, J.C., 1983, Ice ages recorded in Gondwanan continents: Geological Society of South Africa, Transactions, v. 86, p. 237-263.

Crowley, T.J. and Baum, S.K., 1991, Estimating Carboniferous sea-level fluctuations from Gondwanan ice extent: Geology, v. 19, p. 975-977.

Davydov, V., Wardlaw, B.R., and Gradstein, F.M., 2004, The Carboniferous Period, *in* Gradstein, F.M., Ogg, J.G., and Smith, A.G., eds., A Geologic Time Scale 2004: New York, Cambridge University Press, p. 222-248.

Epshteyn, O.G., 1981a, Middle Carboniferous ice-marine deposits of northeastern U.S.S.R., *in* Hambrey, M.J. and Harland, W.B. (eds.), Earth's pre-Pleistocene glacial record. Cambridge University Press, Cambridge, UK, p. 268-269.

Epshteyn, O.G., 1981b, Late Permian ice-marine deposits of the Atkan Formation in the Kolyma river headwaters region, U.S.S.R., *in* Hambrey, M.J. and Harland, W.B. (eds.), Earth's pre-Pleistocene glacial record. Cambridge University Press, Cambridge, UK, p. 270-273.

Fielding, C.R., Frank, T.D., Birgenheier, L.P., Rygel, M.C., Jones, A.T. and Roberts, J., 2008, Stratigraphic imprint of the Late Paleozoic ice age in eastern Australia: a record of alternating glacial and non-glacial climate regime: Geological Society of London Journal, v. 165, p. 129-140.

Goldstein, R.H. and Franseen, E.K., 1995, Pinning Points: a method providing quantitative constraints on relative sea-level history: Sedimentary Geology, v. 95, p. 1-10.

Heckel, P.H., 1994, Evaluation of evidence for glacio-eustatic control over marine Pennsylvanian cyclothems in North America and consideration of possible tectonic events, *in* Dennison, J.M. and Ettensohn, F.R., eds., Tectonic and Eustatic Controls on Sedimentary Cycles: SEPM, Concepts in Sedimentology and Paleontology 4, p. 65-87.

Hendrickson, D. M., 1986, Stratigraphy and Sedimentology of the Pennsylvanian and lower Permian Fountain Formation in Perry Park, Douglas County, Colorado: MA thesis, Colorado School of Mines, 296 p.

Houck, K.J., 1997, Effects of sedimentation, tectonics, and glacio-eustasy on depositional sequences, Pennsylvanian Minturn Formation, north-central Colorado: American Association of Petroleum Geologists Bulletin, v. 81, p. 1510-1533.

Hoy, R.G. and Ridgway, K.D., 2002, Syndepositional thrust-related deformation and sedimentation in an ancestral Rocky Mountains basin, Central Colorado trough, Colorado, USA: Geological Society of America Bulletin, vol. 114, p. 804-828.

Isbell, J.L., Miller, M.F., Wolfe, K.L., and Lenaker, P.A., 2003. Timing of Late Paleozoic glaciation in Gondwana: was glaciation responsible for the development of northern hemisphere cyclothems? In: Chan, M.A. and Archer, A.W. (eds.), Extreme depositional environments: mega end members in geologic time. Geological Society of America Special Paper 370, pp. 5-24.

Joachimiski, M.M., von Bitter, P.H., and Buggisch, W., 2006, Constraints on Pennsylvanian glacioeustatic sea-level changes using oxygen isotopes of conodont apatite: Geology, v. 34, p. 277-280.

Kairo, S., Suttner, L.J., and Dutta, P.K., 1993, Variability in sandstone composition as a function of depositional environment in coarse-grained delta systems: Geological Society of America Special Paper 284, p. 263-283.

Klein, D.D., 1994, Depth determination and quantitative distinction of the influence of tectonic subsidence and climate on changing sea level during deposition of Midcontinent Pennsylvanian cyclothems, *in* Dennison, J.M. and Ettensohn, F.R., eds., Tectonic and Eustatic Controls on Sedimentary Cycles: SEPM, Concepts in Sedimentology and Paleontology 4, p. 35-50.

Kluth, C.F., and Coney, P.J., 1981, Plate tectonics of the Ancestral Rocky Mountains: Geology, v. 9, p. 10-15.

Kluth, C.F., and McCreary, J.A., 2006, Reinterpretation of the geometry and orientation of the late Paleozoic Frontrange Uplift: Abstracts with Programs—Geological Society of America, v. 38, no. 6, p. 29.

Maples, C.G. and Suttner, L.J., 1990, Trace fossils and marine-nonmarine cyclicity in the Fountain Formation (Pennsylvanian; Morrowan/Atokan) near Manitou Springs, Colorado: Journal of Paleontology, vol. 64, p.859-880.

Paola, C. and Mohrig, D., 1996, Palaeohydraulics revisited: palaeoslope estimation in coarse-grained braided rivers: Basin Research, v. 8, p. 243-254.

Plint, A.G., Eyles, N., Eyles, C.H., and Walker, R.G., 1992, Control of sea level change, *in* Walker, R.G. and James, N.P., eds., Facies Models; Response to Sea Level Change: St. Johns, Newfoundland, Geological Assocaition of Canada, p. 15-25.

Rygel, M.C., Fielding, C.R., Frank, T.D., and Birgenheier, L.P., 2008, The magnitude of late Paleozoic glacioeustatic fluctuations: A synthesis: Journal of Sedimentary Research, v. 78, p. 500-511.

Suttner, L.J., Langford, R.P., and O'Connell, A.F., 1984. New interpretation of the stratigraphic relationship between the Fountain Formation and its Glen Eyrie Member. In: Suttner, L.J., (Ed), Sedimentology of the Fountain fan-delta complex near Manitou Springs and Canon City, Colorado. Society of Economic Paleontologists and Mineralogists field guidebook, pp. 31-61.

Sweet, D.E. and Soreghan, G.S., 2008, Polygonal cracking in coarse clastics records cold temperatures in the equatorial Fountain Formation (Pennsylvanian-Permian, Colorado): Palaeogeography, Palaeoclimatology, Palaeoecology, v. 268, no. 3-4, p. 193-204.

Sweet, D.E. and Soreghan, G.S., in review, Late Paleozoic tectonics and paleogeography of the Ancestral Front Range: Structural, stratigraphic and sedimentological evidence from the Fountain Formation (Manitou Springs, Colorado): [submitted GSA Bulletin, September 2008]

Trimble, D.E. and Machette, M.N., 1979, Geologic map of the Colorado Springs-Castle Rock area, Front Range Urban Corridor, Colorado: U.S.G.S. Map I-857-F, 1:100,000.

Veevers, J.J. and Powell, C.McA., 1987, Late Paleozoic glacial episodes in Gondwanaland reflected in transgressive-regressive depositional sequences in Euramerica: Geological Society of America Bulletin, v. 98, 475-487.

Wanless, H.R. and Shepard, F.P., 1936, Sea level and climatic changes related to late Paleozoic cycles: Geological Society of America Bulletin, v. 47, p. 1177-1206.

APPENDIX A. SAMPLE LIST AND LOCATIONS

Portions of the USGS 7.5’ minute Manitou Springs and Cascade, Colorado quadrangles with exact locations of measured sections discussed in text and shown on Figures 2.4-2.7 and Appendix E. Anotated white hexagons denote locations of samples not tied to measured sections and are keyed to the Appendix Table A on next page.

Appendix Table A: Sample list and location key

Location Keyed	Sample Name	Tectonostratigraphic Unit	SEM	Grain Size	Gravel Composition
MSXN-I, 1 mab	msp-i_1.0	lower	X		
MSXN-I, 10.1 mab	msp-i_10.1	lower	X		
MSXN-I, 21 mab	p-sol 1a_18	lower		X	
MSXN-I, 33.8 mab	msp-ii_21.8	lower	X		
MSXN-I, 51 mab	msp-ii_39.8	lower	X		
TOPO, (H)	COG lower	lower		X	X
TOPO, (G)	COG upper	middle		X	X
MSXN-I, 62 mab	msp-ii_52	middle	X	X	X
MSXN-I, 128 mab	msp-iii_39.1	middle		X	
MSXN-I, 142 mab	msp-iii_53	middle	X	X	X
MSXN-I, 162 mab	msp-iii_73	middle			X
MSXN-I, 186 mab	msp-iii_99.8	middle	X		
TOPO, (F)	School	middle		X	X
MSXN-I, 232.2 mab	msp-iv_49.1	middle	X		
MSXN-II, 16.7 mab	msp-v_16.7	middle	X		
MSXN-II, 37.8 mab	msp-v_37.8	middle	X		
MSXN-II, 102.4 mab	msp-vi_12.4	middle	X		
MSXN-II, 122.8 mab	msp-vi_32.8	middle	X		
TOPO, (E)	GOTG-Z	middle		X	X
MSXN-III, 60 mab	msp-viii_28	upper			X
TOPO, (C)	RRVW-Z	upper	X	X	
TOPO, (B)	RRVW-D	upper	X	X	X
MSXN-IV, 68.7 mab	msp-ix_68.7	upper		X	
MSXN-IV, 134.5 mab	msp-ix_134.5	upper			X
MSXN-IV, 229 mab	msp-ix_229	upper			X
MSXN-IV, 230.4 mab	msp-ix_230.4	upper	X	X	
TOPO, (A)	RRVE-A	upper		X	X
TOPO, (D)	upper outer	upper		X	

MSXN = measured section (displayed in Appendix E and Figs. 2.4-2.7)
TOPO = topographic map shown on previous page
mab = meters above base

APPENDIX B. GRAIN-SIZE DISTRIBUTION DATA

Grain-size analyses were conducted on the coarsest beds (inferred from visual inspection) to quantitatively assess the spatial and temporal degree of fining away from the AUPF. Data on the > 2 cm fraction was obtained by placing a 0.5 m^2 net with ~5 cm grid size on the outcrop and recording sizes of clasts > 2 cm (A-axis) at grid intersections. For clasts larger than the grid size, all intersections were counted. Data for the > 2 cm fraction was tallied into 5 cm bins. The matrix (< 2 cm fraction) of each site was then sampled for further grain size analysis through disaggregation and standard sieve analysis. Additionally, grain-size analysis was conducted through standard sieve methods on muddy granular sandstone facies (described later) to assess the proportion of mud to sand.

Appendix Table B (on next page displays raw data). Histograms of the grain-size distribution are displayed on the subsequent pages.

Appendix Table B: Grain-size distribution data													
SAMPLE	% ≤.125 mm	% .3-.125 mm	% .7-.3 mm	% 1.5-.7 mm	% 3-1.5 mm	% 20-3 mm	% 2-6 cm	% 7-10 cm	% 11-15 cm	%16-20 cm	%21-25 cm	%>26 cm	Total
Fluvial deposits													
upper outer	n/a	n/a	n/a	n/a	n/a	n/a	15.00%	1.00%	0.00%	0.00%	0.00%	0.00%	n/a
msp-ix_230.4	4.87%	6.69%	6.48%	8.90%	16.62%	29.45%	20.00%	7.00%	0.00%	0.00%	0.00%	0.00%	100.01%
RRVE-A	4.65%	9.52%	7.67%	8.50%	16.36%	41.31%	10.00%	2.00%	0.00%	0.00%	0.00%	0.00%	100.01%
RRVW-Z	3.93%	7.29%	6.50%	9.46%	17.85%	27.95%	24.00%	2.00%	0.00%	0.00%	0.00%	0.00%	98.98%
RRVW-D	5.74%	13.10%	11.54%	15.22%	26.49%	16.91%	9.00%	3.00%	0.00%	0.00%	0.00%	0.00%	101.00%
COG-lower	8.64%	10.16%	9.52%	12.25%	21.48%	14.95%	10.00%	8.00%	5.00%	0.00%	0.00%	0.00%	100.00%
COG-upper	4.75%	5.48%	6.51%	7.34%	5.65%	3.26%	13.00%	12.00%	20.00%	7.00%	16.00%	0.00%	100.99%
School	3.30%	4.53%	4.90%	5.29%	6.20%	5.77%	34.00%	15.00%	9.00%	4.00%	3.00%	5.00%	99.99%
msp-ii_52	2.18%	4.06%	3.85%	4.21%	3.64%	6.05%	20.00%	20.00%	19.00%	10.00%	7.00%	0.00%	99.99%
msp-iii_53	1.77%	9.94%	9.22%	11.08%	12.42%	6.57%	26.00%	12.00%	7.00%	3.00%	0.00%	0.00%	99.00%
GOTG-Z	10.35%	27.72%	19.99%	5.56%	2.47%	2.91%	23.00%	5.00%	0.00%	3.00%	0.00%	0.00%	100.00%
Debris flow deposits	clay	f. silt	c. silt	v.f.-f.sand	m.-c. sand	v.c sand-granule	pebble						
P-sol 1a-18	5.34%	5.70%	6.80%	14.39%	31.22%	26.19%	8.71%						
msp-iii_39	20.07%	16.59%	11.50%	12.18%	13.56%	6.25%	0.78%						
msp-ix_68.7	12.13%	13.21%	17.05%	27.92%	11.89%	2.39%	0.94%						

Grain-size distribution histograms

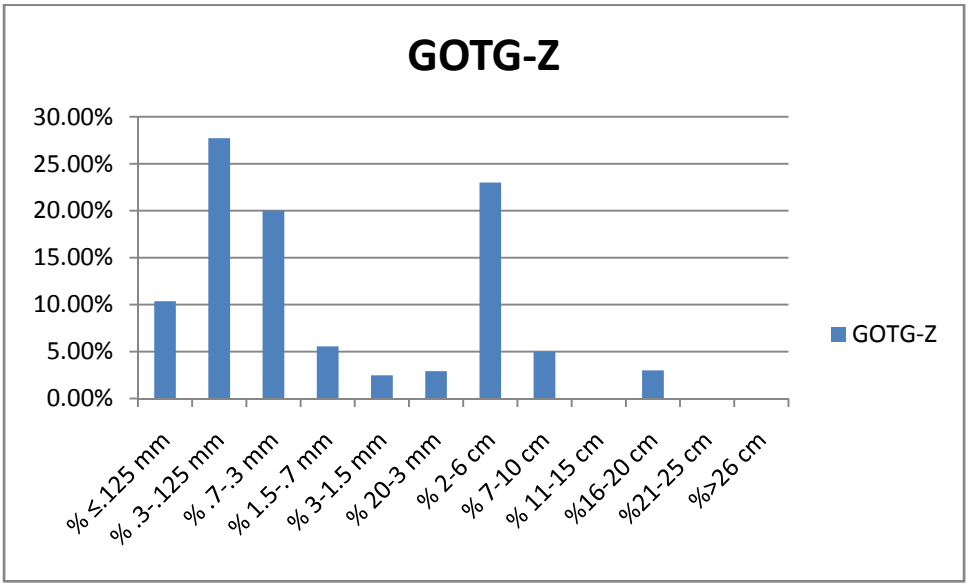

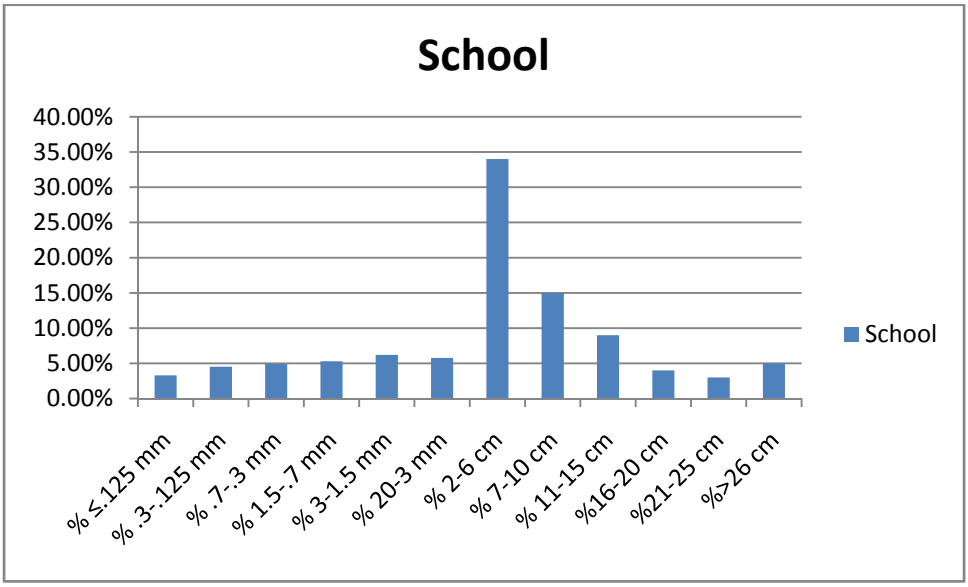

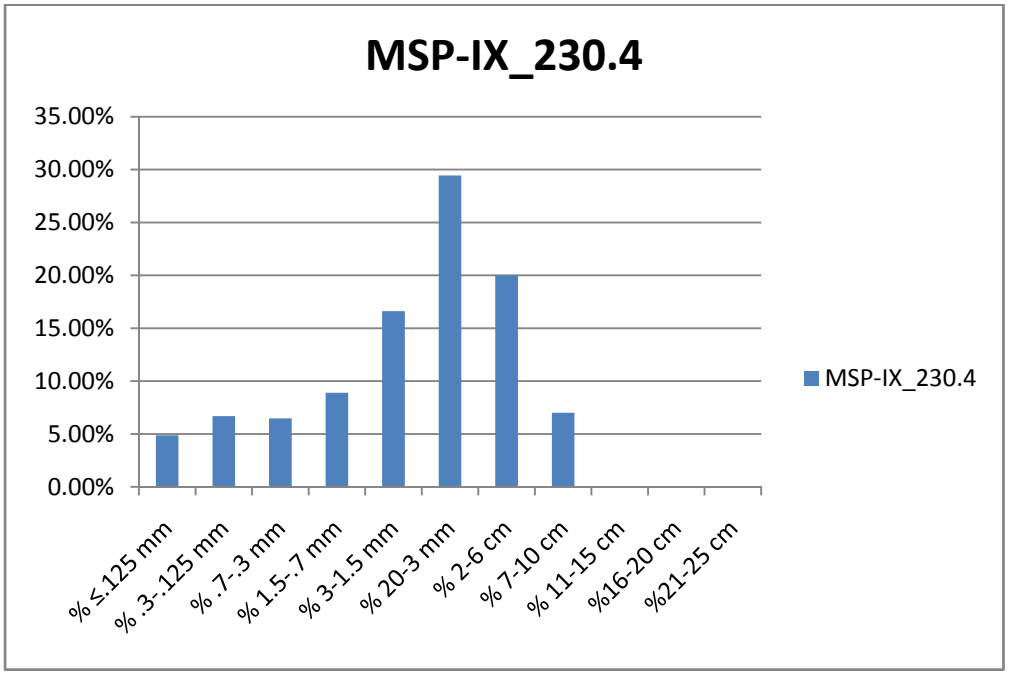
MSP-IX_230.4
35.00%
30.00%
25.00%
20.00%
15.00%
10.00%
5.00%
0.00%
% ≤.125 mm
% .3-.125 mm
% .7-.3 mm
% 1.5-.7 mm
% 3-1.5 mm
% 20-3 mm
% 2-6 cm
% 7-10 cm
% 11-15 cm
%16-20 cm
%21-25 cm
MSP-IX_230.4

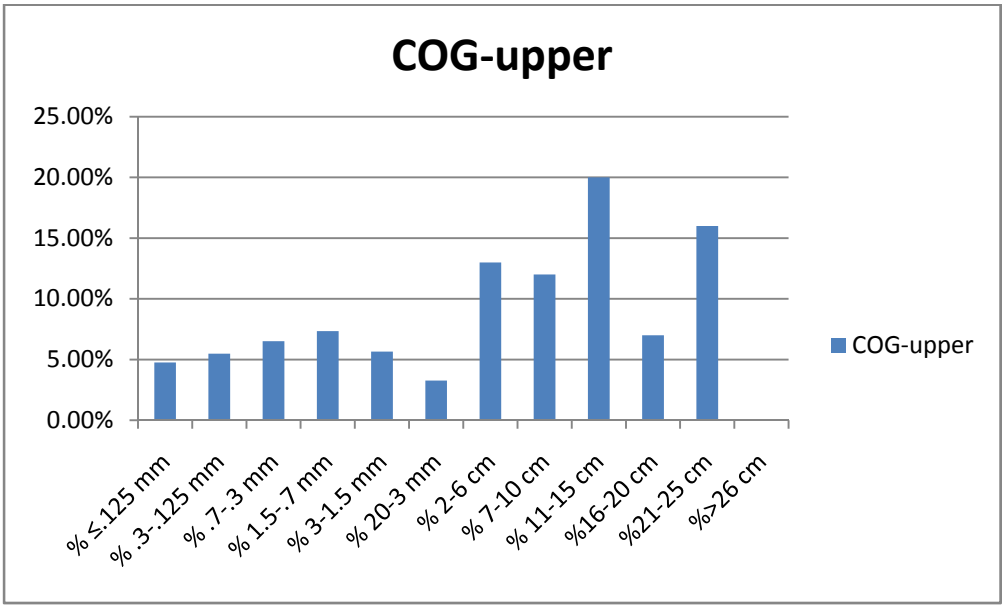
COG-upper
25.00%
20.00%
15.00%
10.00%
5.00%
0.00%
% ≤.125 mm
% .3-.125 mm
% .7-.3 mm
% 1.5-.7 mm
% 3-1.5 mm
% 20-3 mm
% 2-6 cm
% 7-10 cm
% 11-15 cm
%16-20 cm
%21-25 cm
%>26 cm
COG-upper

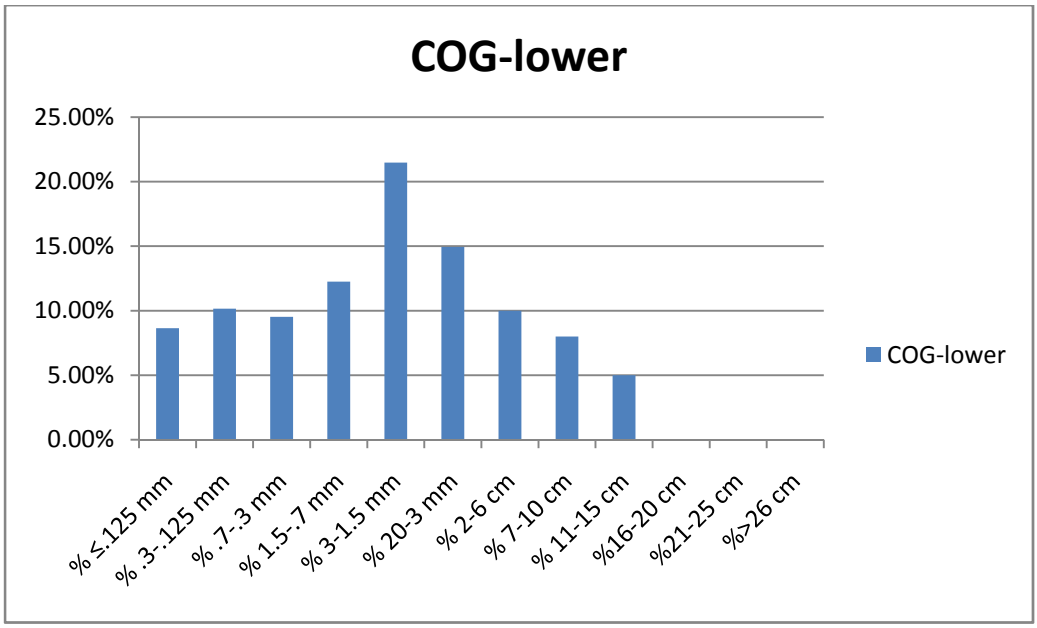
COG-lower
25.00%
20.00%
15.00%
10.00%
5.00%
0.00%
% ≤.125 mm
% .3-.125 mm
% .7-.3 mm
% 1.5-.7 mm
% 3-1.5 mm
% 20-3 mm
% 2-6 cm
% 7-10 cm
% 11-15 cm
%16-20 cm
%21-25 cm
%>26 cm
COG-lower

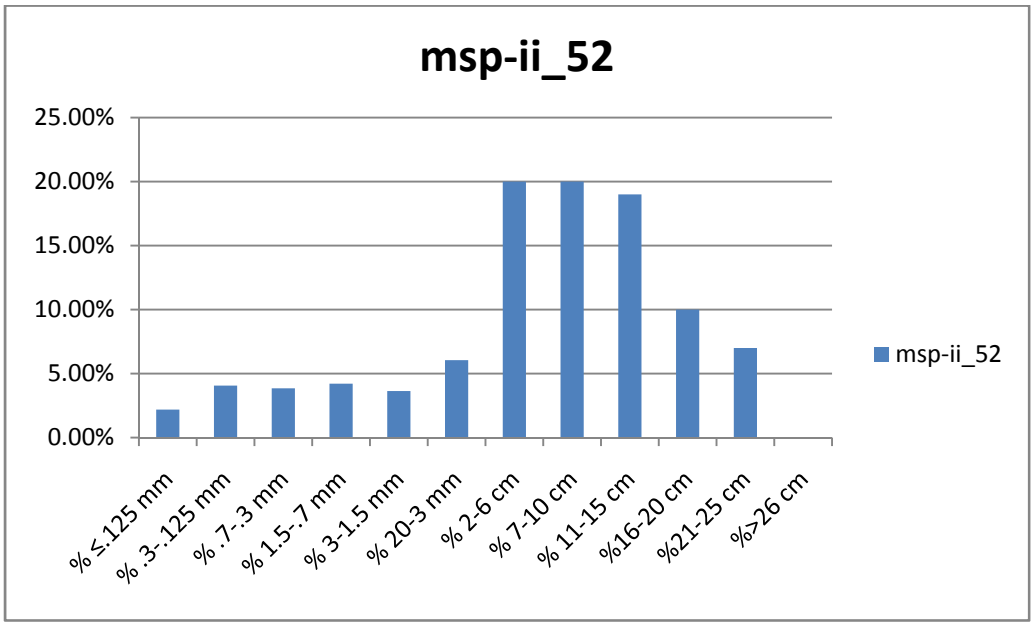
msp-ii_52
25.00%
20.00%
15.00%
10.00%
5.00%
0.00%
% ≤.125 mm
% .3-.125 mm
% .7-.3 mm
% 1.5-.7 mm
% 3-1.5 mm
% 20-3 mm
% 2-6 cm
% 7-10 cm
% 11-15 cm
%16-20 cm
%21-25 cm
%>26 cm
msp-ii_52

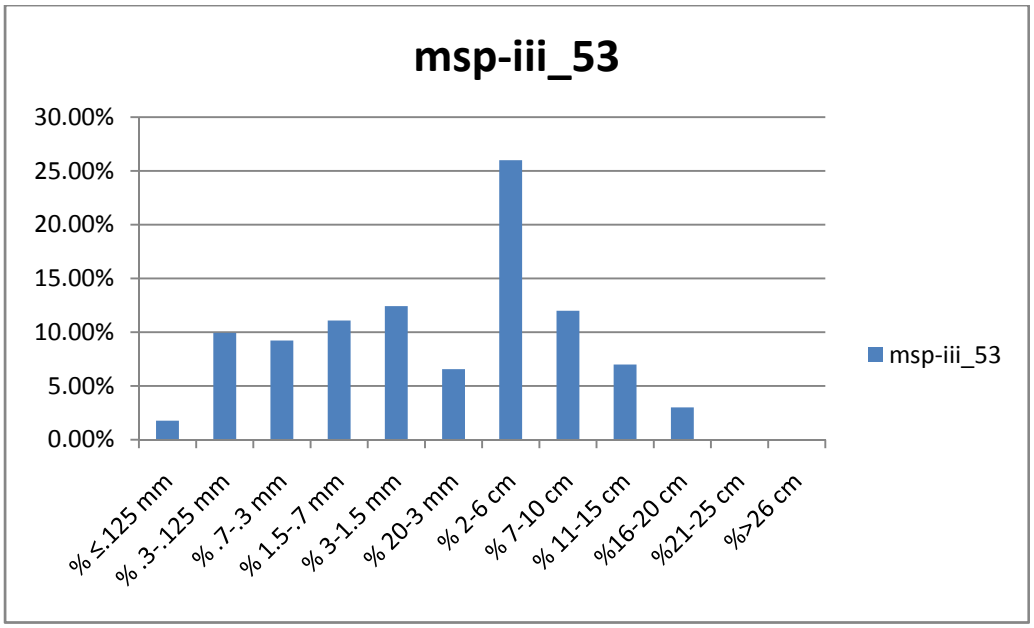
msp-iii_53
30.00%
25.00%
20.00%
15.00%
10.00%
5.00%
0.00%
% ≤.125 mm
% .3-.125 mm
% .7-.3 mm
% 1.5-.7 mm
% 3-1.5 mm
% 20-3 mm
% 2-6 cm
% 7-10 cm
% 11-15 cm
%16-20 cm
%21-25 cm
%>26 cm
msp-iii_53

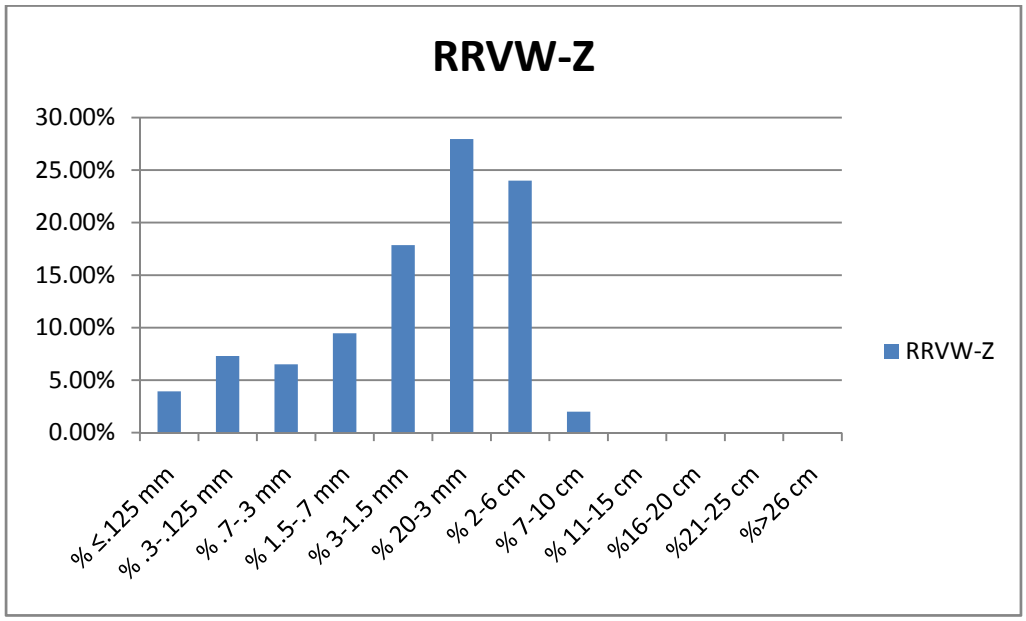
RRVW-Z
30.00%
25.00%
20.00%
15.00%
10.00%
5.00%
0.00%
% ≤.125 mm
% .3-.125 mm
% .7-.3 mm
% 1.5-.7 mm
% 3-1.5 mm
% 20-3 mm
% 2-6 cm
% 7-10 cm
% 11-15 cm
%16-20 cm
%21-25 cm
%>26 cm
RRVW-Z

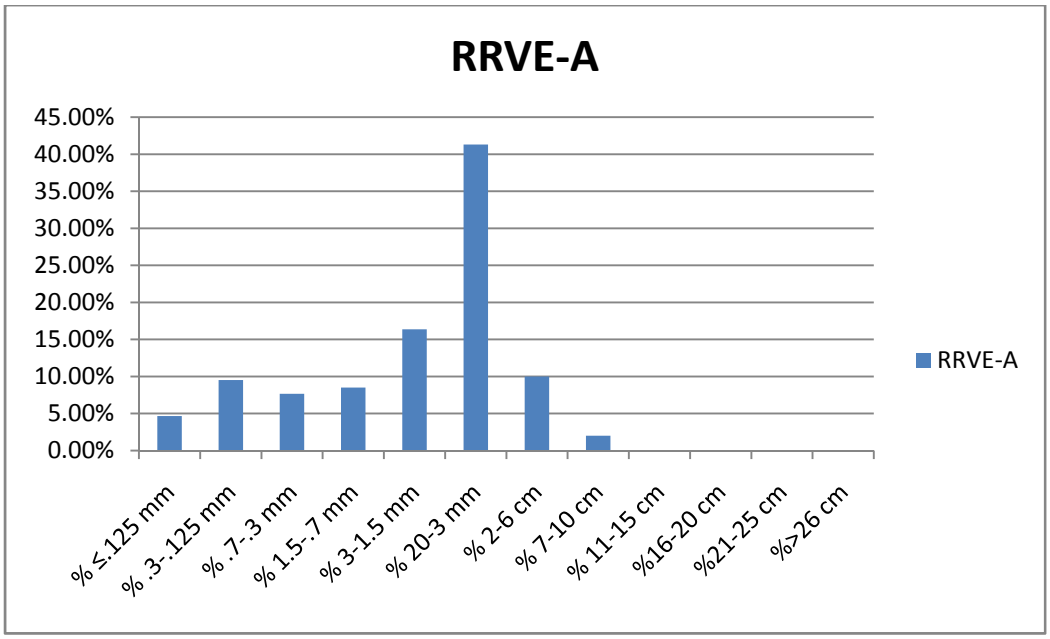
RRVE-A
45.00%
40.00%
35.00%
30.00%
25.00%
20.00%
15.00%
10.00%
5.00%
0.00%
% ≤.125 mm
% .3-.125 mm
% .7-.3 mm
% 1.5-.7 mm
% 3-1.5 mm
% 20-3 mm
% 2-6 cm
% 7-10 cm
% 11-15 cm
%16-20 cm
%21-25 cm
%>26 cm
RRVE-A

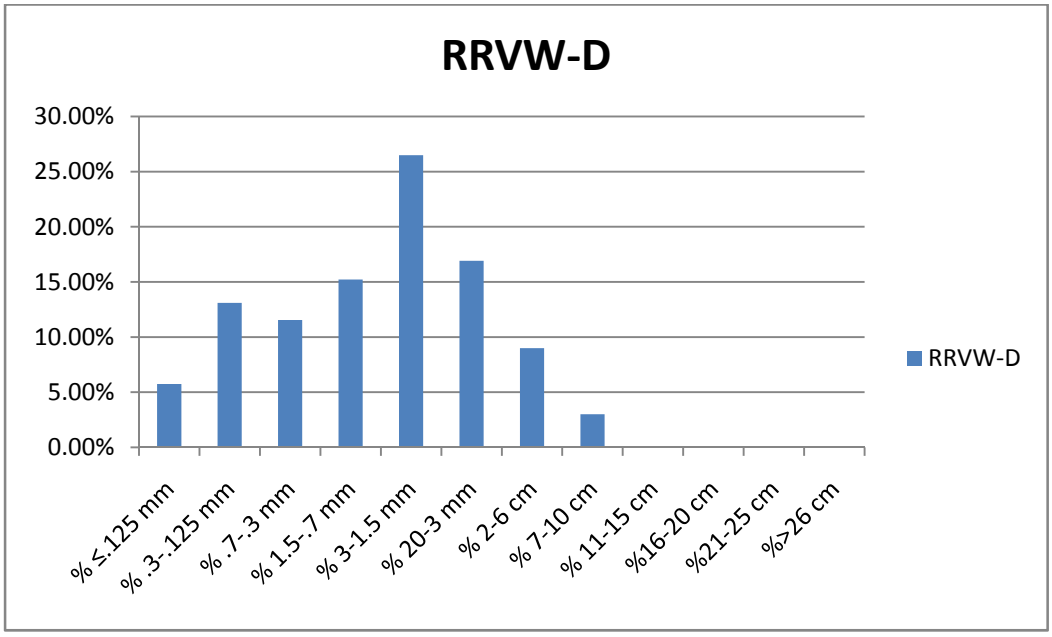
RRVW-D
30.00%
25.00%
20.00%
15.00%
10.00%
5.00%
0.00%
% ≤.125 mm
% .3-.125 mm
% .7-.3 mm
% 1.5-.7 mm
% 3-1.5 mm
% 20-3 mm
% 2-6 cm
% 7-10 cm
% 11-15 cm
%16-20 cm
%21-25 cm
%>26 cm
RRVW-D

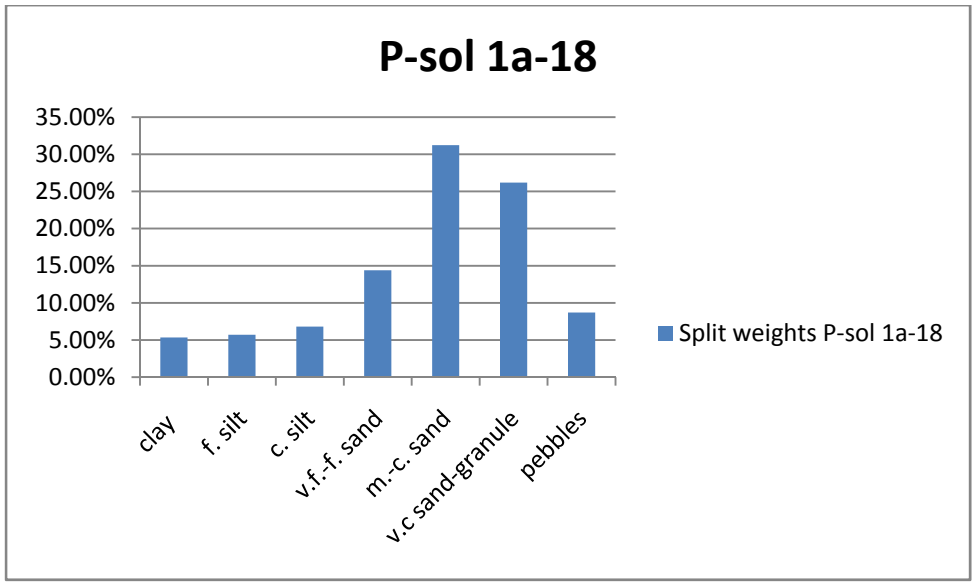
P-sol 1a-18
35.00%
30.00%
25.00%
20.00%
15.00%
10.00%
5.00%
0.00%
clay
f. silt
c. silt
v.f.-f. sand
m.-c. sand
v.c sand-granule
pebbles
Split weights P-sol 1a-18

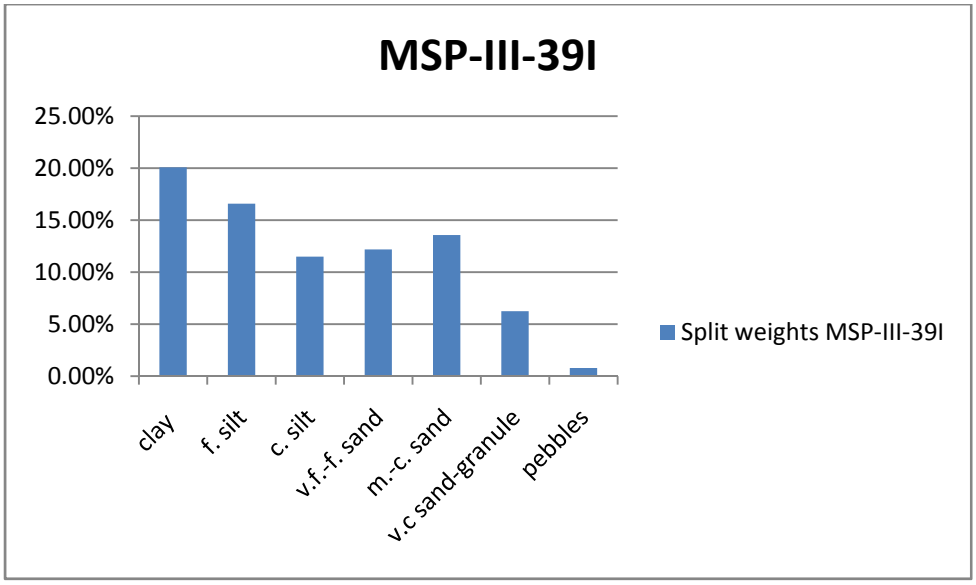
MSP-III-39I
25.00%
20.00%
15.00%
10.00%
5.00%
0.00%
clay
f. silt
c. silt
v.f.-f. sand
m.-c. sand
v.c sand-granule
pebbles
Split weights MSP-III-39I

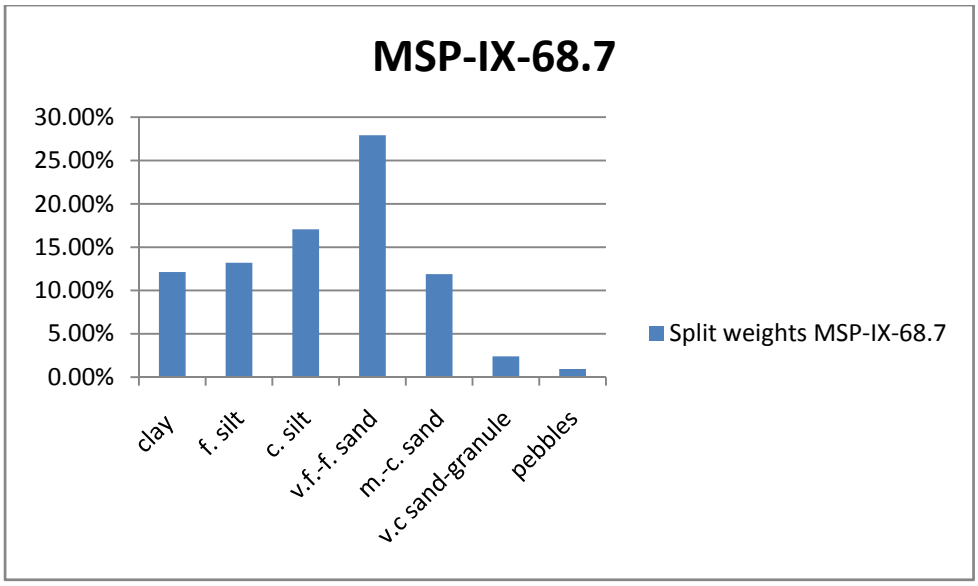
MSP-IX-68.7
30.00%
25.00%
20.00%
15.00%
10.00%
5.00%
0.00%
clay
f. silt
c. silt
v.f.-f. sand
m.-c. sand
v.c sand-granule
pebbles
Split weights MSP-IX-68.7

APPENDIX C. COMPOSITION DATA FOR CLASTS > 2 CM

Data was collected on the > 2 cm fraction by placing a 0.5 m^2 net with ~5 cm grid size on the outcrop and recording composition of clasts > 2 cm (A-axis) at grid intersections. For clasts larger than the grid size, all intersections were counted. Although they varied, no attempt was made to differentiate different types of granite and metamorphic clasts.

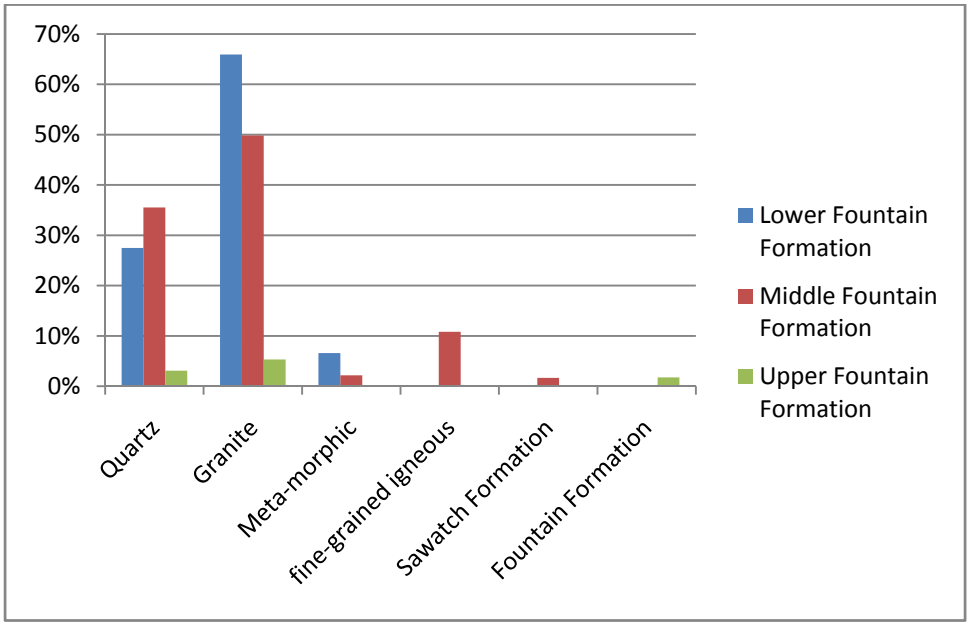

Bar-graph displaying the compositional variation of clasts larger than 2 cm in the lower, middle and upper Fountain Tectonostratigraphic units.

Appendix Table C: Fountain Formation composition of clasts > 2 cm

SAMPLE SITE	CLAST TYPE						TOTAL COUNT
	Quartz	Granite	Meta-morphic	Fine-grained igneous	Sawatch Formation	Fountain Formation	
Lower Fountain							
COG lower	25	60	6				91
total	25	60	6				91
percentage	27%	66%	7%	0%	0%	0%	
Middle Fountain							
COG Upper	4	76	1		4		85
SXN-III-53	20	36		12	1		69
SXN-III-73	60	112		20	5		197
GOTG-Z	54	90	2	26			172
School	154	183	22	60	9		428
SXN-II-52	116	75		6			197
total	408	572	25	124	19		1148
percentage	36%	50%	2%	11%	2%	0%	
Upper Fountain							
RRVW-D	1	14	3				18
RRVE-A	20	27					47
SXN-IX-134.5	11	25					36
SXN-IX-229	18	15	2				35
RRVW-Uncon	17	34				38	89
total	67	115	5	0	0	38	2170
percentage	3%	5%	0%	0%	0%	2%	

APPENDIX D. SEM MICROTEXTURAL DATA

Samples were collected from 3 facies—fluvial, debris flow and marine shoreface—in conjunction with description of the measured section presented in Sweet and Soreghan (in review). Fifteen samples were collected and 10-55 individual quartz grains from each sample were analyzed by SEM.

Samples were disaggregated for microtextural analyses by removing iron-oxide cement with the citrate-bicarbonate-dithionite (CBD) method (Mehra and Jackson, 1960; Janitzky, 1986). The sand + gravel fraction was wet-sieved and the 3-1.5 mm, 1.5-0.7 mm and 0.7-0.3 mm fractions were analyzed. No sonication was used during the disaggregation process. Quartz grains were randomly selected with a binocular microscope for SEM analysis as outlined by Mahaney et al. (1988).

Individual grains were placed on an aluminum SEM stub and sputter coated with a gold-palladium mixture. Grains were examined with a Zeiss 960 SEM, tungsten filament and 15 Kv. All grains were individually verified as quartz by energy dispersive spectrum (EDS) analysis.

The atlases of Krinsley and Doornkamp (1973) and Mahaney (2002) were used for identification of microtextures. Each microtexture evaluated was noted as either present or not present following the methods of Mahaney (2002); no attempt was made to estimate percentage of grain covered or relative importance of certain microtextures. Quantitative summary analyses were plotted similarly to methods outlined in Mahaney and Kalm (2000) and Mahaney et al. (2001).

Appendix Table D: Raw SEM microtexture data

Sample	MAB	Facies	total grains	grains with textures	percent with late Paleozoic textures	percussion counts	polygenetic counts	high-stress counts	Percent percussion	Percent polygenetic	Percent high-stress
msp-i_1.0	1	offshore	48	39	81.25%	36	48	9	39%	52%	10%
msp-i_10.1	10.1	fluvial	53	32	60.38%	30	48	12	33%	53%	13%
msp-ii_21.8	31	fluvial	32	24	75.00%	25	27	9	41%	44%	15%
msp-ii_42	51	fluvial	55	22	40.00%	17	20	3	43%	50%	8%
msp-ii_52	62	fluvial	33	27	81.82%	29	39	14	35%	48%	17%
msp-iii_53	143	fluvial	34	11	32.35%	5	17	1	22%	74%	4%
msp-iii_99.8	188.8	foreshore	46	21	45.65%	12	26	6	27%	59%	14%
msp-iv_49.1	232	fluvial	10	7	70.00%	3	8	5	19%	50%	31%
msp-v_16.7	281.7	debris flow	22	14	63.64%	6	23	5	18%	68%	15%
msp-v_37.8	302.8	fluvial	39	28	71.79%	25	63	23	23%	57%	21%
msp-vi_12.4	367.4	fluvial	22	18	81.82%	8	32	7	17%	68%	15%
msp-vi_32.8	387.8	fluvial	27	18	66.67%	6	21	3	20%	70%	10%
RRVW-Z	583	fluvial	35	23	65.71%	22	35	7	34%	55%	11%
RRVW-D	684	fluvial	43	17	39.53%	17	28	0	38%	62%	0%
msp-ix_230.4	909.4	fluvial	42	29	69.05%	28	41	15	33%	49%	18%